TRAJECTORY OPTIMIZATION FOR ASTEROID CAPTURE

A Dissertation

Submitted to the Faculty

of

Purdue University

by

Jay Iuliano

In Partial Fulfillment of the

Requirements for the Degree

of

Doctor of Philosophy

December 2020

Purdue University

West Lafayette, Indiana

THE PURDUE UNIVERSITY GRADUATE SCHOOL
STATEMENT OF DISSERTATION APPROVAL

Dr. David Spencer, Chair

School of Aeronautics and Astronautics

Dr. James Longuski

School of Aeronautics and Astronautics

Dr. Dengfeng Sun

School of Aeronautics and Astronautics

Dr. Daniel DeLaurentis

School of Aeronautics and Astronautics

Approved by:

Dr. Gregory Blaisdell

Head of the School Graduate Program

Dedicated to my dearest friends and my wonderful girlfriend, whose companionship has gotten me through many tough times, and to my wonderful professors, whose erudition and endless patience has made me who I am today.

"Friendship is far more tragic than love. It lasts longer."

- Oscar Wilde

ACKNOWLEDGMENTS

Foremost, I would like to express my gratitude to my advisor, Professor David Spencer for his support and involvement during my Ph.D. research, for his patience, dedication, and wealth of experience. His guidance has helped me improve both my research and my writing, and his contributions to those cannot be understated.

I would also like to thank the rest of my thesis committee: Prof. James Longuski, Prof. Daniel DeLaurentis, and Prof. Dengfeng Sun for their perspective and insight on my work. Their decades of experience as researchers, and professors has been invaluable to my work.

I would also like to thank all of my lab mates in the Space Flights Project Laboratory, who always had encouraging and interesting perspectives that helped advance and clarify my work. Specifically, I would like to acknowledge my labmate Sylvain Renevey, and my old roommate, Robert Potter, who's insights into astrodynamics have helped me better understand and improve my ideas numerous times. And I would like to thank some of my best friends: Dr. Conner Farley, Dr. Camden DeBruler, and Trevor Jones who, despite their expertise in disparate fields, have had a tremendous impact on the quality of my research and my intellectual discourse.

Finally, and by no order of merit, I would like to thank my pervious professors: Dr. Kira Abercromby, and Dr. Paul Miklowitz. Their understanding, their expertise, and their mentorship has greatly influenced my perspective as an intellectual, and has made me both a better researcher, and a better person.

TABLE OF CONTENTS

LIST OF TABLES

Table Page

LIST OF FIGURES

Figure Page

SYMBOLS

a	semi-major axis
$a_{(source)}$	inertial acceleration from (source)
A	area
c_{srp}	solar radiation pressure constant
C	Jacobi energy
C_r	coefficient of reflectivity
$\varnothing$	diameter
m	mass
μ	gravitational parameter
N	total number of burns
Δp	change in momentum
p_{srp}	average solar radiation pressure at 1 AU
q	perihelion
Q	aphelion
r	radius
Ω	right-ascension of the ascending node
t	time
T	Tisserand parameter
T_{max}	maximum thrust
θ_s	angular position of the sun in the Earth-Moon synodic frame
v	velocity
ΔV	change in velocity
v_∞	hyperbolic excess velocity

ABBREVIATIONS

AU	Astronomical Units
BCR4BM	Bicircular Restricted Four Body Model
CR3BP	Circular Restricted Three Body Problem
DRO	Distant Retrograde Orbit
NEA	Near-Earth Asteroid
NEO	Near-Earth Objects
PHA	Potentially Hazardous Asteroids
SRP	Solar Radiation Pressure

ABSTRACT

Iuliano, Jay PhD, Purdue University, December 2020. Trajectory Optimization for Asteroid Capture . Major Professor: David Spencer.

In this work, capturing Near-Earth Asteroids (NEAs) into Near-Earth orbits is investigated. A general optimization strategy is employed whereby a genetic algorithm is used to seed a sequential quadratic programming (SQP) method for the first step, and then nearby solutions seed further SQP runs. A large number of solutions are produced for several asteroids with varying levels of thrust, and under the effects of various perturbations. Solutions are found over a range of epochs and times of flight as opposed to many traditional methods of optimizing point solutions. This methodology proved effective, finding low-thrust capture solutions within 10% of the required ΔV for analytically estimated transfers, and matching results from other optimization programs such as MALTO. It is found that the effects of solar radiation pressure (SRP) and n-body effects do not have a significant impact on the optimized transfer costs, nor do the perturbations significantly affect the shapes and trends of the optimized solution space.

These optimized results are then used to develop analytic models for both optimized transfer costs and flight times. These models are then used to estimate the transfer costs and flight times for all listed Near Earth Asteroids from the JPL Small Body Database. This analysis is then used to determine the nominal properties of potentially capturable asteroids. The characteristics are then related to a series of different asteroid transfer technologies, elucidating each technology's capabilities and potential capture targets. Finally, this analysis concludes with a brief roadmap of the major decisions mission designers should consider for future asteroid capture missions.

1. INTRODUCTION

Asteroid capture has become a topic of increasing interest in recent years with numerous recent missions to asteroids as well as the emergence of more advanced propulsion technologies. The advancements in technology have turned asteroid deflection and capture from sci-fi speculation to a real-world proposition. The consistent improvement of low thrust systems as well as the development of new types of propulsive technologies such as kinetic impactors, and gravity tractors, makes the concept feasible and approachable.

1.1 State-of-the-Art in Asteroid Capture and Deflection

The prospect of planetary defense has become feasible in the last 20 years with observational abilities and efforts increasing and with the advancement of more efficient and powerful transportation methods. Asteroid capture has become a topic of greater interest in the last decade as asteroid deflection becomes well understood and the prospect of bringing an asteroid back to a stable orbit in a controlled way becomes reasonable. Fortunately, much of the work on asteroid deflection is applicable to the asteroid capture problem. Of course, there are several notable differences, but the deflection effort remains a strong groundwork for the capture effort.

1.1.1 Transfer Optimization

Transfer optimization has been a topic interest since orbital mechanics was studied and has been a wealth of amazing and interesting research since. In general, there is no concrete way to distill the transfer optimization problem completely and concretely. In the broader field of mathematical optimization, there are two camps that optimizations generally fall into - local optimization and global optimization [1]. These methodologies differ in the scope of the space that they search and their benefits in doing so. Global algorithms are able to search large and unrelated areas in the solution space but often fail to converge with the same precision as local optimizers. Local optimizers are very good at converging to true optima, but struggle to move away from their initial guess or to converge at all if their initial guess is poor. Orbital transfer optimization is usually taken as a local optimization problem where a significant effort has been made to generate good initial guesses for a number of different transfer scenarios.

While initial guess generation in general is heavily dependent on the problem, there are numerous common techniques that have been developed. For simple orbital transfers, where the goal is simply to optimize the transfer from one orbit to another, even in the presence of complex dynamical perturbations, one traditional method for generating initial guesses is to use a Lambert arc. The Lambert arc pulls all of the transfer into two impulses and finds the time-fixed solution to go between them [2,3]. Under the right conditions, an optimizer can use this initial guess and match it to the problems constraints and control law to then generate a more accurate and an often more optimized result. This is the technique that JPL's interplanetary optimization tool MATLO uses to great success [4]. Optimizations with complex control laws, or constraints not directly related to the physical structure of the transfer (total radiation dosage, for example), can also utilize this technique but the farther the bounds of the problem pull the transfer from a coasting arc, the more difficult it will be for the optimizer to converge using the Lambert solution as an initial guess.

Another common technique is to use the state transition matrix (STM) of the system dynamics in order to actively converge upon nearly correct initial guesses before allowing the optimizer to take control of the trajectory. The STM is a linearization of the dynamics over some small fixed timestep that allows for an accurate prediction of the behavior of the transfer given certain desired perturbations in the initial and final state. This can be used to iteratively converge on trajectories that shoot towards given constraint points, or that follow certain rules of the problem.

One technique for solving the initial guess problem that has become increasingly popular as computation has become more efficient is the use of hybrid optimizers [5–7]. Hybrid optimizers use a global optimizer to find an initial solution that can be input as the first guess for a local optimizer. The global optimizer ensures that the location of the initial guess has merit over a large amount of the solution space while the local optimizer ensures that the given guess converges to the best possible answer in that neighborhood. These are extremely powerful as they utilize both qualities of global and local optimizers, though they have the drawback of being significantly more computationally expensive than using just a single optimizer. See Fu or Wagner ([5–7]) for more examples. As such, hybrid structures are best used for single-point solutions that require high fidelity, or problems where generating an initial guess is difficult.

There are two major optimization techniques to consider for transfer optimization - indirect optimization, which formulates the problem in terms of the necessary and sufficient conditions for optimality and then solves for the parameters that enforce those conditions, and direct optimization, which formulates the problem explicitly in terms of the input parameters of the system. The terms 'direct' and 'indirect' refer to the way that the cost function and the constraints are setup and which variables are modified in order to affect the cost. Indirect methods formulate mathematical counterparts to the states of the system called costates. Costates often have no physical meaning, making them very difficult to guess, but have been shown to represent certain conditions that prove the given transfer is truly optimal [1]. By using indirect methods and ensuring all constraints are met, it can be shown that the given solution is mathematically optimal. This is an advantage over direct methods which determine optimality through methods related to examining the gradient of the cost function at different points. While this works well and often finds nearly optimal solutions, optimality is not explicitly dictated in direct methods. The major drawback to indirect methods is the description of these costates and the associated conditions of optimality. Costates require length derivatives, and change every time the cost changes, constraints are added, or the dynamics or controls of the system are altered. This is unwieldy, slow, difficult, and often decreases the convergence rate of the optimizer, but it carries with it the claim of true optimality [1, 8].

Neither method is better in general, and each has been shown to have valid use cases. Indirect methods are often used when highly precise optimal solutions are required or when continuous control needs to be optimized for. Direct methods are often used when a large number of low-fidelity solutions are desired or where discrete control can be applied. Direct optimization can accommodate continuous control, it is just more difficult and often not worth the considerations it requires when an indirect method could be used in its place. This is similarly true for indirect methods and discrete control.

Much of the initial work in transfer optimization separated the optimization question into "finite thrust" and "infinite thrust", where the former was meant to be a refinement of the latter and the latter is more commonly referred to now as impulsive thrust optimization. Numerous techniques and methodologies have been developed and thoroughly tested for optimizing low-thrust trajectories. The low-thrust transfer problem has been examined thoroughly for minimum time transfer solutions and for minimum fuel transfer solutions. The number of different studies into the subject include interplanetary studies, rendezvous problems, flyby transfers, transfers to time-variant regimes, and so forth. It has been shown by Sims and Flanagan [9] that even very low thrust systems can be successfully approximated to a low degree of fidelity using impulsive approximations. Sims and Flanagan achieve this approximation by segmenting the transfer trajectory and representing the continuous thrust as accumulated thrust at defined nodes. This segmentation has also been shown to be an effective optimization tool for continuous thrust trajectories with complex control laws [10].

High-thrust optimization is rarely studied anymore because it is more concretely contextualized by the infinite-thrust cases that make up the majority of early research into orbital transfer optimization. It is also becoming commonplace for missions to attempt complex transfers as low-thrust systems become the norm. For pushing asteroids around, all modern propulsion systems are functionally equivalent to low-thrust systems since the mass of asteroids is so much higher than that of spacecraft.

In the context of asteroid deflection, there has been a serious effort to characterize the capabilities of low-thrust transfers. While asteroid deflection specifically is very different from asteroid capture, the two have enough similarities that deflection results act as a good backbone for capture scenarios. One of the most extensive surveys of the problem was produced by NASA in 2006 [11]. This report gives an overview of the technological deflection capabilities of several technologies with different launch vehicles, asteroid targets, and deflection techniques. This report also gives a concrete look at the technological readiness of each of these deflection options and their various benefits and drawbacks. Another significant report with similar content was delivered to the National Research Council in 2010 [12]. Stahl [13], in 2008, developed a tool for assessing the validity of different options for NEA deflection. Izzo [14] went through the basics of optimal deflection and orbital mechanics, examining b-plane deflection strategies for impulsive and continuous maneuvers. Wie [15] showed the dynamical techniques for asteroid deflection while Ketema [16] showed how asteroid deflection with gravity tractors could be improved using orbits that move relative to the asteroid. Mazanek [17] also talks of several methods to improve upon gravity tractor deflection techniques. Later, Wagner and Wie [7] developed an optimization methodology for low-thrust asteroid deflection and redirect missions. Vasile talks at length of different optimal strategies for asteroid deflection [18, 19]. Olds takes the problem from the perspective of mass drivers and examines how deflection efforts could be improved upon with this technology [20]. In his dissertation, Paek [21] goes into depth about how to integrate and attack uncertainty into asteroid deflection campaigns. Eggl continues this effort in 2016 [22].

There has also been a considerable effort for optimizing asteroid capture transfer scenarios as well. A wonderful literature review by Sanchez et al. [23] gives a short summary of the work done up to 2018 that includes explicitly transfer costs for asteroid capture. In 2010, Yarnoz et al. [24] made a list of the easily retrievable NEOs. In his work, Yarnoz uses Sun-Earth three body motion to exploit transfers into vertical Lyapunov and halo orbits, finding transfers that cost as low as 58 m/s. Baoyin et al. [25] explored how asteroids could be captured using low-energy transfers in the Sun-Earth-NEO three body system. The results found here were successful, finding transfers with a ΔV cost of 400 m/s. Brophy et al. [26] investigates the technological feasibility of capturing NEAs to the ISS. Despite the difficult capture orbit, Brophy finds transfers on the order of 2 km/s or less. The Asteroid Retrievability Study [27] found return transfers for approximately 170 m/s given select asteroids and flight conditions. Llado [28] showed how NEOs could be captured into Sun-Earth Lagrangian points. Llado also uses a similar methodology to that developed in this work. Strange et al. [29] studied how asteroids could be transferred into Earth-Mars resonant cycler orbits for as little as 36 m/s. In 2015, Gong talked about several techniques for capturing asteroids using lunar flyby techniques with resulting captures costing less than 1 km/s, and even one capture costing only 49 m/s ΔV. Bao et al. [30] used a swarm optimization technique to find capture transfers into bounded orbits around Earth. This study looked at several flyby techniques and showed that transfer costs as low as 79 m/s could be achieved. Urrutxua and Bombardelli [31] look at an interesting class of asteroids known as "temporarily captured asteroids". These objects are naturally captured in the Earth-Moon gravity well and maintain in the system until they escape. The duration of this capture depends on several factors such as the physical properties of the asteroid and the strength of the perturbational forces. Urrutxua and Bombardelli show that these natural dynamics can be utilized to purposefully induce temporary capture in asteroids. Their work extends to find transfers as low as 31 m/s for a capture duration of 5.5 years. Tan et al. [32] investigated capturing NEAs into bounded periodic orbits around the Sun-Earth L_1 and L_2 points. Tan examines several asteroids and finds transfers on the order of 40 m/s. Neves and Sanchez [33] detailed a methodology for capturing into Sun-Earth Libration orbits using a multi-fidelity approach whereby the dynamics fidelity is increased successively as quality solutions are found. Transfers as low as 73 m/s are found using this technique.

1.1.2 Transfer Technologies

There are a considerable number of different potential transfer technologies that have been proposed. In general, these are divided into two categories: 1) fast technologies, and 2) slow technologies. Fast technologies include destructive options such as kinetic impactors, nuclear blasts, and mass drivers, and nondestructive options such as chemical propulsion. Slow technologies include a variety of different suggestions including solar sails, gravity tractors, low-thrust tugs, and so forth. The slow options offer an outlet for more creative ways to manipulate the trajectory of the asteroid but offer less control authority over the asteroid in most cases and significantly longer mission times.

As of right now, the most developed and understood potential candidates for asteroid transfer applications are gravity tractors [34]. Gravity tractors, also known as gravity tethers, are systems where a satellite orbits near or around a massive body so as to pull it off course with its own gravity. While this is likely one of the cheapest solutions (other than kinetic impactors), they are difficult to control and require a very long time to change the trajectories of asteroids significantly. They also require much more complex transfer trajectories since they are always within the gravitational influence of the asteroid itself [35]. The momentum exchange provided by these systems is miniscule, but they have high ΔV potentials as they can apply changes to the asteroid's trajectory for the entire lifetime of the spacecraft. Because of the inherent simplicity of this technology, it is currently the only technology that could be flown for an asteroid capture mission without need for further development. After gravity tractors, propulsive technologies are the most well vetted and understood choice. Electric propulsion offers extremely high ΔV potential but adds transfers inefficiencies compared to energy minimum (Hohmann) transfers, as well as the associated difficulties of elongated missions [36]. Chemical thrusters decrease the inherent inefficiencies of low-thrust transfers and require less complex transfer trajectories, but do not have nearly as high ΔV capabilities. Chemical systems also require more complex systems in order to work properly (pressurants, oxidizers, etc.).

Solar sails are becoming more understood as more and more missions employ them for their ability to apply small changes in velocity with relatively lightweight systems [37, 38]. These have the benefit of high ΔV potentials but have very little control authority over the asteroid and require that the asteroid be sun-side relative to the target orbit in order to work.

Other suggested solutions to the transfer problem have included ion Sheppard beams, enhanced Yarkovsky effect systems, and laser ablation systems. These are unique in that they have a minimal impact on the asteroid itself (gravity tractors are included here), as opposed to anything that tethers to the asteroid itself (propulsion systems and solar sails) or explicitly destructive options. Tethers can easily damage important parts of an asteroid or potentially reduce their valuable contents for mining, making these choices less desirable for both scientific and commercial approaches, but they offer the benefits of using well understood and flight-tested propulsive technologies.

Ion beams are projected onto an asteroid from some orbital standoff distance that slowly push the asteroid to a new orbit [39, 40]. The Yarkovsky effect is a force that acts on rotating bodies in space whereby one side is heating by the sun, rotates away from the sun, and the resulting emission of thermal photons carry enough momentum to slightly alter the path of the body. Some have proposed coating asteroids in a material that would enhance this effect [41]. Laser ablation systems work by focusing energy on certain parts of the asteroid, which are then heated and ablate from the surface, causing thrust [42]. These technologies are still in their preliminary stages of their development and have very low ΔV potentials, making them better suited for long term deflection campaigns than asteroid capture.

Nuclear standoff is another theoretical technology of interest to asteroid deflection [11]. The idea is to detonate a nuclear blast at some standoff distance from an asteroid. The blast superheats the surface particles of an asteroid, causing them to become a plasma and eject from the surface. This ejection results in a small ΔV. The amount of ΔV, on the order of centimeters per second, is enough to cause significant changes the asteroid's trajectory in a relatively short period of time with only a single mission, but it is not well suited to capture trajectories as it requires a different blast for every change in velocity. The physics of the blast are also not fully understood as no such thing has ever been attempted.

Kinetic impactors are simply satellites meant to ram into a body to disturb its course [44]. These are by far the simplest and cheapest technology to employ of those listed here, but their effectiveness is limited by the geometry of the asteroid's orbit with respect to Earth's. While this technology is very well suited for deflecting bodies in any safe direction, precisely impacting a target can require complicated intercepting trajectories and can be subject to single-point-failures. While some proposed kinetic impactor missions have decided to stop and survey a target before impacting it, the most potential ΔV would come from impacting it at full velocity from a different heliocentric orbit. If the impactor misses, it would have to wait several years before it could try to impact again depending on the asteroid's orbit. Nonetheless, for small transfers with few impulses, this seems like a feasible option.

Mass drivers are an extremely interesting technology that is closer to science-fiction than science at this point but would not be infeasible within the next 50 years. A mass driver is a drill/ejection system that attaches to an asteroid. The system drills into the body, collecting mass from it, and then drives the mass into space - hence the name. These theoretically have the highest ΔV capacity of any of the proposed technologies but no such system has ever been made on the scale required, let alone tested or used [20].

1.1.3 Mission Design

Thus far, only five missions have ever impacted or landed on small bodies in our solar system - Deep Impact, Hayabusa I, Hayabusa II, NEAR Shoemaker, and Rosetta/Philae. Deep Impact was the first mission to impact comet, ejecting an impactor from an orbiter which caused a crater to form. NEAR Shoemaker passed by the NEA Eros and orbited and landed on the asteroid 253 Mathilde. This was the first mission to soft-land on an asteroid [45]. The first Hayabusa mission was the first attempt to return an asteroid sample collected from the asteroid's surface to Earth, and the second Hayabusa mission is currently attempting a similar task. The Rosetta mission, which set the Philae lander on the comet 67P/Churyumov–Gerasimenko, was the first mission to soft-land on a comet [46]. While comets and asteroids are different, they are similar enough that this mission is still highly relevant for missions to asteroids. OSIRIS-Rex is a JPL mission currently being flown that is attempting to collect asteroid samples. It has been successful thus far (August 2020), and is planning to attempt full sample return soon. If it succeeds, it will add its name to this short list of spacecrafts to visit small bodies in the solar system.

There have also been some notable theoretical designs for asteroid capture missions [26, 27, 47, 48]. The most prominent of these is the NASA Asteroid Redirect Mission (ARM) which was in development until Dec. 2017 when the White House issued the White House Space Policy Directive 1 [49]. Also, of note is NASA's Double Asteroid Redirection Test (DART) Mission, which plans to be the first mission to test kinetic impactor technology for asteroid deflection. DART is part of joint effort between NASA and the ESA. The ESA is building the spacecraft for their Asteroid Impact Mission (AIM), which will fly with DART in a combined mission known as the Asteroid Impact Deflection Assessment (AIDA). There have also been a few independent studies for capture and deflection missions from JPL [11, 12, 27].

Other efforts have looked at the asteroid capture problem from a mission overview perspective, namely the works of Brophy [26, 47], Barbee et al. [50], and Gleaves et al. [51]. Barbee et al. completed a comprehensive survey of the most feasible NEA population, characterizing each by how easy they would be to reach and capture from a mission overview perspective. Gleaves et al. completed a multi-part overview of transfers to and capture around trans-Neptunian objects. While this is not strictly the same as asteroid capture, it has important implications for the early mission timeline where a spacecraft will have to reach and orbit around a NEA.

1.2 Contributions

All of the work thus far suffers from a few similar shortcomings: 1) All the work done on transfer optimization for asteroids thus far has focused on point-design, picking objects out of a catalogue of thousands with ideal characteristics and returning single optimal solutions for each. While this has merits for later in the mission design process and it gives a great overview of the possibilities of lower limits for transfer costs, this more esoteric look at transfer optimization shoehorns any potential mission designs into using the conditions specified in the problem. Real world considerations such as technology cost or availability, fluctuating flight times for transfers due to errors in insitu trajectory measurements, and the possibility of changing targets in relatively short timeframes requires that the results from transfer optimization be general enough that they inform a large breadth of different possible input parameters - no such study for asteroid capture optimization yet exists. 2) The direct effects of perturbations such as solar radiation pressure and n-body effects has not been studied for asteroid transfer to great length and no study of the optimized asteroid capture problem has studied the effects of non-conservative perturbations [23]. These are the largest interplanetary orbital perturbations and should be concretely understood in the context of asteroid transfer. While it is likely that these effects are small, their effects on the general shape of the trajectory optimization solution space has not yet been explicitly studied.

The contributions of this research are as follows:

1. Development of a generalized framework for optimizing asteroid capture trajectories on a large scale in order to expedite and simplify mission design and planning. Asteroid transfer optimization has previously been examined by other sources using indirect optimization methods and with specific asteroids in mind. The results found in these studies are valuable, but they do not provide a general framework from which to work. This research aims to provide that framework.

2. This work will examine optimal asteroid capture trajectories including solar radiation pressure and n-body perturbations. Thus far, the asteroid capture problem has been largely examined only with two-body dynamics or without inclusion of the other major interplanetary perturbations, SRP and n-body effects. This work will include those perturbations so as to get a concrete and explicit idea of their effects on asteroid transfer.

3. This work will also generalize the optimal asteroid capture problem with respect to thrust capability instead of with respect to a given technology. This system will also be setup such that the dynamics can vary greatly without affecting performance. By formulating the optimization problem in a specific way, the particularity of optimal solutions is bypassed; instead of only understanding optimal solutions for one asteroid, with one system of dynamics, and one particular technology, this research gives an overview of many such possibilities without tying the design of missions to specific inputs to the optimization.

4. Finally, this work will provide bounds or parameter ranges for inputs to asteroid capture mission design that can be used to assess the suitability of various technologies based on the optimal trajectory analysis, the chosen asteroid mass, the desired time-of-flight, and the various possible technologies a particular mission might be interested in using. This work will also make recommendations on choosing these parameters as well.

2. CHARACTERISTICS OF NEOS FOR POTENTIAL CAPTURE

The number of potential objects in the solar system that might be worth studying or capturing for either scientific or commercial purposes is far too vast to simply pick and choose at random. On top of technological considerations, there are very few asteroids that are near enough to Earth, are small enough, have orbits close enough to Earth's, and that have been observed well enough to concretely determine all of these characteristics. The total number of known near-Earth asteroids is about 22000 according the JPL Small-Body database. Only 850 of these objects have been observed well enough to estimate their diameter without making difficult assumptions, and, of those, only 140 of them have a diameter less than 250 meters. The numbers dwindle further once things like semimajor axis, eccentricity, and inclination are considered as well.

Of the Near-Earth Asteroids (NEAs), there are four basic orbital classifications: Atiras, Atens, Apollos, and Amors [52]. Atiras orbits are strictly inside Earth's orbit with both the aphelion (Q) and perihelion (q) being less than 0.983 AU, the approximate value of Earth's perihelion. Atens orbits have a semimajor axis less than one AU and cross Earth's orbit. Apollos have a semi-major axis greater than one AU and cross Earth's orbit (therefore q less than 1.017 AU, the aphelion of earth). Amors have orbits strictly outside the Earth's orbit.

It is not clear from these categorizations alone which will be the easiest to capture, though in general, Earth-crossing orbits seem to be the best candidates. As long as the orbital energy is close enough to Earth's and the asteroid is sufficiently small, any asteroid should be capturable with similar amounts of ΔV. Capturing into specific orbits can sometimes affect which regime the body needs to begin as well. For exam-

Table 2.1.. Orbital Groups of Near-Earth Asteroids

Group	**Perihelion**	**Semimajor Axis**	**Aphelion**	**Earth-Crossing**	**NEO Population %**
Atiras	-	a $<$ 1 AU	Q $<$ 0.983 AU	✗	0.2%
Atens	-	a $<$ 1 AU	Q $>$ 0.983 AU	✓	7.3%
Apollos	q $<$ 1.017 AU	a $>$ 1 AU	-	✓	49.7%
Amors	q $>$ 1.017 AU	a $>$ 1 AU	-	✗	42.2%

ple, non-permanent captures necessitate Earth-crossing orbits as initial conditions to achieve their extremely low transfer ΔV values (some have reported as low as $31\frac{m}{s}$ to redirect an asteroid into the Earth vicinity [31]).

Table 2.2.. Size Bins of Near-Earth Asteroids

Size Bin ($\varnothing$ in m)	**Approximate Number Observed**	**Estimated Total Number**
0 - 100	3000	1000000+
100 - 300	5200	13700
300 - 500	1100	2400
500 - 1000	1200	1500
1000+	910	980

Beyond the difficulties of the orbital transfer itself, only certain orbital regimes have been catalogued well enough to determine feasible targets. The Atens and Apollos regions have the largest number of well observed asteroids due to the fact that they can be easily observed from ground observations. While there are likely significant and interesting candidates in other regions, especially the Amors region, far fewer observations have been made for asteroids in these regimes.

The largest number of asteroids are smaller than 30m across at their widest point, with some estimates putting the total number of small NEAs at over 1 million. While they are the most abundant and the easiest to capture, these are also the most difficult asteroids to observe. Not only are small asteroids less bright, the variance in their surface features makes things such as density and rotation rate difficult to estimate from ground observations. There are some asteroids that have been observed to have characteristics within a feasible bound to make them targets for capture, but a lot is left to speculation. Knowing the rotation rate of the asteroid, for example, is required before any mission can take place because of the effect it has on the chosen transfer technology. An asteroid being pushed by a kinetic impactor would have fewer problems deflecting a fast-rotating body, but anything that needs to attach to the body might not be able to if the rotation rate is too high. As time goes on and the observations of NEAs becomes more complete, this problem will become less relevant.

2.1 Asteroid Classifications

Although there is much debate on which taxonomic system is most appropriate for asteroids, the most commonly used systems are the Thoren system, the SMASII system, and that correlating asteroid types to those of meteorites. The problem of agreement comes largely from the lack of highly detailed information about asteroids. Classifications beyond basic spectral measurements are few and far between, which would otherwise be useful for a range of scientific and engineering studies.

Nonetheless, the current classifications do provide some insight into the relevant characteristics of different asteroids.

The last consideration for NEA selection is the scientific relevance of the proposed target. At this point, so little is known about asteroids, that any target would provide significant scientific insight. The larger the asteroid, the more significant samples can be obtained, and the more likely the asteroid is to have unique characteristics, but any asteroid is worth collecting. Once asteroid capture and mining become more

Table 2.3.. Asteroid Spectral Classifications. Low, moderate, high, and very high albedo ranges are $0.0-0.15$, $0.15-0.25$, $0.25-0.35$, and $+0.35$ respectively.

Meteorite Type	Thoren Type	SMASII Type	Density ($\frac{g}{cm^3}$)	Albedo
C	B	B	1.38	moderate
	C	C, Cb, Ch, Cg, Chg		low
	D	D		low
	G	-		-
	P	X, Xc, Xe, Xk		low
	T	T		low
S	A	A	2.71	moderate
	E	X, Xc, Xe, Xk		very high
	K	K		moderate
	Q	Q		moderate
	R	R		moderate
	S	S, Sa, Sk, Sl, Sq, Sr		moderate
	V	V		moderate
M	M	X, Xc, Xe, Xk	5.32	varies
Other	-	-	2.0	moderate

commonplace ventures, it may become more desirable to find asteroids with rarer internal compositions, focusing on things such as Germanium and Iridium content for mining, or unusual density properties or chemical compositions.

2.2 Asteroid Selection Process

The asteroid selection process is two-fold. On one hand, the asteroid's chosen for analysis need to be reasonable targets for capture; they need to be relatively small, and they should be in orbits that are not too far from Earth. On the other, the point of this research is not to find a single perfect optimal transfer solution, but to look broadly at the solution space of many transfer types. This means that it is also desirable to pick asteroids with a reasonable variance in size and orbital characteristics. To deal with the diverging set of needs, the smallest asteroids with well defined characteristics are chosen, ones that are not unique either in mass or orbital characteristics are discarded, and transfers are solved starting from that set. As more solutions are found and the optimizer becomes more concretely understood, heavier asteroids are added to the selection and analysis pool to give a more general understanding of the transfer solution space.

JPL's Small Body Database gives a convenient listing of the currently observed Near-Earth objects, asteroids, and comets. The first round of selection limits the search by constraining the inclination to be less than 5 degrees, and diameter to be greater than 0 and less than 50. The diameter needs to be constrained in this counterintuitive way because there are a large number of asteroids that have not been observed well enough to estimate their diameter. In general, if asteroid's are small enough, the best way to estimate their size is by a logarithmic fit equation that correlates the asteroid's observed absolute magnitude, H, the visual magnitude an observer would record if the asteroid is placed 1 AU away, and 1 AU from the Sun and at a zero phase angle. Geometric albedo is the ratio of its actual brightness as seen from the light source (i.e. at zero phase angle) to that of an idealized flat, fully reflecting, diffusively scattering disk with the same cross-section [53]. Of these two characteristics, the absolute magnitude is much more frequently observed than the geometric albedo, but both are required in order to approximate the mass (of smaller bodies). The geometric albedo is difficult to guess and can have a large impact on the estimated mass. As such, those objects without a concrete estimation of both absolute magnitude and geometric albedo are left out of this initial analysis.

The initial candidates chosen are summarized in Table 2.4. The masses are estimated from the diameters of the objects via the tabulated correlation:

$$m \approx \frac{\pi abc\rho}{6} \tag{2.1}$$

where a, b, and c are the semimajor axes of the equivalent ellipsoid [54]. All the observations here give the diameter of the equivalent spheroid, so this equation simplifies to:

$$m \approx \frac{\pi d^3 \rho}{48} \tag{2.2}$$

where d is the diameter of the asteroid. For these calculations it also assumed that the density of the asteroids, ρ, is an average value of 2.0 $\frac{g}{cm^3}$ [54].

Asteroids that are considered too heavy for an initial analysis are discarded as are asteroids with redundancies in mass and orbital characteristics. Since the transfers from interplanetary space required both, this list remained longer. Transfers from Earth SOI to DROs, however, are only mass dependent as they all have the same initial conditions. This meant that there only needed to be a small set of chosen candidates. The chosen candidates for this analysis are shown in Table. 2.5.

Table 2.4.. Initial set of asteroids to choose from for trajectory analysis

Asteroid	Diameter (m)	Mass (kg)	Orbital Class	Semimajor Axis (AU)	Eccentricity	Inclination (deg)
2010 FD6	8	6.70e13	Apollo	1.447191593	0.435651257	0.458983426
2010 XB112	2.5	2.05e12	Apollo	1.028875864	0.1446215	1.321926423
2010 KV7	13	2.88e14	Apollo	1.214105986	0.218541731	0.31448546
2010 GH7	8	6.70e13	Apollo	1.401426337	0.300326726	3.53372036
2010 TN4	18	7.63e14	Apollo	1.724665885	0.434997457	3.029741156
2010 DL	19	8.98e14	Apollo	1.352697504	0.313792782	2.567788025
2010 FW9	24	1.81e15	Apollo	1.641598636	0.432591385	3.767056195
2010 YD	26	2.30e15	Apollo	2.041264173	0.538223404	0.438510919
2002 JR100	28	2.87e15	Atens	0.923729452	0.298742132	3.692301757
1998 KY26	30	3.53e15	Apollo	1.232902162	0.201841404	1.481034424
2010 FX9	30	3.53e15	Apollo	1.131420926	0.367061528	3.780780196
2010 HA	32	4.29e15	Atens	0.959831625	0.195902439	2.182787752
2010 JJ3	32	4.29e15	Apollo	2.2339863	0.578048291	2.393483205
2010 QG2	38	7.18e15	Apollo	1.673579209	0.517356794	4.697165543
2010 JW39	39	7.76e15	Apollo	1.637098683	0.390271222	3.00271953
2010 FE7	45	1.19e16	Apollo	1.951248316	0.552364068	1.552088805

Table 2.5.. Initial set of asteroids to choose from for trajectory analysis

Interplanetary Transfer Candidates						
Asteroid	Diameter (m)	Mass (kg)	Orbital Class	Semimajor Axis (AU)	Eccentricity	Inclination (deg)
2010 FD6	8	6.70e13	Apollo	1.447191593	0.435651257	0.458983426
2010 XB112	2.5	2.05e12	Apollo	1.028875864	0.1446215	1.321926423
2010 KV7	13	2.88e14	Apollo	1.214105986	0.218541731	0.31448546
2010 TN4	18	7.63e14	Apollo	1.724665885	0.434997457	3.029741156
2010 FW9	24	1.81e15	Apollo	1.641598636	0.432591385	3.767056195
2010 YD	26	2.30e15	Apollo	2.041264173	0.538223404	0.438510919
2002 JR100	28	2.87e15	Atens	0.923729452	0.298742132	3.692301757

DRO Transfer Candidates						
Asteroid	Diameter (m)	Mass (kg)	Orbital Class	Semimajor Axis (AU)	Eccentricity	Inclination (deg)
2010 FD6	8	6.70e13	Apollo	1.447191593	0.435651257	0.458983426
2010 DL	19	8.98e14	Apollo	1.352697504	0.313792782	2.567788025
2002 JR100	28	2.87e15	Atens	0.923729452	0.298742132	3.692301757

3. MATHEMATICAL MODELS

3.1 Trajectory Model

Figure 3.1 shows the trajectory model used for the optimization problem. This model is based on the methodology proposed by Sims and Flanagan [9] with some minor differences. The trajectory is divided into N segments and an impulsive burn is applied at nodes. If there are a sufficient number of nodes, the impulsive burns act as a good approximation of low thrust without the associated difficulties of using an excessive number of burns for low thrust or integrating a continuous thrust arc over the trajectory. This method requires that an initial state, X_i, and a final state, X_f, be specified. The initial state is propagated forward with impulses applied at nodes, and the final state is propagated backwards similarly. The only constraint is that the patch points, X_1 and X_2, have the same position and velocity to within a given tolerance.

In order to approximate low thrust, the ΔV applied at each node is bounded to be less than a prescribed ΔV_{max}, which is found by calculating the total accumulated thrust over the segment:

$$\Delta V_{max} = \frac{T_{max}}{m}\Delta t \tag{3.1}$$

where Δt represents the total transfer time divided by the total number of nodes, and m is the mass of the asteroid.

$$\Delta t = \frac{t_{transfer}}{N} \tag{3.2}$$

In this way, the impulse imposed at each node represents the total possible ΔV that would be imparted to the system had the thruster been burning for the entire segment. Cases that look at high thrust engines calculate the ΔV_{max} in the same way except

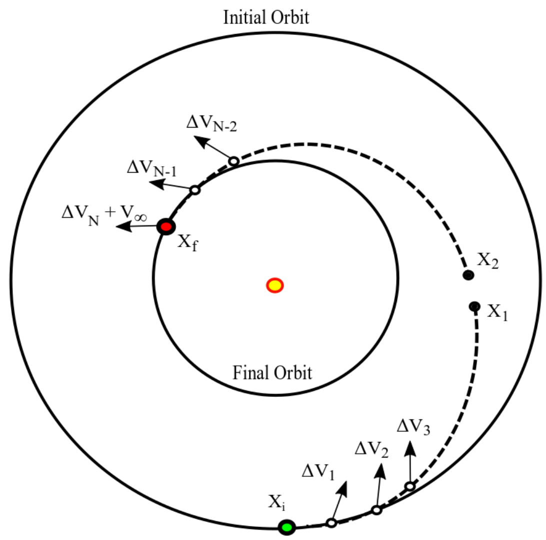

Figure 3.1.. Impulsive ΔV transcription based on Sims and Flanagan

Δt is calculated using the max burn time of the thruster instead of the time of the segment.

There are two major differences between the one used in this work and the one proposed by Sims and Flanagan. First, in this model, impulses are applied at the end of segments instead of the beginning. This is done because of the second major difference, the inclusion of an arrival V_∞. Since the idea is to put asteroids into capture orbits, the objects must arrive at Earth with a non-zero velocity difference depending on the target orbit. Since the arrival V_∞ can be functionally treated as its own ΔV vector, the final impulse is added to this vector to simplify the overall optimization. As such, the last impulse is allowed to be greater than the other impulses by a factor scaled to a commanded arrival V_∞ and the number of impulses remains N. The secondary effect of this is that impulses need to be applied at the end of the trajectory segments instead of in the middle. This proved to be an effective method and had no negative impact on the accuracy of the results.

3.1.1 Interplanetary Propagation

One of the goals of this research is the examination of the asteroid capture problem including major perturbations. The largest perturbations to the motion of an asteroid in interplanetary space are SRP and n-body gravitational effects so these are added to the propagation between nodes. However, since the problem becomes very non-linear once these perturbations are included, it is still necessary to utilize two-body orbit propagation solution to seed the higher-fidelity trajectory model. This served a double purpose of both seeding the more complex dynamical solutions and providing a baseline for solutions that could be found much quicker. The more complex motion required numeric integration, but two-body dynamics are solved using a Lambert solution for speed. It is also shown that the SRP perturbation could be included in a Lambert solver using a few assumptions.

If the state of the system is given as $X = \begin{bmatrix} x & y & z & v_x & v_y & v_z \end{bmatrix}^T = \begin{bmatrix} \vec{r} & \vec{v} \end{bmatrix}^T$, the equations of motion for an asteroid including gravity and SRP are:

$$\dot{X} = \begin{bmatrix} \vec{v} \\ \vec{a}_g + \vec{a}_{SRP} \end{bmatrix} = \begin{bmatrix} \vec{v} \\ -\frac{\mu}{r^3}\vec{r} + p_{SRP}\ (\frac{1AU}{r})^2\ C_r \frac{A_{sun}}{m}\ \hat{r} \end{bmatrix} \tag{3.3}$$

where p_{SRP} is the solar radiation pressure at 1 AU. The $(\frac{1AU}{r})^2$ term serves to scale this value to the distance the object is currently at relative to the sun. If the r^2 term in the denominator is pulled out and multiplied into the $\hat{r}$ term, then the acceleration can be rewritten as:

$$\vec{a} = -\frac{\mu}{r^3}\vec{r} + \frac{c_{srp}}{r^3}\vec{r} \tag{3.4}$$

where

$$c_{srp} = p_{SRP}\ (1AU)^2\ C_r \frac{A_{sun}}{m} \tag{3.5}$$

It is an assumption that the sun-facing area of the asteroid remains constant, but unless more is known in advance about the body, this is a good assumption in general. This also assumes that the body is always sun-lit which is a fine assumption for any propagation far from an occulting body. As such, the entire expression for the gravity and the effect of SRP can be combined into a single term where it is apparent that SRP acts purely as an anti-gravitational perturbation.

$$\vec{a} = (-\mu + c_{srp})\frac{\vec{r}}{r^3} \tag{3.6}$$

This simplification means that a propagation including SRP can be done using a Lambert solver with μ set to $\mu - c_{srp}$. This is key in seeding the more complex dynamical optimization with a good guess. The Lambert solution with SRP is orders of magnitude faster than a solution that requires integration but is closer to the full dynamics than the two-body solution.

The full set of equations of motion for the interplanetary body including SRP and n-body effects is:

$$\dot{X} = \begin{bmatrix} \vec{v} \\ \vec{a}_g + \vec{a}_{SRP} + \vec{a}_n \end{bmatrix} = \begin{bmatrix} \vec{v} \\ \frac{c_{srp}-\mu}{r^3}\ \vec{r}\ +\ \sum_{i=1}^{n} \mu_i(\frac{\vec{r}_i}{r_i^3} - \frac{\vec{r}_{sun\to i}}{r_{sun\to i}^3}) \end{bmatrix} \tag{3.7}$$

where $\vec{r}_i = \vec{r} - \vec{r}_{sun\to i}$ and $\vec{r}_{sun\to i}$ is the vector from the sun to the i^{th} gravitational body.

One of the largest challenges with incorporating complex dynamics into optimizers is not the complexity of the equations of motion, but the dramatic increase in computation time that highly accurate propagators add to the optimization. Since even very small iteration optimizations can run internal integrations thousands of times, reducing the computation time as much as possible is very important.

To reduce the computation time for the effect of SRP, the c_{srp} simplification allowes the perturbation to be treating as a scaling factor to the gravitational acceleration from the Sun, but n-body perturbations has no such simplification. In order to counteract the high computation time, two major assumptions are used for n-body computations. First, it is assumed that the only gravitational bodies with significant perturbations would be the Earth-Moon system, Jupiter, and Venus. Asteroids that are in capturable orbits are generally near Earth where the major n-body perturbations are from the Earth-Moon system (on the order of $10^{-4} - 10^{-6}\frac{km}{s^2}$ at 1 AU), Jupiter (10^{-8}), and Venus (10^{-8}). The effect of Saturn and Mars is another order of magnitude smaller than that of Jupiter and Venus in orbits near Earth. For asteroids farther into the main belt, this assumption might not be accurate, but since the Asteroids examined in this study are chosen specifically for their potential capturability, this assumption remains valid.

Second, it is assumed that the dynamics of the system can be accurately modeled if the positions of the extra gravitational bodies are only updated at a fixed time interval. This assumption is equivalent to an averaging of the n-body perturbation over a fixed timestep of the planet. Other work has shown how this averaging can also be modified to include the averaging over the timestep of the satellite [**?**], but this approximation is beyond the scope of this work. This assumption is made purely for the purpose of speeding up the integration without losing a significant amount of accuracy, while still including the effects of n-body perturbations. This assumption means that the planets do not need to be integrated alongside the asteroid and their positions can be passed into the integrator as constants beforehand. This can cause some inaccuracies if the timestep between each update is too large, but if it is too small, the data passed into the integrator isbe enormous and any time saved from recalculating the positions of the planets is eliminated. A timestep of 1 day is a sufficient middle ground for this analysis. This is a less accurate assumption for the innermost planets, and for Earth's Moon, this is potentially problematic, however, since the perturbation from the Moon's gravity is very small, the Earth's gravity overpowering it, the inaccuracy of the 1 day timestep is diminished for the Earth-Moon system in general. Earth, Jupiter, and Venus are in large enough orbits that the timestep of 1 day is a relatively small change in their position.

3.1.2 Earth-Moon System Propagation

Propagation in the Earth-Moon system is not as straightforward as interplanetary propagation due to the large effect of the Moon's gravity. The simplest form of

Earth-Moon dynamics is given by the solution to the Circular Restricted Three Body Problem (CR3BP) as follows:

$$\dot{X} = \begin{bmatrix} \vec{v} \\ \vec{a} \end{bmatrix} = \begin{bmatrix} \dot{x} \\ \dot{y} \\ \dot{z} \\ 2\dot{y} + x - \frac{(1-\mu^*)(x+\mu^*)}{r_{13}^3} - \frac{\mu^*(x-1+\mu^*)}{r_{23}^3} \\ -2\dot{x} + y - \frac{(1-\mu^*)y}{r_{13}^3} - \frac{\mu^* y}{r_{23}^3} \\ -\frac{(1-\mu^*)z}{r_{13}^3} - \frac{\mu^* z}{r_{23}^3} \end{bmatrix} \tag{3.8}$$

where $r_{13} = \sqrt{(x+\mu^*)^2 + y^2 + z^2}$ and $r_{23} = \sqrt{(x-1+\mu^*)^2 + y^2 + z^2}$, and μ^* is the nondimensional mass parameter ($\mu^* = \frac{m_{Moon}}{m_{Moon}+m_{Earth}}$). The vector components are in the Earth-Moon rotating frame relative to the Earth-Moon barycenter and scaled to the masses of the three-body system, the distance between the Earth and the Moon, and the Moon's synodic period. See Vallado [**?**] for details. These dynamics give a baseline for results with more complex dynamics as they are more thoroughly studied and produce results much faster than dynamics that include n body effects. Unfortunately, there exists no method as quick as Lambert solvers for multi-body system dynamics. but, to include the effects of solar gravity, the Bicircular Restricted Four Body Problem (BCR4BP) is used. The equations of motion are given as:

$$\dot{X} = \begin{bmatrix} \dot{x} \\ \dot{y} \\ \dot{z} \\ 2\dot{y} + x - \frac{(1-\mu^*)(x+\mu^*)}{r_{13}^3} - \frac{\mu^*(x-1+\mu^*)}{r_{23}^3} - \frac{m_s(x-x_s)}{r_{s3}^3} - \frac{m_s}{a_s}x_s \\ -2\dot{x} + y - \frac{(1-\mu^*)y}{r_{13}^3} - \frac{\mu^* y}{r_{23}^3} - \frac{m_s(y-y_s)}{r_{s3}^3} - \frac{m_s}{a_s}y_s \\ -\frac{(1-\mu^*)z}{r_{13}^3} - \frac{\mu^* z}{r_{23}^3} - \frac{m_s(z-z_s)}{r_{s3}^3} - \frac{m_s}{a_s}z_s \end{bmatrix} \tag{3.9}$$

where m_s is the system the Sun scaled to the system, $\vec{r}_{s3} = \vec{r} - \vec{r}_s$, and a_s is the distance from the major body (Earth) to the Sun in canonical units. The Sun is assumed to be in constant circular motion relative to the Earth-Moon frame so its position can be described solely in terms of its rotational position relative to the synodic frame, θ_s. Since the rotational rate is assumed constant, $\theta_s = \omega_s t$. For the Earth-Moon system, $\omega_s = -0.9253\ \frac{rad}{TU}$ [56]. With this, the position of the Sun can be calculated very efficiently.

$$\vec{r}_s = \begin{bmatrix} x_s \\ y_s \\ z_s \end{bmatrix} = a_s \begin{bmatrix} \cos(\theta_s - \Omega)\cos(\Omega) - \sin(\theta_s - \Omega)\sin(\Omega)\cos(i) \\ \cos(\theta_s - \Omega)\sin(\Omega) + \sin(\theta_s - \Omega)\cos(\Omega)\cos(i) \\ \sin(\theta_s - \Omega)\sin(i) \end{bmatrix} \tag{3.10}$$

where Ω and i are the longitude of the descending node and the inclination of the Sun in the Earth-Moon frame, respectively. See Boudad [56] for more details.

To include the effects of SRP and keep the integration efficient, a similar logic is used here as in the interplanetary propagator. It is assumed that the body is in constant sunlight and the sun-facing area remains constant, meaning that SRP can be modeled as a weakening of the direct gravitational effect of the Sun. Since the gravity of the Sun is not given in terms of the gravitational parameter in these equations of motion, the mass of the Sun is scaled by the ratio between c_{srp}, the interplanetary solar pressure constant described earlier, and μ_s, the gravitational parameter, i.e. $m_s^* = \frac{m_s(\mu_s - c_{srp})}{\mu_s}$. Only the first Solar mass term is scaled because the second term represents the indirect gravitational effect, the perturbation from the pull the Sun has on the Earth and would not be directly impacted by outward radial effects of SRP in this way. This simplification allowed the inclusion of SRP without any additional terms beyond the BCR4BP.

$$\dot{X} = \begin{bmatrix} \dot{x} \\ \dot{y} \\ \dot{z} \\ 2\dot{y} + x - \frac{(1-\mu^*)(x+\mu^*)}{r_{13}^3} - \frac{\mu^*(x-1+\mu^*)}{r_{23}^3} - \frac{m_s^*(x-x_s)}{r_{s3}^3} - \frac{m_s}{a_s}x_s \\ -2\dot{x} + y - \frac{(1-\mu^*)y}{r_{13}^3} - \frac{\mu^* y}{r_{23}^3} - \frac{m_s^*(y-y_s)}{r_{s3}^3} - \frac{m_s}{a_s}y_s \\ -\frac{(1-\mu^*)z}{r_{13}^3} - \frac{\mu^* z}{r_{23}^3} - \frac{m_s^*(z-z_s)}{r_{s3}^3} - \frac{m_s}{a_s}z_s \end{bmatrix} \tag{3.11}$$

The inclusion of additional n-body perturbations is similar to the inclusion of the Sun's effect. The direct and indirect effects of the additional bodies take a similar form, with fewer simplifications.

$$\dot{X} = \begin{bmatrix} \dot{x} \\ \dot{y} \\ \dot{z} \\ a_{xBC4BP} - \sum_{i=1}^{N} m_i(\frac{x-x_i}{r_{i3}^3} - \frac{x_i}{r_i^3}) \\ a_{yBC4BP} - \sum_{i=1}^{N} m_i(\frac{y-y_i}{r_{i3}^3} - \frac{y_i}{r_i^3}) \\ a_{zBC4BP} - \sum_{i=1}^{N} m_i(\frac{z-z_i}{r_{i3}^3} - \frac{z_i}{r_i^3}) \end{bmatrix} \tag{3.12}$$

Here the mass of the i^{th} body can be used in place of its gravitational parameter because the units are scaled to the Earth-Moon system, much in the same way that the gravitational effects of the Sun in the BCR4BP are given only in terms of the Sun's mass.

As with the interplanetary propagation, this perturbed bi-circular four body model incorporates the n-body effects under the assumption that the positions of the planets only needed to be updated once a day. Since the bicircular model already includes the Earth, Sun, and Moon directly and continuously, this 1-day timestep only applies to the perturbation caused by Jupiter and Venus and thus remains a good assumption. The inaccuracies of this assumption are further reduced by the proximity that the asteroid has to the Earth and Moon.

3.2 Optimization Methodology

In general, there are two types of optimization methods to consider - indirect optimization, which formulates the problem in terms of the necessary and sufficient conditions for optimality and then solves for the parameters that enforce those conditions, and direct optimization, which formulates the problem explicitly in terms of the input parameters of the system. Neither is better in general, and each has their drawbacks. Indirect optimization requires the explicit formulations of the problems gradients, as well as other non-trivial equations, but the results can be very accurate and are useful when the required equations are not too unwieldly. Direct methods are far simpler to setup and can solve without very good initial guesses, but they can be less accurate. They also tend to create good, but non-optimal (locally optimal) solutions since no conditions of optimality are given as constraints to the problem [**?**, 8].

Many different methods are tried for this problem ([6, 57, 58, 103]) before settling on a direct method based on the impulsive ΔV transcription method described by Sims and Flanagan [9, 59]. The generality and simplicity of the setup is not only effective, but efficient as well, finding results on timescales of the same order of magnitude as MALTO when run using Lambert arcs. However, since this work looks at complex dynamical systems, creating an initial guess requires more sophistication than using a Lambert arc and perturbing it based on the system's dyanmics. The local optimizer alone is not effective enough to find solutions without a good first guess in cases where the dynamics are too complex. To bypass this difficulty, and to construct good initial guesses for seeding the local optimizer, a global optimizer provides the most consistent and effective starting point for finding good solutions and guaranteeing consistent convergence.

3.2.1 Problem Formulation

Regardless of the specifics of the transfer problem, the fundamentals of the problem statement is the same. An asteroid begins in some initial orbit, with a fixed initial state fed into the optimizer, and with some target state (meaning the final state is a fixed input into the optimizer as well). Then some transfer is simulated via a finite number of impulsive nodes to transition to a near-Earth target orbit by propagating the initial state forward in time and the final state backward in time with impulsive burns being applied at each node (except the first node as the thruster needs to "accumulate thrust" to more accurately mimic a continuous low thrust profile). These forward and backward propagations meet at a central patch point that is constrained to be equal within a given tolerance. The tolerance for both the position and velocity of the states are set to the same value. Even though this means that the tolerance would be a different relative magnitude for the position and velocity, convergence is much more consistent when the same tolerance is used for both. Other than the bounds on the control vector, the only constraint is that the patch points, X_1 and X_2 are equal.

$$\vec{c} = X_1 - X_2 \tag{3.13}$$

The impulses applied at each of the N nodes are expressed in terms of three parameters: the relative magnitude of the thrust, and the two spherical angles corresponding to the direction of the thrust.

$$\Delta\vec{V_i} = \Delta V_{max}\ k_i \left[\cos(\alpha_i)\cos(\beta_i) \quad \sin(\alpha_i)\cos(\beta_i) \quad sin(\beta_i)\right] \tag{3.14}$$

The control thrust magnitude, k_i, is bounded between 0 and 1. The spherical angles, α and β, are bounded between 0 and 2π, and $-\frac{\pi}{2}$ and $\frac{\pi}{2}$ respectively. Here, 'i' represents the i^{th} burn. For simplicity, the time of flight of the problem is fixed as an input to the problem and then varied to give a family of solutions. This meant that all of the free variables of the optimization are given by the $3N$ components of the ΔV vector, $\vec{k}$, $\vec{\alpha}$, and $\vec{\beta}$.

The minimum ΔV transfer is equivalent to the minimum control vector, so the cost function is written as

$$J = \sum_{i=1}^{N} k_i \tag{3.15}$$

This formulation is also applied almost identically to the transfers in the Earth-Moon system, the only difference being the dynamics. In essence, this formulation boils down to three inputs - the initial state, the final state, and the time of flight - and one constraint.

This is a simplistic problem formulation when compared to a lot of modern optimizations, but the way that each of the pieces in the optimization are defined greatly impacts the way the optimizer must be setup and the potential success of the optimizer. Since the idea is to create a catalogue of solutions, the optimizer needs to be fast, reliable, and generic. Too much focus on satisfying difficult properties that guarantee global optima might produce slightly better answers but doing so also makes solutions more difficult to find, and risks making the optimizer extremely sensitive to inputs or only viable for a single set of inputs or dynamics.

3.2.2 Global Optimization

The global optimization is arguably the most important part of the optimizer architecture since it is used as the first guess at more accurate solutions and thus determines the quality of the solutions as a whole. Local optimizers are generally faster and better at finding precise solutions in local minima, but they require good first guesses in order to converge. Global optimizers are generally much slower but can search a larger range of the solution space and can often function without a good initial guess or without an initial guess at all. By feeding a lower fidelity solution from a global optimizer into a local optimizer, the benefits of both types of optimizers are utilized.

The architecture of the optimizer is twofold. First a global optimizer searches the solution space for viable trajectories with a relaxed constraint tolerance and is allowed to run for a fair amount of time to increase the likelihood of finding global solutions. These solutions are then fed into a local optimizer that can more easily converge on a solution with a much tighter constraint tolerance. Thisis much more effective than just using a global or a local optimizer on its own. Problems with simple dynamics, such as lambert arcs, can effectively utilize only a local optimizer with an initial guess based on analytic models (much like MALTO), but the inclusion of n-body dynamics perturbed the solutions enough that a local optimizer alone often fail to converge consistently. Conversely, using only a global optimizer is effective for all problems, but takes much longer and often has difficulties converging when constraints are too tight. The generality of the hybrid approach makes it possible to use the optimizer for all forms of the problem examined in this thesis, regardless of dynamics, the initial or final conditions, the thruster properties, the asteroid properties, or the constraint tolerance.

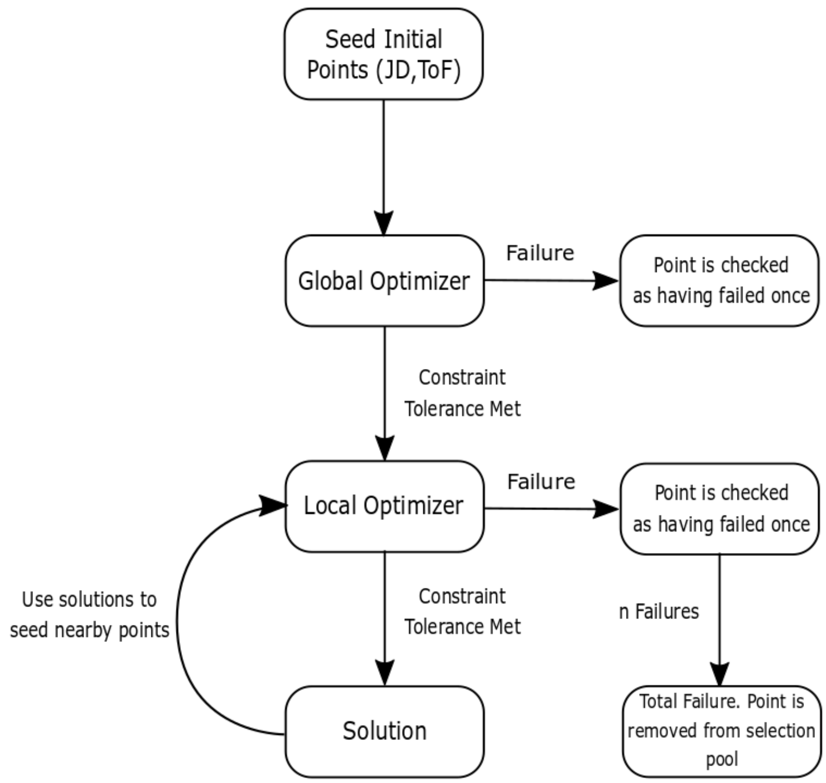

Figure 3.2.. Optimizer Architecture Overview

There are numerous types of global optimizers that are effective for a large range of problems and many are tried for this problem. Types of global optimizers tested include simulated annealing, direct searches, differential evolution, and genetic algorithms. The No Free Lunch Theorem shows that no optimization algorithm outperforms any other when averaged over a large set of problems [60] so there is no way to decide from the outset which method would be the most effective for this problem. A large subset of cases is run to test for convergence rates, computational speeds, and the generality of the setup for each the different methods. In the end, the genetic algorithm hasthe best overall properties this problem. Though it is slower than most other methods, the genetic algorithm is the most consistent for a large range of initial and final conditions and between disparaged sets of dynamics. On top of that, a genetic algorithm requires no initial guess which is essential for transfers in the Earth-Moon system where transfers are complex and guessing near-optimal transfers analytically is difficult.

Specifically, MATLAB's global optimization toolbox genetic algorithm ga is employed with a population size of 250. Though in general, it is recommended that genetic algorithms have a population sized roughly according to:

$$N_{pop} \approx 4 * \sum bits \tag{3.16}$$

where the bits are the total number of bits assigned to your free variables. For this work, the quality of the results does not improve past a population size of 250. For comparison, a transfer with 10 burns would have 30 free variables, and a minimum of 2 bits per variable. This would have a population size of 240. A lower population size tends to cause the global optimizer to find local optima that the local optimizer would try to move away from, actually producing local solutions with worse results than the initial global solution. A higher population size dramatically increased the runtime without increasing the quality of the results for a majority of cases. As will be discussed in further detail in the results section, there are cases where this small population caused unexpected irregularities in the solutions but these abnormalities neither detracted from the results related to the primary focus of this work nor do they hinder the progression of this research in general. Any issues from the low population size are meant to be captured by the solutions from the local optimizer.

3.2.3 Local Optimization

The overall optimization architecture has a twofold structure, the initial global optimizer creates a general solution and the local optimizer then uses this initial global solution and corrects it to a local minimum. The local optimizer does not need to have the robustness and general power of the global optimizer, but it does need to converge on optima consistently and quickly. The local optimizer also has to be fast and accurate in order to maximize its efficiency in the overall structure and to compensate for the large computation times of the genetic algorithm.

A number of different methods are tried for the local optimizer as well, including interior point methods, active set methods, grading projection methods, and numerous quadratic programming methods.The most effective optimizer for this problem is an SQP method, specifically MATLAB's fmincon is used. Though handwritten optimizers tend to be faster than the built-in optimizers, MATLAB's function is more robust to the point that its benefits outweigh the runtime cost.

The local solutions also act as a sort of starting point while searching for a large range of solutions in the date grid (the date grid is similar to those used in pork chop plots and bacon plots). Instead of finding a global solution for every single point, it is much quicker to use nearby local solutions that are already converged upon as an initial condition to seed other local optimizations for unsolved points nearby in the date grid. In this way, the global optimizer seeds the entirety of the solution space at a few select points, and the local optimizer finds all of the solutions therefrom. This combination maximizes the benefits of both types of optimizers. The global optimizer finds global minima in the solution space and the local optimizer uses those as a jumping-off point to converge upon more exact solutions. This is essential since the genetic algorithm is very slow in comparison, and it helps to maximize the efficiency of the overall architecture by utilizing the local optimizer as much as possible.

The second benefit to this architecture is the simplicity of the cost and constraints relative to both optimizers. Though many different cases are tested, the most effective way to get good solutions from both optimizers used in tandem is to give them the same cost function and constraints with different tolerances. No other inputs are changed between each of these optimizers. It is possible that there is a more efficient way to combine these algorithms, but these tests are time expensive and are considered outside the scope of this work. Some other works have combined hybrid architectures in more clever ways [?,5,8,61], but it is difficult to conclude whether or not the overall architecture of this problem could be improved by these methods.

3.3 Seeding and Searching Algorithms

The way that the solution space is seeded and searched is one of the most difficult and important parts of this problem. The hope is that simplifying the optimization problem enough by fixing the time-of-flight in each optimization, and by reducing the constraints and the number of free variables is much as possible, the problem can be solved quickly enough that it can be solved for a large range of points in a relatively small amount of time. By doing this instead of trying to find time optimal solutions, a large range of solutions can be found with a various number of initial conditions (i.e. starting dates and time-of-flight's) that can then be used to determine the best solution and the overall trends of the solution space. The global optimizer is far too time expensive to use on every single point in the solution space, but it is also too valuable to be used only once. The global optimizer has to be used enough that the range of solutions are still likely to be global minima or at least near global minima, but it cannot be used so much that it would be a large detriment to the run time. Determining how and where the global optimizer can run inside a range of initial dates and times of flight is what will be referred to as the seeding algorithm. How these initial solutions then spread through the rest of the solution space and initialized other local optimizations will be referred to as the searching algorithm.

The seeding and searching algorithms are coupled with respect to the success of the solutions. Fixing one searching algorithm that is sub-optimal and then testing a range of different possible seeding algorithms can yield results that might have been different than choosing a different searching algorithm and running the same tests. Because of this difficulty and because of the inherent problems with quantifying the efficacy of each of these algorithms without an intuitive or precise way of differentiating them, the results shown here are not found in a way consistent with a rigorous testing methodology. For each successive iteration of testing, the search or seeding method is modified until it is improved upon. A summary of these methods is necessary for this work, and a comprehensive and rigorous testing of these methods will be necessary for future works.

The comparison of methods shown here is given chronologically. One methodology is tested and then progressively modified in order to produce better results. All of the following results are run for the same Asteroid, 2010 FD6, with starting dates that range from January 2030 to January 2035, and times of flight ranging from 250 days to 1200 days. The maneuvers use a moderate thrust profile (100 N of equivalent continuous thrust) and 40 impulsive nodes. For the sake of consistency, all of the graphs are given the same coloring scheme relative to the results (i.e. blue is low ΔV and red is high), but the color bar is purposefully omitted as not to distract from the purpose of this section. The purpose of this section is to display how seeding and searching algorithms affect the behavior of the results, not the specifics of the results themselves. Those are given with the relevant discussion in the Trajectory Analysis chapter. Regardless, the colorbars maintain a consistent range between tests where red represents high-cost solutions, and blue represents low-cost solutions.

The first method tried is employed in a number of different optimization schemes. A point in the middle of the date and time of flight range is selected as an initial point for the global optimizer to run. That global optimization result is then used as the initial condition for the local optimizer that same first point. When that solution is found, the surrounding points in the grid are then initialized with that first solution and so on. So, in this instance, there is one seed (one run of the global optimizer), and the search extends from that point linearly. Nearby points are only allowed to use solutions that are adjacent horizontally or vertically from an already found solution point, hence a linear search.

This method has been shown to work well in JPL's transfer tool MATLO [4], but it is ineffective for the problems examined in this work. As shown in Figure 3.3, this method tends to find high cost solutions and then continuously propagate those bad solutions horizontally or vertically. Though some solutions do appear to be good solutions, the number of bad solutions is overwhelming. The results should have clear patterns that smoothly transfer from one type of result to another, where it is evident instead that there are certain valleys of low-cost solutions that are being covered up by poor solutions. Transfers with a small difference in epoch or time of flight (or both) should be almost identical in shape and transfer cost with a few exceptions. Having a large number of dramatic jumps from high to low cost solutions is a strong indication that the solution is incorrect or non-optimal.

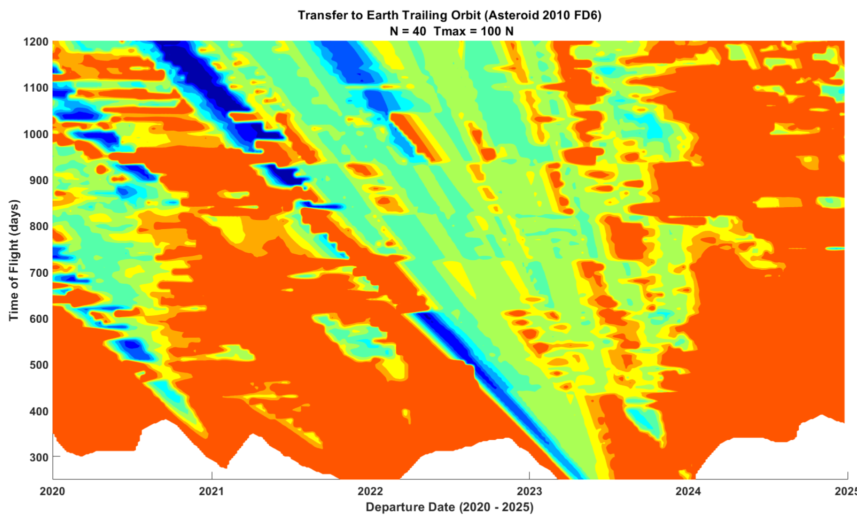

Figure 3.3.. One seed, one solution, and a linear search

The next method runs a single initial point as before, but searching from that point radially instead of linearly, the only difference being that diagonally adjacent points are allowed to be used as initial conditions as well as vertically and horizontally adjacent ones. This change has dramatic effects on the results as shown in Figure 3.4. Now the single valley of local minimum solutions that was being partially covered up with the linear search is clearly shown, though there are still apparent issues as you get farther away from the initial seeding point. Similar issues as in the first case start

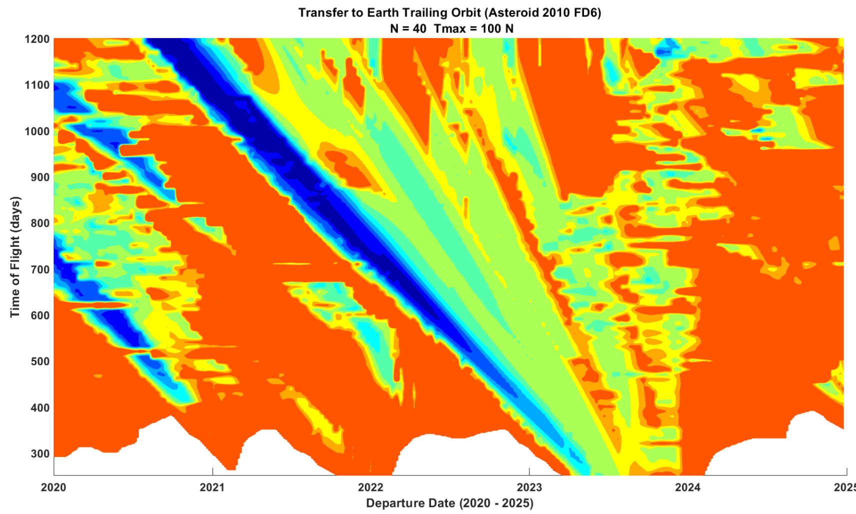

Figure 3.4.. One seed, one solution, and a radial search

appearing the farther away points are from that initial seed. Again, bad answers will eventually start to propagate horizontally, vertically, and now, diagonally through the date grid.

In order to eliminate this tendency to hold onto bad solutions, multiple seeds are run and then the best solution among them is used. If the quality of the initial seed's solution is high enough, it is possible that the poorer solutions will show up less, mitigating this issue. The results of this method are shown in Figure 3.5.

Since these differences are due to where the initial seed is placed, it is assumed that a better solution could be found if all of the initial seeds are used as starting points. This way, any advantages that are found from starting at any one point could be utilized without having to worry if the solution used as the initial seed is better or worse than any of the others. If bad solutions only start to propagate through after a certain distance in either epoch or time of flight, adding multiple seeds should functionally reduce that distance and help mitigate this problem. Figure 3.6 shows a run where 25 initial seeds are used, and the search spread out from every single one of those initial seeds radially. The quality of the results is now evidently dependent

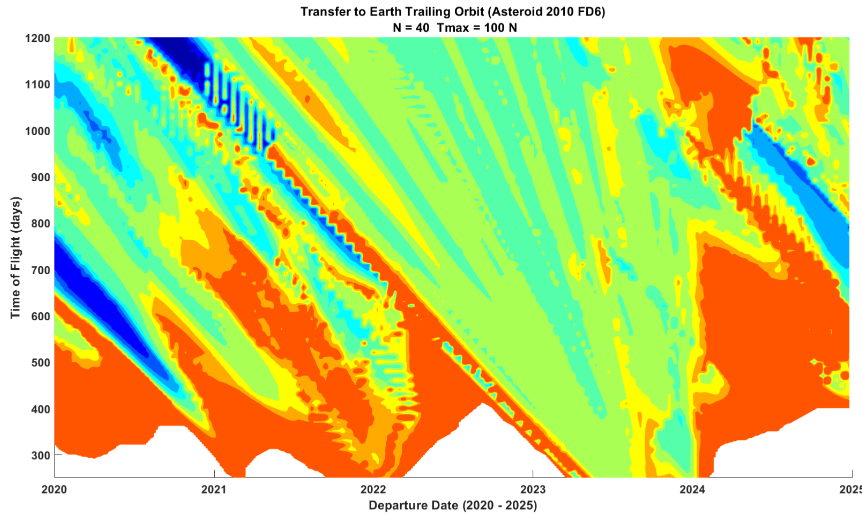

Figure 3.5.. Many seeds, one solution, and a radial search

on the quality of the solutions of the initial seeds. In some cases, the initial solutions are very good and the sections of solutions near the high-quality seeds turn out quite well but in others, the initial solutions are much worse and cause nearby solutions to fail as well. These results show a few notable behaviors. The most obvious is the

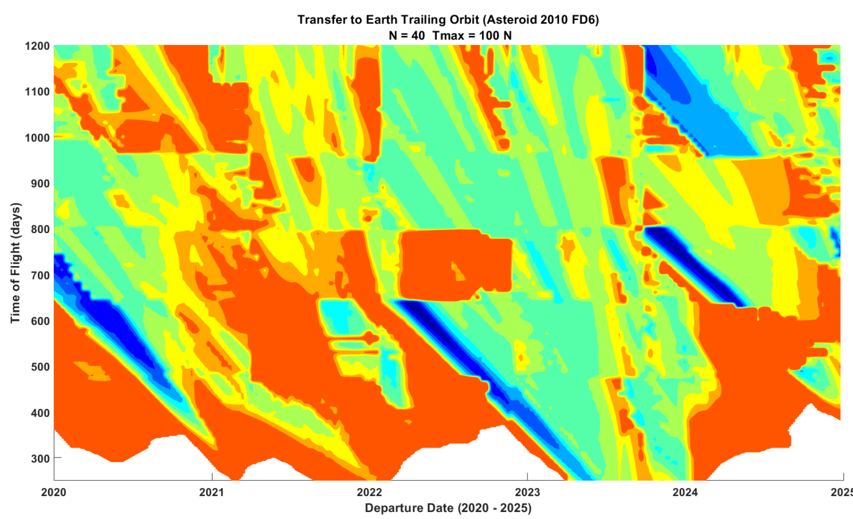

Figure 3.6.. Many seeds, many solutions, and a radial search

sectioning of the results. Most of the found solutions match the quality of the closest seed, with little overlap between seeds. Some of the solutions with lower times of flight manage to show more natural trends, but most of the seeds create non-optimal solutions that the nearby local optimizers use without much change. This creates the shown pockets of solutions, where bad solutions do not propagate through the entire solutions space, but they do spread locally.

Two things are attempted to correct these issues. First, the number of populations in the genetic algorithm is increased to 250 from 100. This improved the quality of the solutions significantly. Increasing it any further does produce higher quality results in these tests. The other major change is to switch from a radial search to a search that, instead of using adjacent points as initial conditions, used points that are both nearby to the point in question and low in ΔV cost. What this means is that each unsolved point searched the entirety of already found results and used the one that was both closest and lowest in delta V as an initial condition. These changes create the biggest improvement overall between any of the different runs. As shown in Figure 3.7, there are now distinct lines or valleys of low ΔV solutions that are showing up inconsistently or not at all when using previous methods. There are still clearly areas that need improvement, however. Bad solutions still seem to leak over valleys of good solutions and bad solutions seem to pepper themselves throughout areas where it seems that there should be lower cost solutions.

After a series of testing, it is discovered that the searching algorithm is allowed too much freedom in exploring the already found solutions. In some cases, new points are initialized with solutions that are very far away in either date or time-of-flight by nature of the way that the searching algorithm is set up. To correct this issue, the searching algorithm is switched to a range limited one. Instead of being allowed to search all found solutions, each new point is only allowed to search solutions a certain distance away from itself. This range is arbitrary, but each time a solution failed, instead of simply taking it out of the pool of candidates, it is flagged and then re-run with a smaller allowed search range. Only after a certain number of failures,

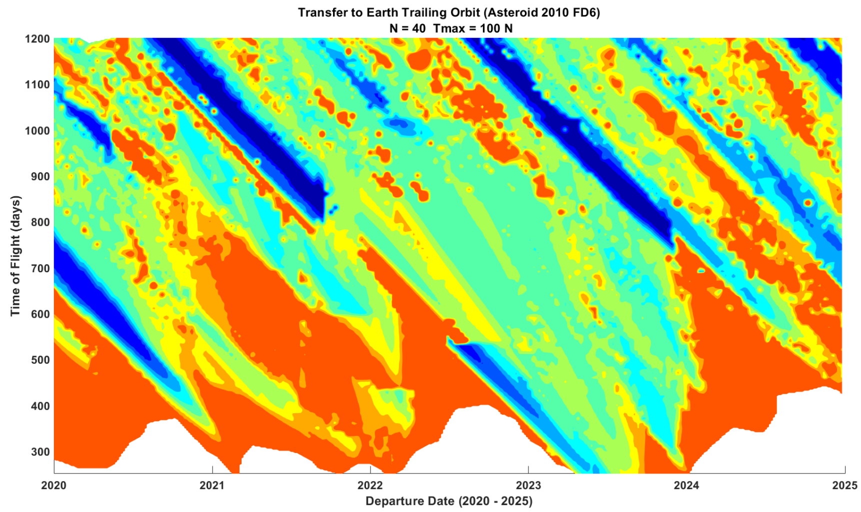

Figure 3.7.. Many seeds, many solutions, and a local minimum search

4 is used as the upper limit, is the point be taken out of the searching space and convergence is considered failed. The results for this method are shown in Figure 3.8. Now the results show much more distinct trends of both good and bad solutions.

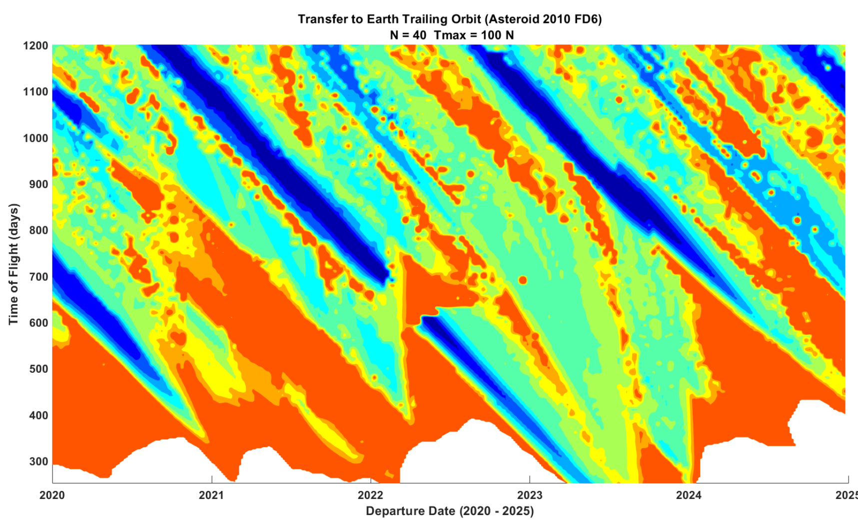

Figure 3.8.. Many seeds, many solutions, and a range-limited local minimum search

Still, there are areas in which bad solutions overlap good ones and good ones do not show consistent trends, so some improvement is still needed.

The next method tested – and the thing that likely carries the most potential in general for a searching algorithm – is a cost-based search. Each solution is initialized using a weighted combination of both of the ΔV cost of the initializing solution and its distance from the new point in the date grid. It would be possible to create cost functions based on a wide range of criteria such as arrival epoch, number of burns, the maximum magnitude of individual burns, etc., but this work only examines cost functions that combined the cost of the initializing solution and its distance in the date grid.

The results shown in Fig. 3.9 display the best results from this methodology. There are significant improvements here over the previous cases. There are distinct valleys that extend fully through the date grid and are not overlapped significantly by poorer solutions. There are not any large striations of poor solutions and the optimizer does not cling to a single solution in any given region. The largest issue with this method is that poor solutions are sprinkled intermittently throughout the tested date range. These poor solutions seem to occur irrespective of location or initial seed, and they occur in places where there should be lower cost solutions.

Almost no modification of the cost function seems to have any notable impact on this behavior, with most cost functions producing results much worse than the one shown. Though it is not clear that this method is bad in general, it is difficult to get working to the required level of accuracy. A much simpler solution is found in testing wherein most of the complexities of the searching algorithm cost function are ignored in favor of a searching algorithm that used the lowest ΔV solution within a given range. This is functionally a cost-based search where the weighting of the distance to the initializing solution is set to zero. The results are shown in Figure 3.10. The results are good– with clear indications of valleys of low ΔV solutions, with little to no overlapping of poor solutions, and with good intermediate solutions between the valleys of relative minima – but far more testing is done to improve these results than

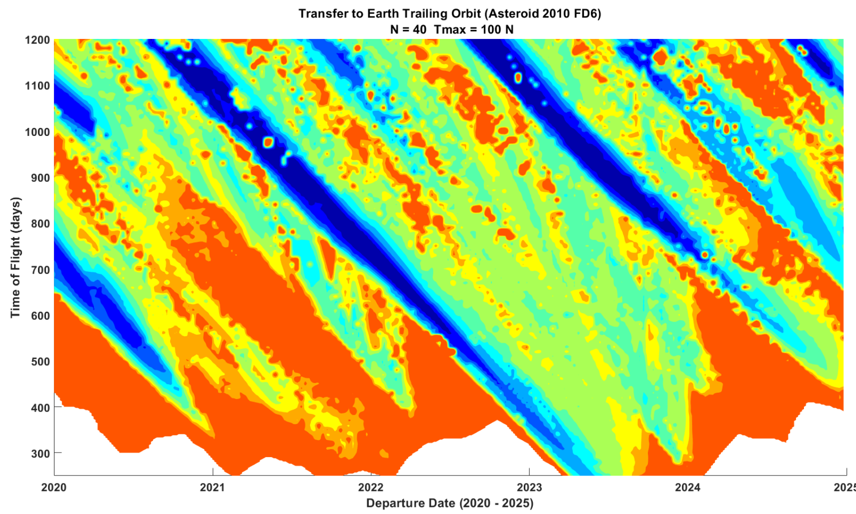

Figure 3.9.. Many seeds, many solutions, and a cost-function based search

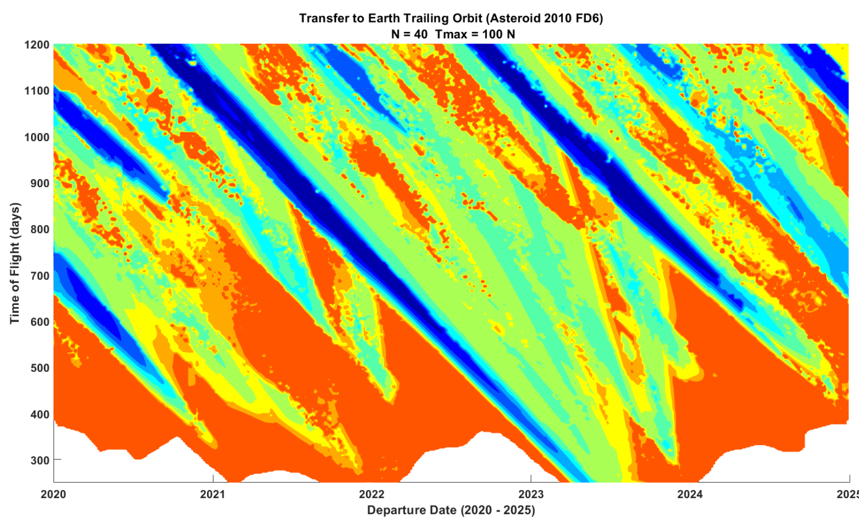

Figure 3.10.. Many seeds, many solutions, and a decreasing-range-limited local minimum search

is worth summarizing here. The results are improved upon further by playing with the various parameters in the searching algorithm. Specifically, the range of allowable solutions and how that range decreased each time a solution failed to converge at a given point are the most important parameters for this particular searching algorithm.

In the end, the range of selectable solutions to use as initial guess for new points began at one fourth of the total solution space. For each failed iteration at that point, the range is decreased by a factor of two, with the minimum possible range of being 1/16 the solution space. If the optimizer could not use a solution within that range to solve for the transfer at the given date and time-of-flight, the range is restricted to adjacent points only and it is tried once more. If it fails to converge with adjacent solutions, it is considered a failed point and is no longer tested.

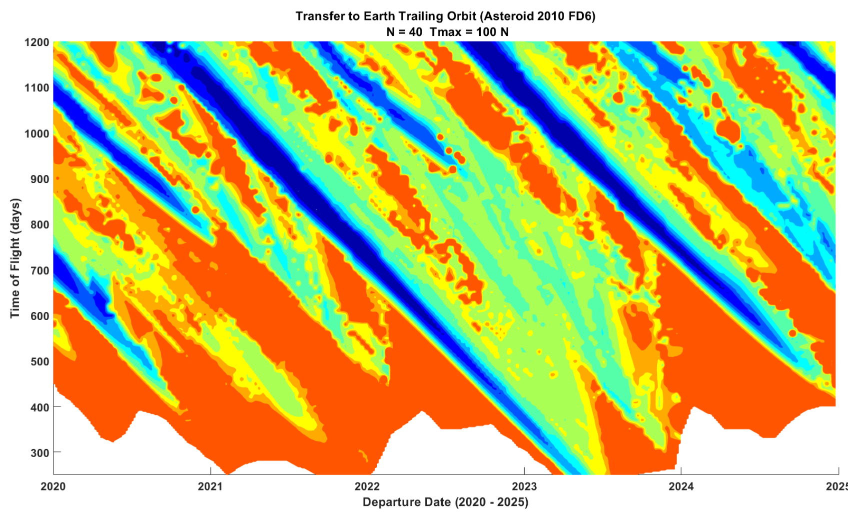

Figure 3.11.. Many seeds, many solutions, and a refined decreasing-range-limited local minimum search

This process can still be improved. Both the way the solution space is seeded with initial solutions found with the global optimizer, and the searching algorithms by which the optimizer decides how to move through the solution space and use found solutions to initialize others, are not perfected yet. A very detailed study would be required in order to fully understand the effects that this has on finding solutions of this type, but for the sake of this work, the methods displayed here are good enough at finding any major trends for the optimization of these transfers. A more concrete and detailed examination of how and where seeds are placed in the solution space and how solutions are then propagated through the remaining unsolved points should be examined in future work.

3.4 Capture Orbit Characteristics

For this work, the focus is on the capture of asteroids for potentially scientific or commercial purposes. As such, the capture orbits need to be close enough to the Earth so that the asteroid could be revisited relatively easily without being so close that it might accidently hit the Earth. The two possibilities examined here are Earth trailing/leading orbits, and Earth-Moon distant retrograde orbits (DROs).

3.4.1 Earth-Trailing Orbits

Choosing Earth-Trailing or Earth-Leading orbits as asteroid capture targets has two benefits. First, from a theoretical perspective, it gives a concrete idea of the requirements to match Earth's energy. From that, generalizations can be made about the cost of doing alternative transfers with the same asteroids; for example, flybys from this regime could save approximately X% in comparison to a Hohmann transfer meaning flyby options could save Y to Z $\frac{m}{s}$ on transfer costs. The second benefit of this option as a target orbit is it is passively safe and potentially easy to retrieve once captured. While sample return mission would not necessarily be cheap from these orbits, they would be easier than other proposed interplanetary orbits such as Earth-Sun halos. The one major drawback worth mentioning is that pushing an asteroid in an Earth orbit turns the asteroid into a potentially hazardous asteroid. This can be mitigated by close monitoring and placement of the asteroid. For example, a minor phasing of the asteroid's final orbit can create an artificially long synodic period between the asteroid's final orbit and Earth, greatly decreasing the threat of future Earth impacts. Nonetheless, this would be a concern mission designers would have to address. Earth trailing and Earth leading orbits are identical from a transfer perspective, the only difference being a minor phasing. To avoid the unnecessary computation, only Earth-trailing orbits are studied. The target states chosen for Earth trailing orbits are found by targeting the position of the Earth 3 days prior to the date of arrival of the transfer. Since this corresponds to approximately 3 degrees of difference in true anomaly from Earth, it remains relatively close to Earth without any threat of entering Earth's sphere of influence in the near future. A diagram of the transfer is given in Figure 3.12.

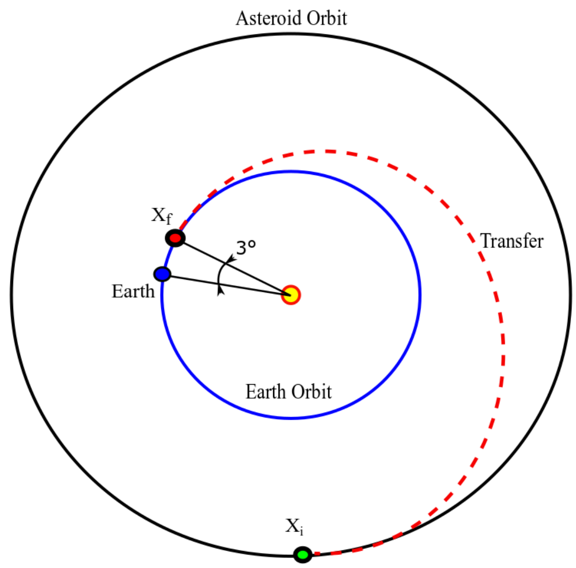

Figure 3.12.. Transfer diagram for transfers to Earth-trailing orbits

3.4.2 Earth-Moon Distant Retrograde Orbits

Distant Retrograde Orbits (DROs) are orbits defined in the circular restricted 3 body problem (CR3BP) that have desirable long-term stability properties. Bezrouk and Parker showed that even with strong perturbations, objects in DROs will remain so for hundreds of years, making them ideal targets for asteroid capture [62]. DROs are defined relative to the Earth-Moon synodic frame so simply using a DRO state as the target state for the entire transfer would require a complex and precise, time-dependent solution corresponding to a particular state in the DRO as the desired final state. This would significantly increase the problem's complexity and would likely result in the optimizer failing to converge. Even state-to-state transfers where only one trajectory is propagated forward (as opposed to the method used here where a forward and backward propagation are constrained to meet in the middle) have been shown to have convergence issues. Trying to incorporate the sensitive Earth-Moon system dynamics with a long transfer in interplanetary space would add needless complexity to the problem. To bypass this issue, transfers into DROs are separated into two distinct transfers: first, the asteroid is transferred to the Earth-Moon system at a specified radius with a fixed arrival v infinity; second, that arrival radius and v infinity are translated into the Earth-Moon system and used as the initial state for a new transfer optimization problem where the dynamics are changed to the PBC4BM and the final state is specified as some point on the DRO. To ensure that the arrival of the interplanetary transfer is consistent and easily mappable to the Earth-Moon initial state, the arrival position is forced to be sun-side with an excess velocity at the chosen v_∞, the velocity in the same direction as Earth's (this corresponds to the anti-Sun velocity vector in the Earth-Moon synodic frame). These modifications to the arrival states ensure that the asteroid will always arrive moving retrograde relative to the Moon. It is possible to have an arrival state with the proper chosen v_∞ at any given position in the Earth-Moon frame, but arriving sun-side is the simplest form that offers the best energy matching properties for asteroids with an initial higher orbital energy that Earth's. Asteroid's with a smaller orbital energy than Earth should arrive on the anti-Sun side for the same transfer benefits. The transfers are outlined in Figure 3.13.

This methodology does not make claims about the overall optimality of splitting the transfer into 2 segments. It is possible that the segmentation of the transfer into distinct optimizations adds inefficiencies to the total transfer cost but making claims about this would require research well beyond the scope of this work. Some of these inefficiencies are noticed in the trajectory results and will be discussed later. In general, the segmentation allows complex transfers to DROs without modifying

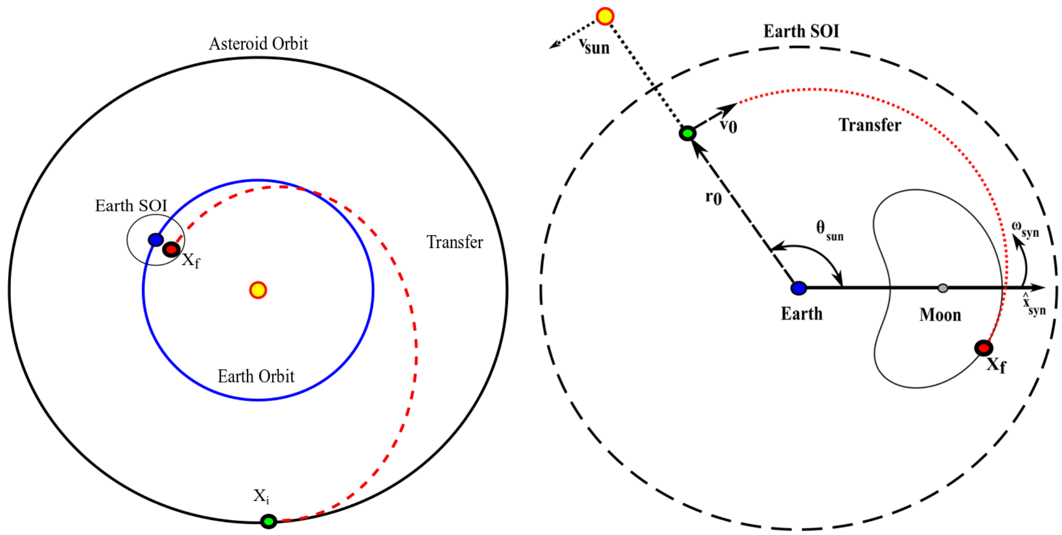

(a) Interplanetary transfer

(b) Earth-Moon system transfer

Figure 3.13.. Transfer diagram to Earth SOI and then to an Earth-Moon DRO

the optimizer itself, thus maintaining the simplicity and generality of the setup. For this reason, and because this work is not attempting to find true optima, but instead to find as many nearly optimal solutions as possible, possible total transfer cost inefficiencies from this methodology are not relevant to this discussion.

A range of the family of planar Lunar DROs is shown in Figure 3.14. In the circular 3 body problem, and in the bi-circular model as well, an equivalent orbital energy is measured by the Jacobi constant, the energy integral of the equations of motion in the system. This parameter is useful for defining certain orbits in the Earth-Moon frame such as DROs. The Tisserand parameter is a unitless measurement that quantifies the relationship between semimajor axis, eccentricity, and inclination of an orbit in 3 body systems. This metric is useful here because the Tisserand parameter can be related to v infinity and the Tisserand parameter is approximately equal to the Jacobi constant for objects far enough from the major body in a 3-body system. This relationship allows a concrete approximation of which arrival v infinity would correspond to which DRO [63]. Plot (a) shows the Jacobi constant of each of the

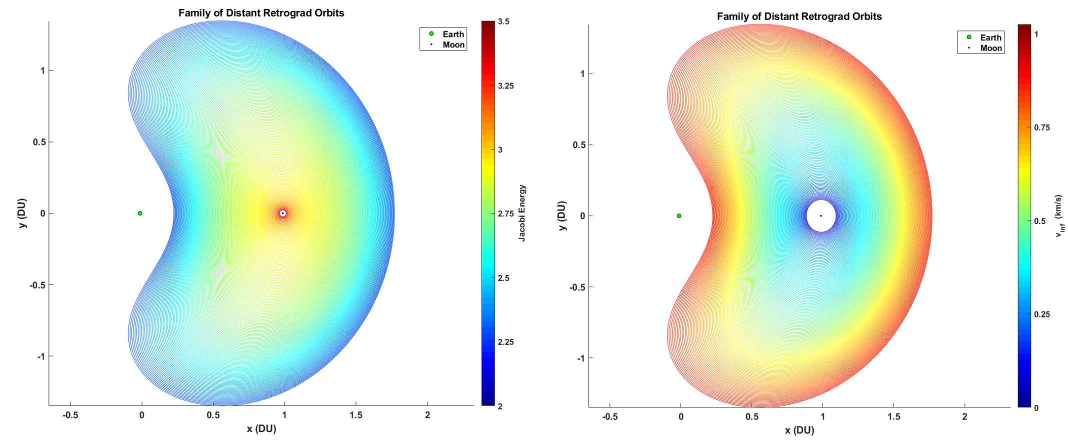

(a) Family of Lunar DROs with Jacobi Energy shown

(b) Family of Lunar DROs with the approximate v infinity from the Tisserand parameter shown.

Figure 3.14.. Family of Lunar Distant Retrograde Orbits

members of the family and plot (b) shows the approximate v infinity corresponding to the Tisserand parameter at the Jacobi energy of the given DRO. The relationship between Jacobi energy and v infinity is given by:

$$C \approx T = 3 - v_\infty^2 \tag{3.17}$$

There is a natural balance here is between choosing a DRO that is easier to get to (higher v infinity), while still being far enough away that the threat of the asteroid falling into the Earth remains small. While some DROs are more stable than others, none of the planar DROs have poor enough stability properties to raise serious concerns. The chosen DRO corresponds to an arrival v infinity of 0.75 km/s. It is left to future work to determine the optimality of this choice.

3.5 Model Verification and Validation

In order to validate the optimization models and methodology, this optimizer is run against results from JPL's optimization tool Mission Analysis Low-Thrust

Optimizer (MALTO). MALTO has a very similar structure to this optimizer, using the Sims and Flanagan model for the transfer, integrating between nodes with a Lambert solver, and producing results in the form of bacon plots. Some important differences are that MALTO outputs transfers not in ΔV costs but in arrival mass, and MALTO has specific logic for arrival and departure energy (C3) values that are only indirectly accessible in this methodology. While these differences are important to note, they should not affect the overall trends of either optimizer and should give a concrete comparison of the efficacy and capabilities of both setups.

Much of the analysis MALTO has been used for has been centered around interplanetary transfers. A test case is taken from Potter where the characteristics of Earth to Mars bacon plots are discussed at length [4]. Transfers begin at Earth and transfer to Mars with specified arrival and departure hyperbolic excess velocity. These transfers are optimized over the Earth-Mars synodic period, just over 2 years, and tested for flight times ranging from 200 to 1000 days. The comparison of one synodic period of results is shown in Figure 3.15, where 3.15(a) are the results found with this methodology and 3.15(b) are the results from MALTO.

Some immediately apparent trends are the shape and location of the wells of low-cost solutions. Both results seem to line up nicely and you can distinctly see that both synodic periods contain two major wells of good solutions, with the cycle of these restarting at the end of period. These results, however, fail to produce the same consistency and convergence rates as those of MALTO. The higher time-of-flight solutions do no converge as quickly, and there are locations where higher-cost solutions are peppered through the solutions space. One possible explanation for this is the way in which MALTO deals with revolutions during transfers. It is shown that the number of revolutions that the transfer is allowed to have can affect the continuity of the solution space for bacon plots [4]. While MATLO handles this issue with additional constraints, the methodology used here does not. It is also worth noting that MATLO's converge is significantly better, with solutions found at every point in the solution space, instead of failing to converge below a certain flight time.

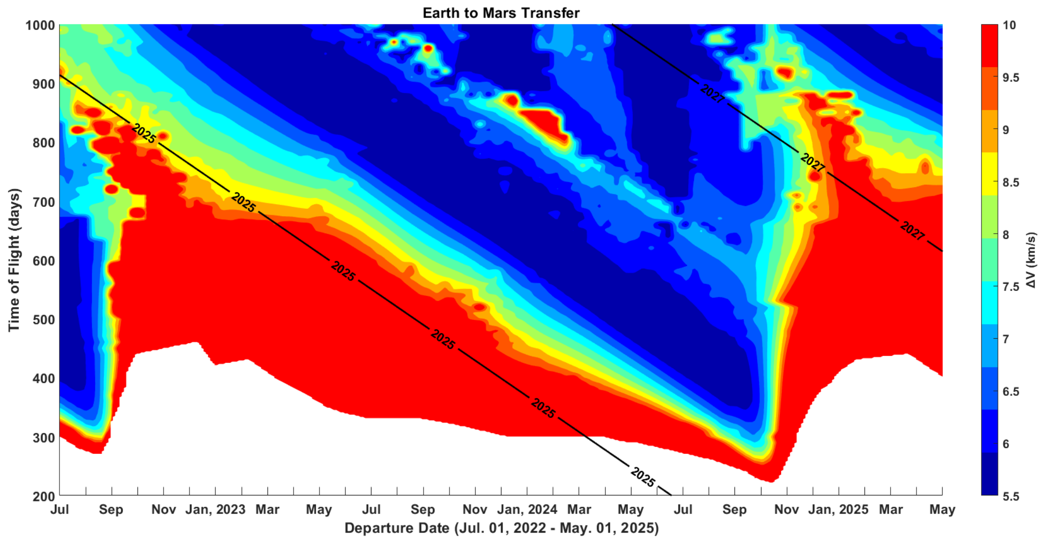

(a) Earth to Mars transfer.

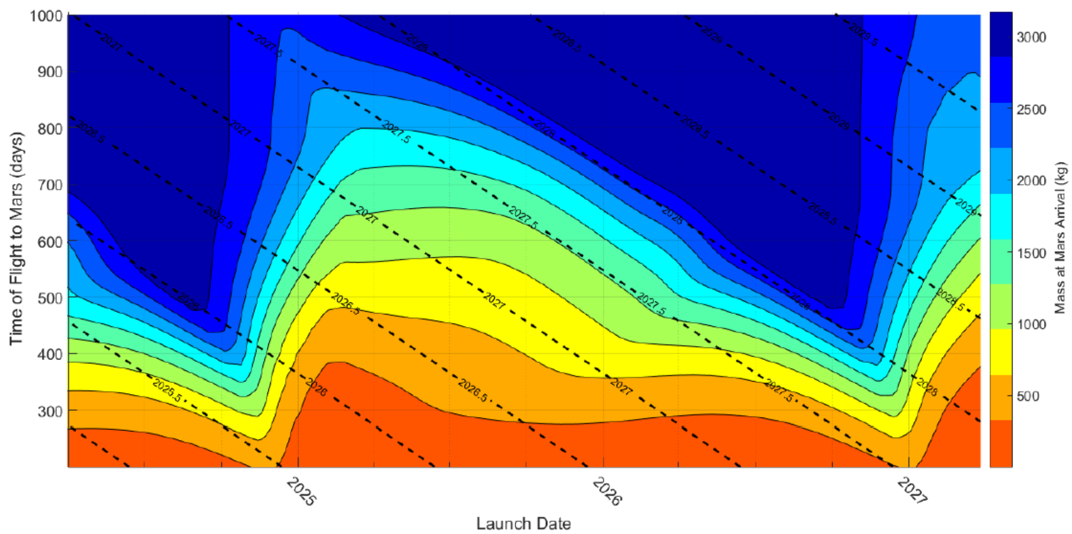

(b) Earth to Mars transfer in MALTO. Taken from Potter [4].

Figure 3.15.. Earth to Mars transfer comparison between this methodology (top) and MALTO (bottom).

While these differences are important, they do not change the results important to this discussion. Both these results and those of MATLO share similar trends and find good solutions of nearly the same cost (and that cost is within 10% of the equivalent

Hohmann transfer cost, another good indicator of the validity of these results). For the sake of generalizing optimized transfer costs, this is enough to move forward. It is left to future work to improve on the continuity and convergence of this methodology.

4. TRAJECTORY ANALYSIS

The trajectory analysis is divided into three components, two interplanetary transfers - one to Earth Trailing orbits, and one to Earth SOI in DRO capture conditions - and transfers from Earth SOI to the chosen DRO. The asteroids chosen are pulled from JPL's small bodies database and are selected based on a wide range of criteria. The goal of this work is not to find one single asteroid that is the easiest to transfer, but to analyze a large range of potential bodies for capture. As such, as many bodies with varied but still feasible characteristics for capture are chosen based on orbital regime, inclination, and size. Asteroids with too similar of characteristics are ignored as redundant though it is possible that similar asteroids could produce important differences; this problem is left to future work. Lastly, the different technologies for asteroid transfer are not considered concretely here. Instead, each transfer is analyzed with a different level of maximum average thrust that can then be mapped back to different technologies based on their individual capabilities. This allows a generic approach for each of the results without hampering the analysis with the complicated specifics of individual technologies and the difficulties of choosing between them.

Each of the transfers and their target capture states are summarized in Table 4.2. The Earth-Trailing captures are constrained to trail the Earth by 3 degrees true anomaly in Earth's orbit. Transfers to Earth's SOI for DRO capture needed to be chosen carefully, and the final state of the transfer to Earth's SOI needed to be the initial state of the DRO capture transfer. The DRO is chosen with a Jacobi energy corresponding to an arrival v_∞ of 0.75 $\frac{km}{s}$. To ensure the asteroid arrives in retrograde motion relative to the Moon, the target radius is shrunk by a small factor so that it will always arrive sun-side, barely inside the Earth's SOI. Arriving sun-side with a heliocentric velocity in the same direction as Earth's ensured the asteroid would always be moving in a retrograde motion relative to the Earth-Moon system. If the

Table 4.1.. Trajectory Analysis Input Summary

Variable	Test Inputs		
Asteroid	2010 FD6 2010 FW9	2012 XB112 2010 YD 2010 TN4	2010 KV7 2002 JR100
Thrust (N)	10	100	1000
Initial Epoch Range	Jan. 01 2030 - Jan. 01 2035		
Time-of-Flight (days)	200 - 3600		50 - 150
Initial Condition	Asteroid Orbit		Earth SOI Capture
Target Orbit	Earth-Trailing	Earth SOI	DRO Capture

asteroid's initial orbit is sun-side the Earth, retrograde arrival could be achieved by aiming for an anti-sun side capture with an heliocentric velocity less than Earth's. This is not relavent for any of the asteroids examined in this work. The capture states are shown in Table 4.2.

For simplicity and speed, the units of each transfer optimization are normalized. This has been shown to considerably improve performance of optimization schemes. This also has the added bonus of scaling the constraints to an order of magnitude of one. For the interplanetary transfers, the distance unit is set to be equivalent to 1 AU, and the time unit is set such that the gravitational parameter of the sun scales to 1 in the normalized units. For the Earth-Moon system, the standard values for distance units and time units are used (the average distance between the Earth and Moon, and the Earth-Moon synodic period respectively). The normalized units for both transfer types are summarized below.

Table 4.2.. Transfer Initial and Final State Summary. The initial epoch is represented by t_0, and t_f represents the initial epoch plus the time-of-flight for the transfer. The states for Earth-trailing capture and transfers to Earth SOI are given in the interplanetary inertial frame and the Earth SOI to DRO capture states are shown in the Earth-Moon synodic frame.

Transfer Type	Initial Position	Initial Velocity
Earth-Trailing Capture	$r_{asteroid}(t_0)$	$v_{\oplus}(t_0)$
Transfer to Earth SOI	$r_{asteroid}(t_0)$	$v_{\oplus}(t_0)$
Earth SOI to DRO Capture	$(500,000\ km)\hat{r}_{\odot}$	$(0.75\ \frac{km}{s})(-\hat{v_{\odot}})$

Transfer Type	Target Position	Target Velocity
Earth-Trailing Capture	$r_{\oplus}(t_f - 3\ days)$	$v_{\oplus}(t_f - 3\ days)$
Transfer to Earth SOI	$(\|\|r_{\oplus}\|\| - 500,000\ km)\hat{r}_{\oplus}(t_f)$	$(\|\|v_{\oplus}\|\| + 0.75\ \frac{km}{s})\hat{v_{\oplus}}(t_f)$
Earth SOI to DRO Capture	r_{DRO}	v_{DRO}

Table 4.3.. Summary of Normalized Units

Constant	Value
$DU_{Interplanetary}$	1.495978e8 km
$TU_{Interplanetary}$	5.022652e6 s
$DU_{Earth-Moon}$	3.84400e5 km
$TU_{Earth-Moon}$	3.751903e5 s

4.1 Transfers to Earth-Trailing Orbits for Asteroid 2010 FD6

The figures here all show the results for optimized transfers with the given epoch and time-of-flight range on the x and y axes, commonly referred to as bacon plots, for asteroid 2010 FD6, a 2.5m diameter Apollo asteroid with an estimated mass of 6.70e13 kg. The initial epoch ranges from January 2030 to 2035, and flight times range from 200 days to 3600 days, just under ten years. The plot on the left of each figure shows the bacon plot, and the plot on the right shows the minimum ΔV transfer found for that solution with the ΔV shown as the individual impulses solved for in the optimization. It is important to note that the ΔV scale changes slightly between each figure in order to maintain a reasonable resolution for each result.

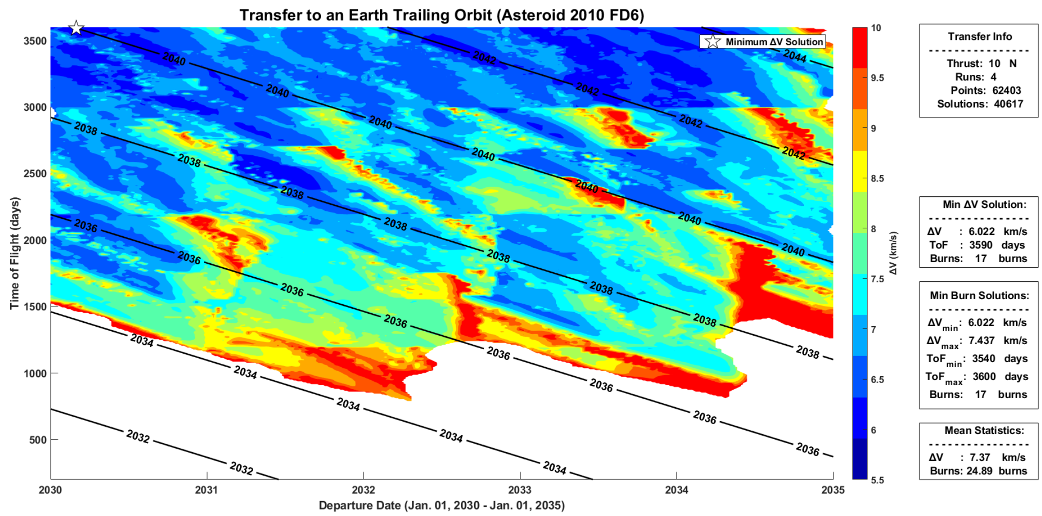

(a) Bacon Plot

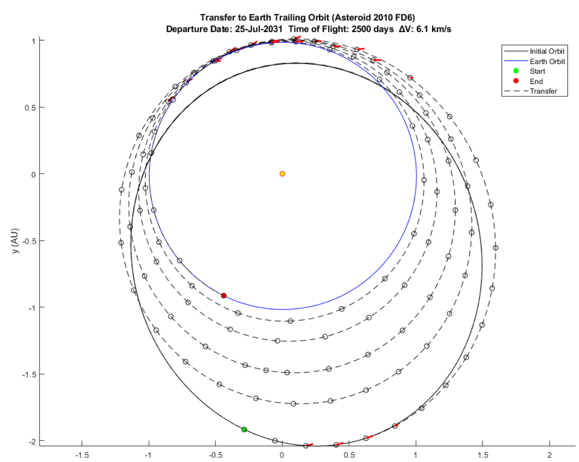

(b) Minimum ΔV solution

Figure 4.1.. Low Impulse (10 N) Transfer of 2010 FD6 to an Earth-Trailing Orbit. The starred solution corresponds to the minimum ΔV transfer found, shown in (b).

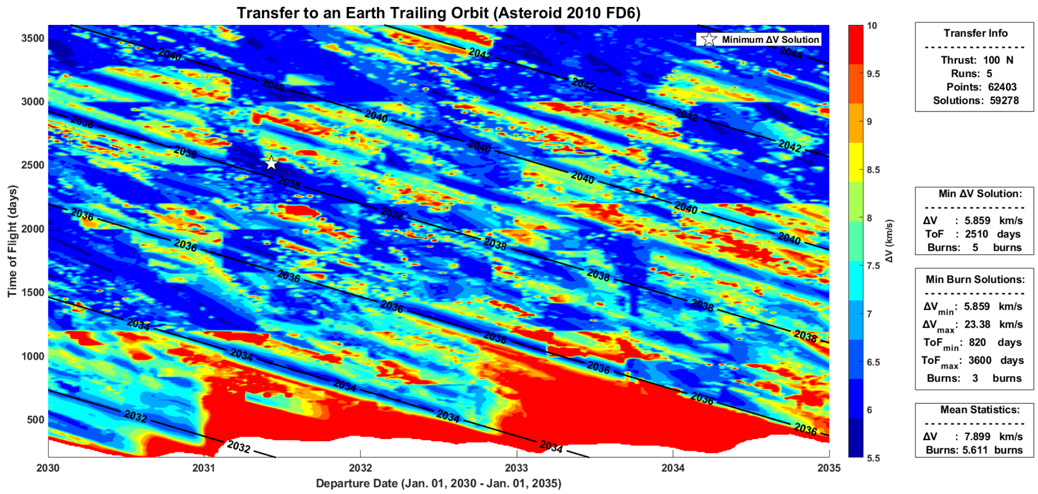

(a) Bacon Plot

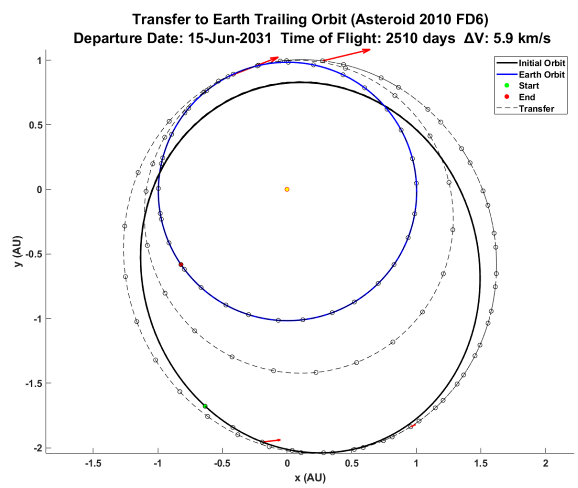

(b) Minimum ΔV solution

Figure 4.2.. Moderate Impulse (100 N) Transfer of 2010 FD6 to an Earth-Trailing Orbit. The starred solution corresponds to the minimum ΔV transfer found, shown in (b).

These results show some prominent trends. Especially in the higher thrust cases, there are clear valleys of low ΔV solutions that follow the constant date lines in the bacon plots. These low-cost solutions continue for the higher times of flight with only marginal decreases in the lowest solution. It is likely that similarly low ΔV transfers could be found for longer flight times, but nothing beyond 3600 days are looked at

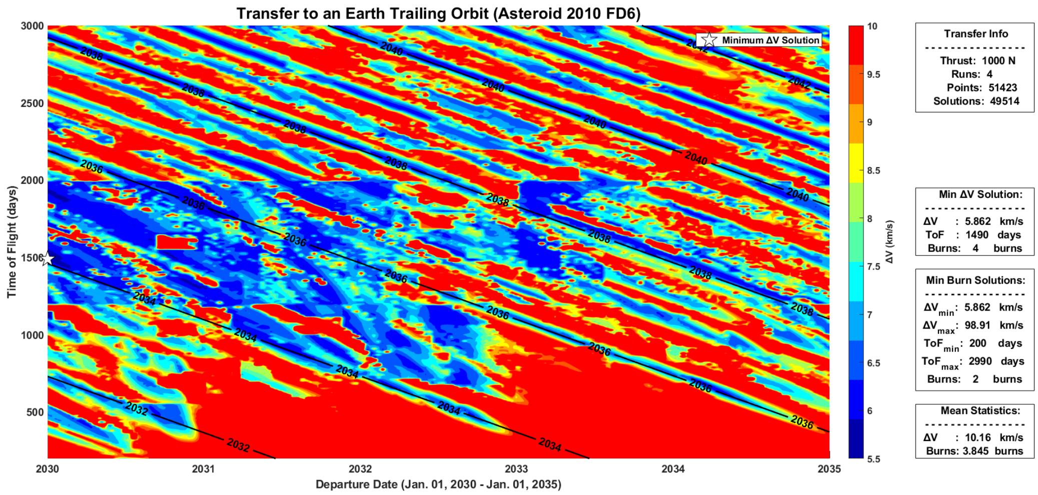

(a) Bacon Plot

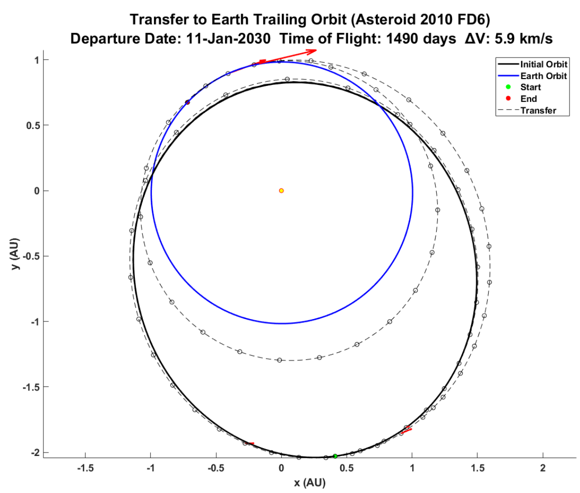

(b) Minimum ΔV solution

Figure 4.3.. High Impulse (1000 N) Transfer of 2010 FD6 to an Earth-Trailing Orbit. The starred solution corresponds to the minimum ΔV transfer found, shown in (b).

in this work. Though there is apparent sensitivity in the results, as shown in Figure 4.1(a) by the dramatic jumps between high and low solutions around 1200 days time-of-flight, the minima shown here are still close enough to the theoretical minimum Hohmann solution to be acceptable; the lower quality of these solutions is due to the optimization routine itself. These runs are sectioned into several smaller time-of-flight ranges so they can be more closely monitored and to improve convergence rates. For each time-of-flight range, the number of burns chosen for all of the runs corresponded to at least 1 burn every 30 days for the highest time-of-flight in the tested range. All transfers in the same run used the same number of burns so that they could easily seed one another without having to deal with the difficulties of trying to seed a transfer with N burns with a solution with M burns. This sensitivity could possibly be improved, but it does not affect the overall ΔV minima for the examined transfers so this is left to future work. It has also been suggested that the convergence of MALTO, which works similarly to this optimizer, is greatly improved by constraining the number of revolutions for each transfer; this optimizer uses no such constraints. It is possible that the abrupt jumps between high and low solutions in these plots is due to sensitivity issues associated with the number of revolutions allowed for each of the transfers. Theoretically, the strength of individual impulses should not necessarily increase the total required transfer cost, it should just change the time-of-flight, but by commanding a flight time and the number of impulses, inefficiencies are automatically built into the system. These results would be good initial guesses to feed into a more precise optimizer. It is evident from these results that there exists some minimum thrust before nearly optimum solutions can be found given a certain fixed time-of-flight. This trend means that increasing the thrust will have no significant effect once nearly optimal thrusts are shown to be achievable. This gives some credence to extrapolating the possibility of transfers given results from lower-thrust technologies. If a low-thrust transfer is found, it is evident here and perhaps obvious from first principles, that a higher thrust system is also capable of completing that or a similarly efficient transfer. Another interesting trend for these transfers is that the minimum Δ solutions for each case confirm basic orbital transfer principles. For any level of thrust, the burns all occur at or near the apogee and perigee of the orbit, the most efficient places to change the perigee and apogee, respectively. This is true of all of the other tested asteroids as well. Some important conclusions can be drawn from this first look at asteroid 2010 FD6. First, the quality of the transfer is not significantly improved when the time-of-flight is increased once nearly optimal solutions are possible. This means that, from a mission design perspective, it is only necessary to test flight times up to 3-5 years and any longer duration missions can be assumed to have equivalently costly transfers (often better). Second, the low-cost solutions are more dependent on the arrival date than the initial epoch or the time-of-flight. This suggests that choosing either of these is not important from a transfer perspective. Feasibly, any epoch or any time-of-flight could be chosen so long as the other is chosen appropriately. It is also clear from these results that the repetition of these results occurs far more frequently than the synodic period of the two bodies. This is confirmed in later sections. If low-cost solutions are common, this means that less time needs to be committed to searching a large date-range. The 5-year range used here is sufficient, but it likely that most transfers could be examined with much smaller ranges without losing important results. Finally, these results suggest that, above a certain threshold, the optimality of a transfer is invariant to the thrust. These conclusions are important. Together, they paint a picture of transfer optimization that is far simpler than what is often imagined. If epoch, time-of-flight, and transfer technology are free variables, each of which can be chosen independently before solving for the rest, then the optimal asteroid capture problem is not a delicate balancing act. Functionally, any technology could be chosen, or any time-of-flight, or any initial epoch, before deciding on the remaining details of the mission.

4.1.1 Comparison of Transfers to Earth-Trailing Orbits for different Asteroids

This section takes a look at transfers to Earth-Trailing orbits for all of the different asteroids tested in this research. Only 1000 N thrust cases are shown here because some of the heavier asteroids only converged to solutions with those levels of thrust. Different from the previous section, here most transfers only have a time-of-flight range of 3-4 years. This is because of the conclusions drawn in the previous section. Runs are attempted at lower flight time ranges until convergence occurred and then the results are continued until the trends of the solutions space are evident from the results. It is also important to note that not all of the color bars shown in the figures here have the same ranges. While these values are meant to be as similar as possible, some trends become invisible on those scales. The currently used color bar ranges are to help visualize those differentiating trends.

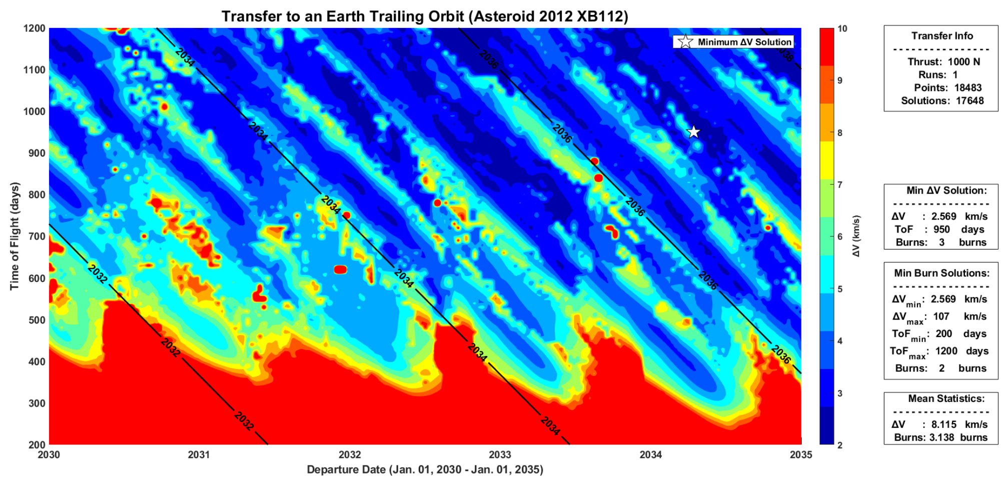

Figure 4.4.. High Impulse (1000 N) Transfer of 2012 XB112 to an Earth-Trailing Orbit.

All of the asteroids here show the same important properties as the transfers for 2010 FD6. There are consistent low-cost solutions along the constant date lines, above a certain threshold, there is no significant improvement in the solutions with higher times-of-flight, and there are equivalently low-cost transfers for any given initial epoch.

The consistency of these results between asteroids either indicates that these trends are true of different asteroids, or more generally, true of any interplanetary transfer, or it indicates that the optimizer tends to produce these types of results. It is unlikely due to the latter reason because similar trends have been witnessed for

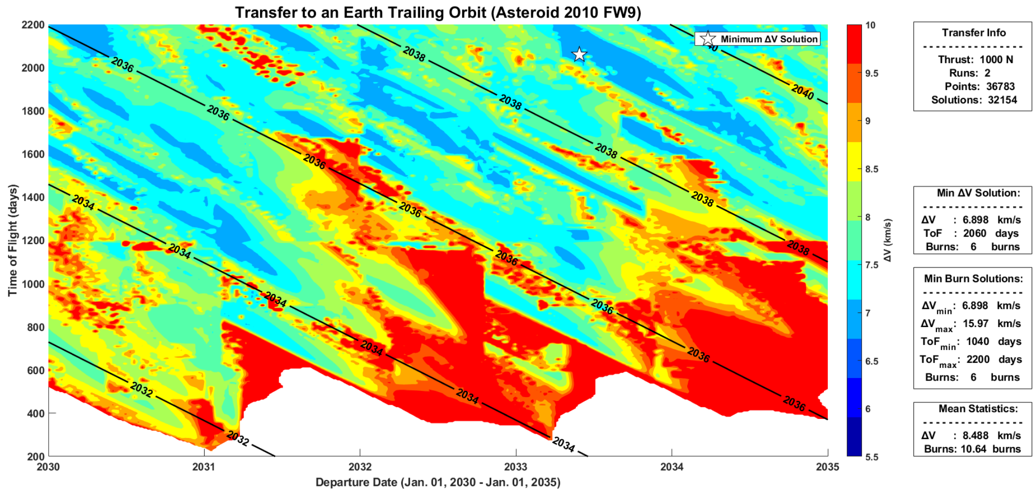

Figure 4.5.. High Impulse (1000 N) Transfer of 2010 FW9 to an Earth-Trailing Orbit.

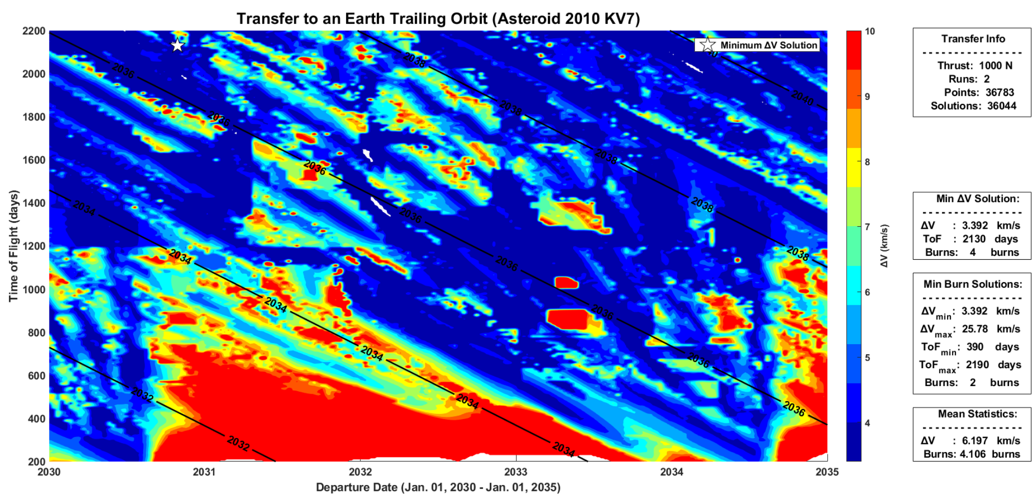

Figure 4.6.. High Impulse (1000 N) Transfer of 2010 KV7 to an Earth-Trailing Orbit.

Earth-Mars transfers [4]. Some preliminary test runs also show that these trends are not as noticeable when testing interplanetary transfers for spacecraft. It is likely that these trends are nominal for any interplanetary transfer and they are more apparent here in part because the asteroids are so massive. The mass of the asteroids reduces

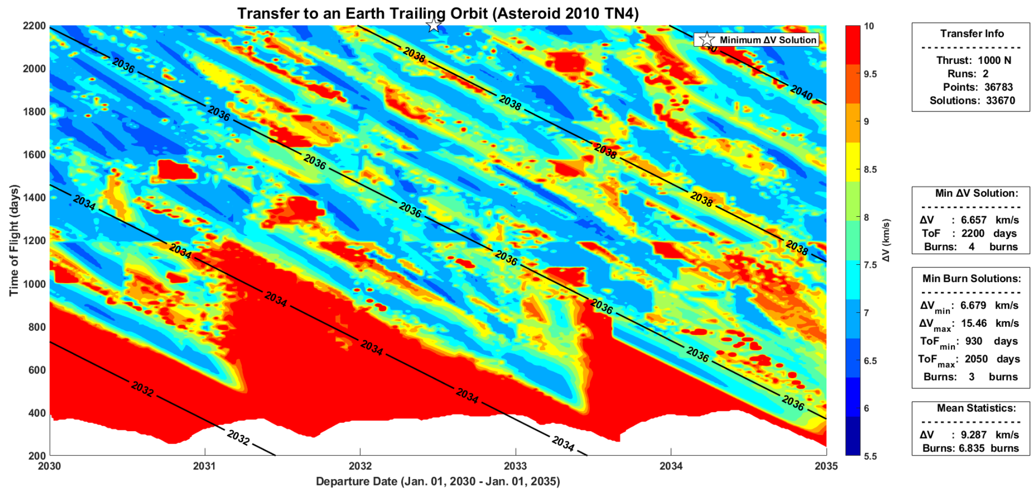

Figure 4.7.. High Impulse (1000 N) Transfer of 2010 TN4 to an Earth-Trailing Orbit.

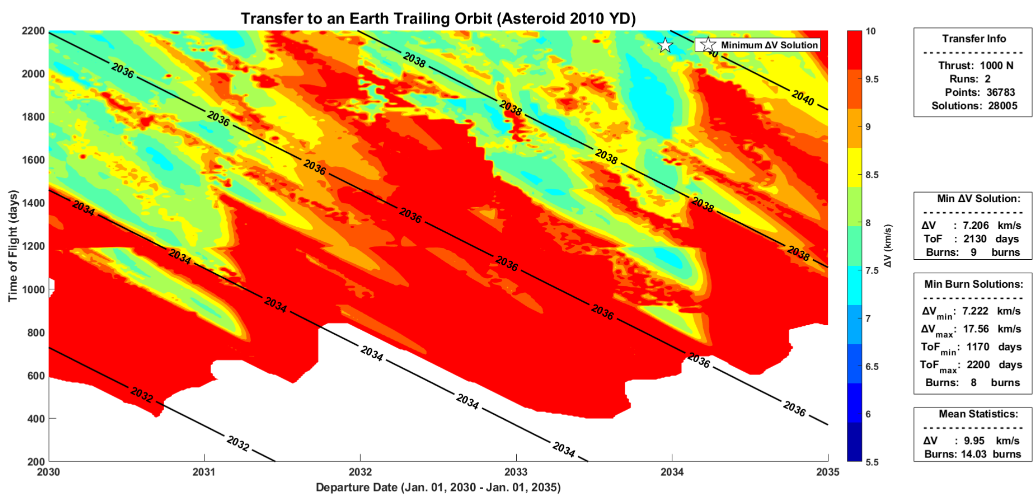

Figure 4.8.. High Impulse (1000 N) Transfer of 2010 YD to an Earth-Trailing Orbit.

the effective thrust and diminishes the total amount of ΔV that can be imposed over a given time span. This means that very heavy objects will either have to find nearly optimal solutions in order to converge at all whereas lighter objects will be able to less optimal transfers without a large increase in transfer cost. Effectively, the high

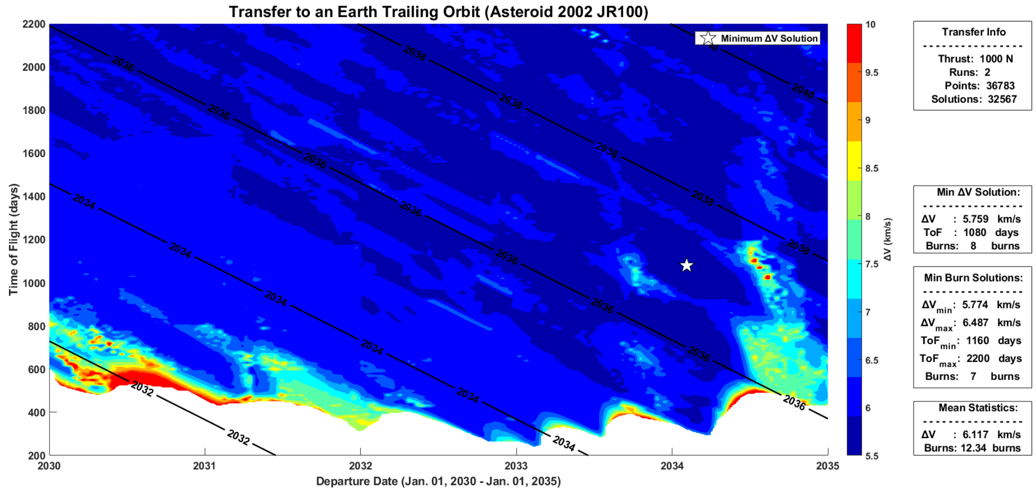

Figure 4.9.. High Impulse (1000 N) Transfer of 2002 JR100 to an Earth-Trailing Orbit.

mass of the asteroids makes the transfers more sensitive, but there is no reason to believe it should change the trends of the transfers in general.

There are also trends in these results that are consistent with those in the previous section that are not evident from these figures alone. For example, in cases where the asteroid's orbits are significantly different than Earth's, there is a consistent trend among the near-optimum transfers in the solutions space where burns tend to occur near apogee and perigee. While this behavior is expected for optimized results in general, it is important both as a deeper kind of verification for the optimizer than surface comparisons, and it also points to the potential for simplifications to the optimization problem. If complex transfer find solutions using burns within 10-15 degrees of apogee and perigee, it would possible to add this as a constraint to the problem, potentially reducing the total number of burn locations and thus greatly reducing the number of free variables inside the optimization.

In a similar vein, for all of the transfers examined here, that the total number of burns required for each transfer is on the order of 10 burns. The Sims-Flanagan method can have an exceedingly large number of potential burn locations due to the even spacing of burn locations and the inclusions of an impulse every x days. With the knowledge that any nearly optimal solution will have fewer than 30 or so burns, it would be possible to reformulate the optimization problem with this addition constraint as well. By only allowing burns near apogee and perigee, and by only allowing a fixed number of impulsive burns, it is feasible from these results that a new version of the Sims-Flanagan method could be constructed with significantly fewer free variables, increasing computational efficiency, and the solver's robustness.

4.2 Capture to Earth-Moon DROs

Transfers to distant retrograde orbits are done in 2 segments. The first is the interplanetary segment and is largely similar to the transfers to Earth-Trailing orbits. The main difference for the interplanetary portion is that, instead of target the Earth's state 3 days prior, the target state for the 1st segment is inside the Earth's sphere of influence with a commanded arrival excess velocity of $0.75\frac{km}{s}$. The second part of the transfer has an initial state at the arrival state of the 1st segment, and transfers into the chosen DRO from there. This segment is fundamentally different since the transfer is done in the Earth-Moon synodic frame. The rotating frame creates some challenges that require a reframing of the solution type. The interplanetary bacon plots are meant to show the relationship between the initial epoch and the transfer flight time. Since the Earth-Moon frame is fixed, regardless of the epoch, and the only thing that changes is the location of the sun, it does not make sense to test a range of epochs. Instead, the arrival condition of the 1st segment is fixed to arrive sun-side, both forcing the arrival motion of the asteroid to be retrograde with respect to the Earth-Moon frame and bypassing the issue of trying to test a wide range of different transfers for every possible initial asteroid insertion angle and initial solar angle. These two angles are forced to be the same. Then several different values of this angle are tested to see if the results vary significantly. With epoch ignored as a free variable for the 2nd segment, there is room to test another unknown in the system. The unknown chosen for this analysis is the state on the DRO to choose as a target. The DRO is an infinite number of states and thus, the transfer to the DRO could be done by targeting any single state on it. In place of testing for epoch, a range of 20 different target states are tested, shown in Figure 4.10.

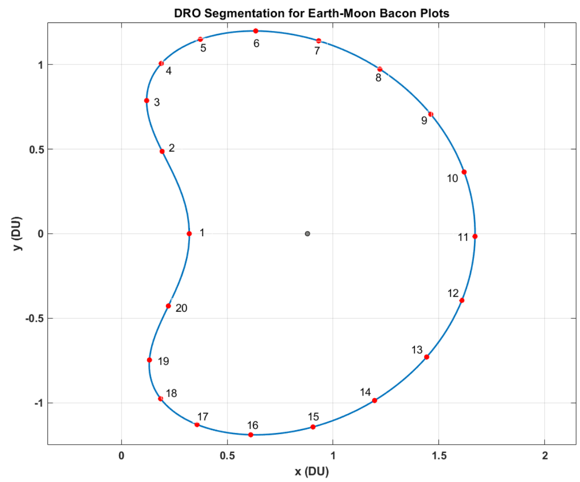

Figure 4.10.. DRO segmentation for Earth-Moon Bacon Plots. Each dot represents the location of one of the final states and is labeled with its respective index.

4.2.1 Interplanetary Transfers to Earth's Sphere of Influence for Asteroid 2010 FD6

The transfers for capture into Earth-Moon DROs display very similar results to capture into Earth-trailing orbits. There are clear and distinct low-cost valleys of solutions that do not change significantly as the time-of-flight increases. There are also equivalently costed transfers regardless of the initial epoch. Both of these trends validate the results from transfers to Earth-Trailing orbits.

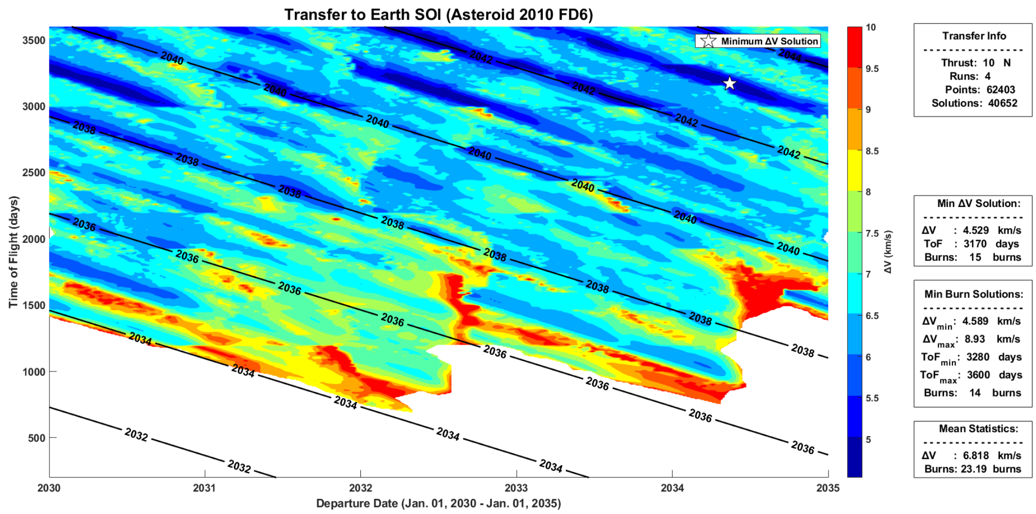

Figure 4.11.. Low Impulse (10 N) Transfer of 2010 FD6 to Earth Sphere of Influence.

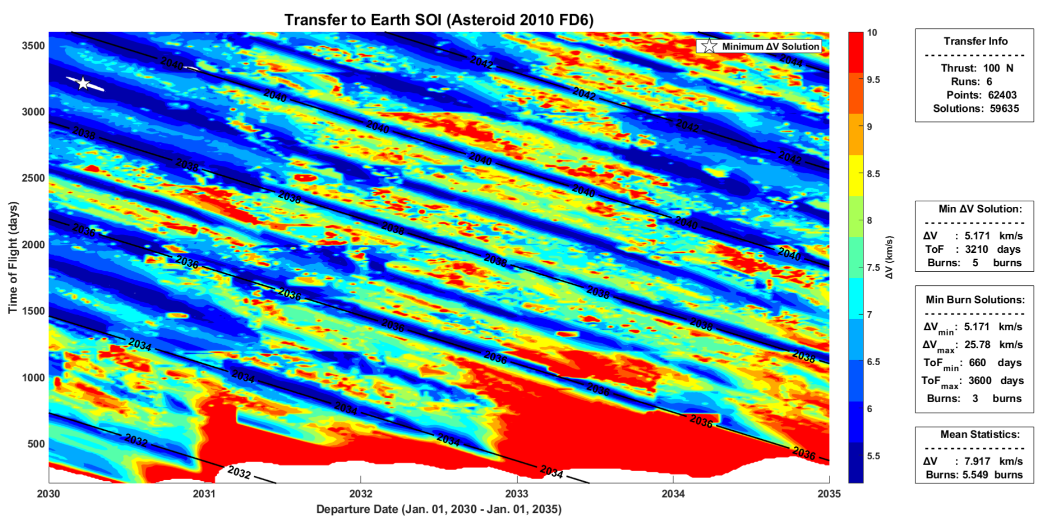

Figure 4.12.. Moderate Impulse (100 N) Transfer of 2010 FD6 to Earth Sphere of Influence.

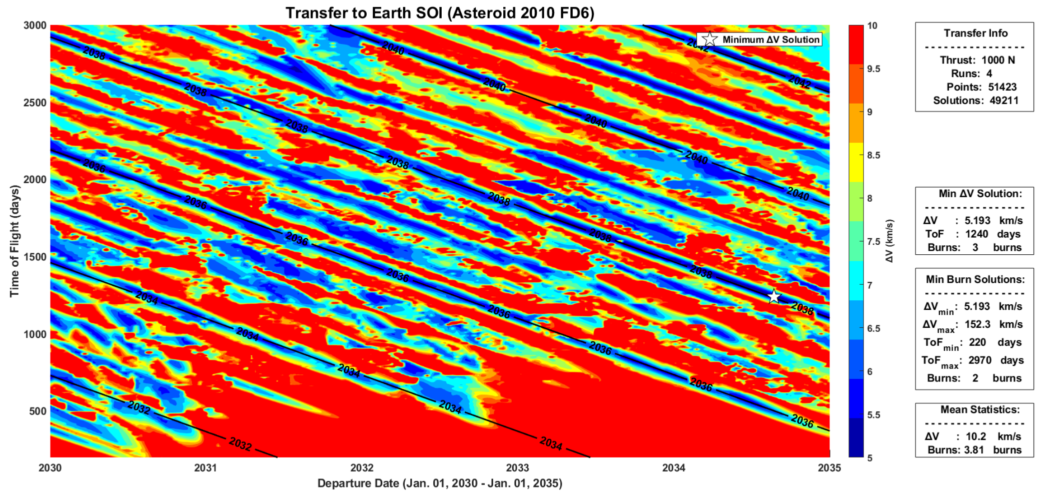

Figure 4.13.. High Impulse (1000 N) Transfer of 2010 FD6 to Earth Sphere of Influence.

It is also worth mentioning that, while not significantly different, the minimum required transfer ΔV for these runs is slightly lower than those to Earth-trailing orbits (by about 0.5 km/s for all thrust values). This is due to the arrival excess velocity of 0.75 km/s for these transfers. While getting the full 0.75 km/s might be theoretically possible, the limitations of this transfer method (nodes are fixed in location and time, for example) are likely the reason that only 0.5 km/s is saved in best cases. This "free" ΔV is only utilized when the transfer can align itself properly with the arrival velocity direction.

4.2.2 Comparison of Transfers to Earth's Sphere of Influence for different Asteroids

This section compares the results for high impulse (1000 N) transfers to DRO insertion. Functionally, the only difference between these transfers and the transfers to Earth-Trailing orbits is the capture condition. Since this target state can be converted into orbital elements, this is no different than simply transferring to a specific point in a non-Earth orbit. In effect, it is like transferring to an Earth-Trailing orbit where the orbit of Earth slightly different. This small difference is enough to notice some changes in the trends of the results, but it is not enough to effect the major trends such as low-cost solutions trending on the constant date lines and the constant value of optimal solutions regardless of the time-of-flight.

One trend in these plots that does stick out is how pronounced the valleys of low-cost solutions are; this is especially noticeable for asteroid 2002 JR100 (compare Figure 4.9 and Figure 4.19). In Earth-Trailing orbits, these valleys tended to blur with other valleys more easily, and they tended to have less pronounced differences in cost from nearby solutions. In these transfers to DRO insertion, the cost of deviating from the optimal date line is greater. This is likely due to the fact that the equivalent capture orbit for these transfers is elliptical, and the asteroids are capturing at what would be the perigee of the orbit. Straying from perigee on capture would violate energy minimum principles and cause more dramatic increases than doing so with a circular capture orbit as a circular orbit has no well-defined perigee and thus, any point on the orbit could be targeted with similar results.

Even so, this trending is not significant and does not change the quality of the best-case results. Comparing the found cost of these transfers with respect to the Hohmann transfer cost to the equivalent orbit, these solutions are still around 110% of the Hohmann transfer cost, the same as the transfers to Earth-Trailing orbits.

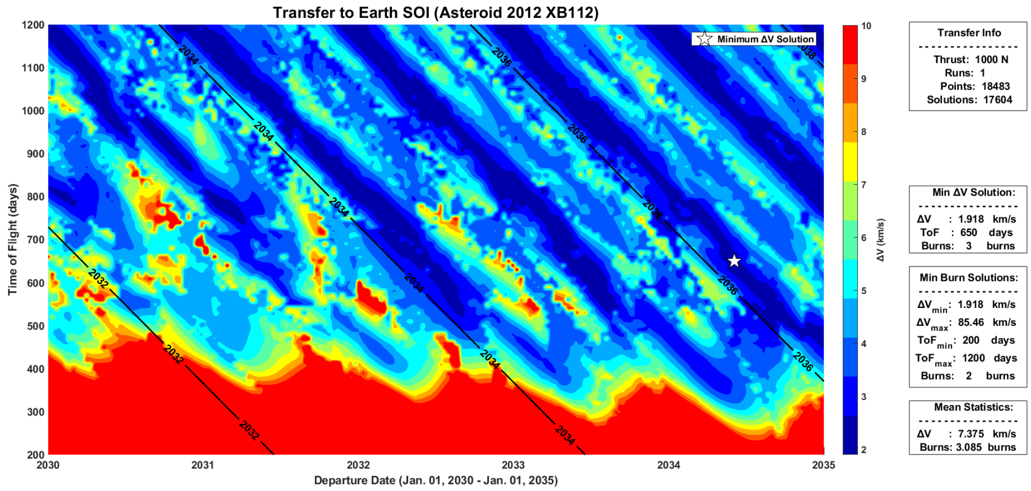

Figure 4.14.. High Impulse (1000 N) Transfer of 2012 XB112 to DRO insertion.

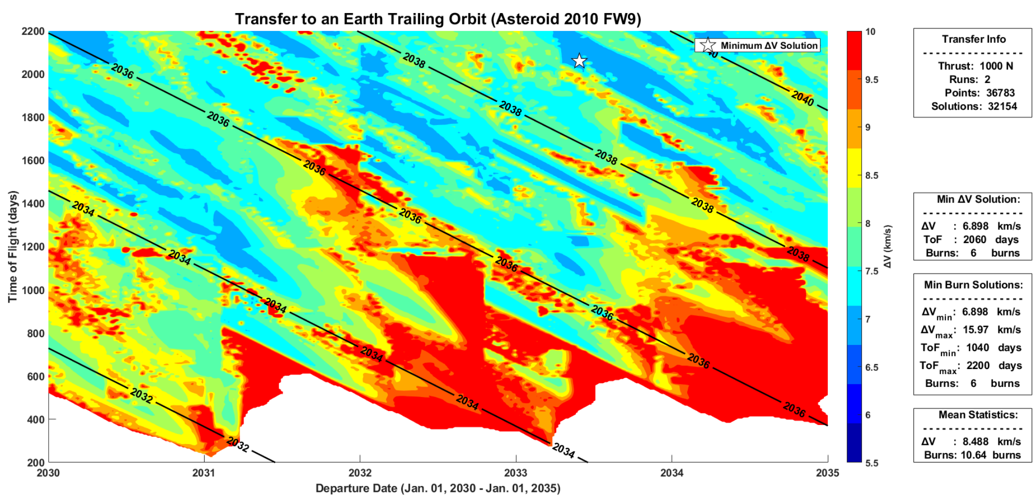

Figure 4.15.. High Impulse (1000 N) Transfer of 2010 FW9 to DRO insertion.

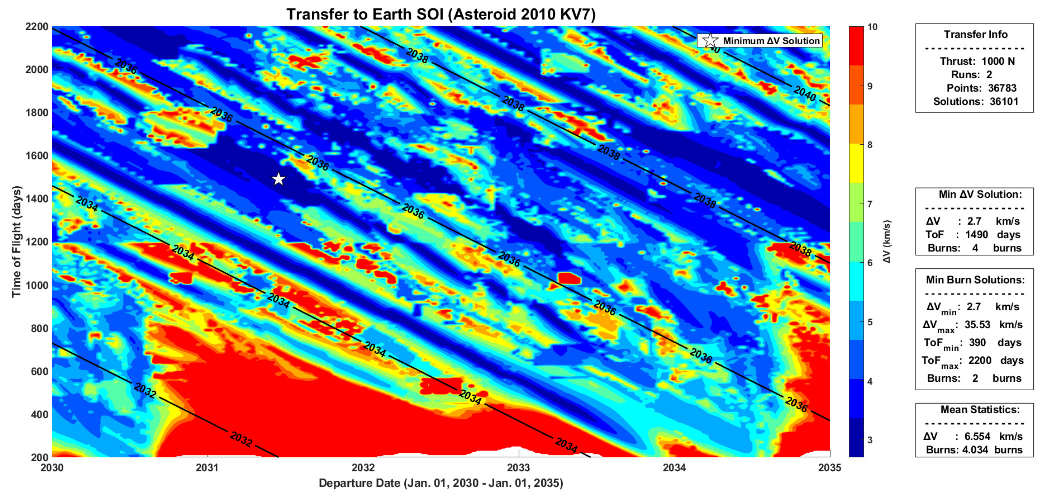

Figure 4.16.. High Impulse (1000 N) Transfer of 2010 KV7 to DRO insertion.

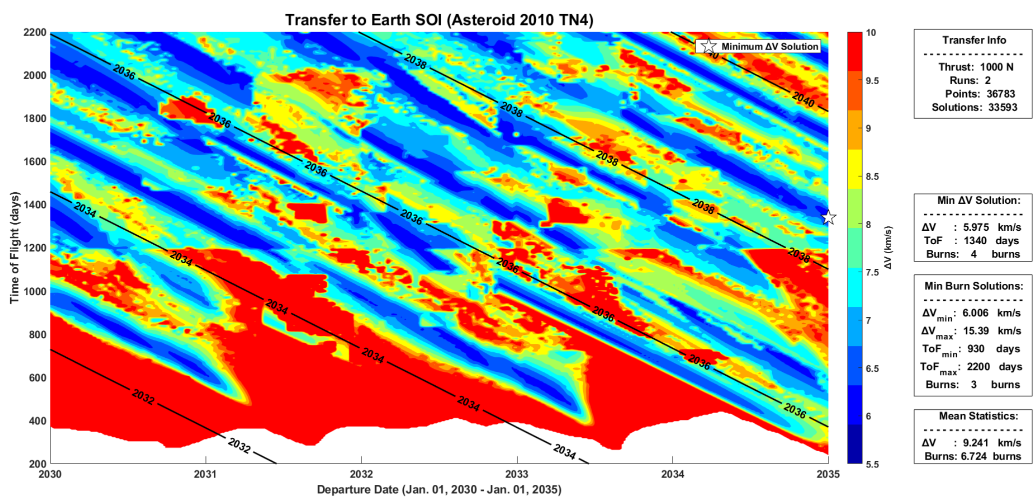

Figure 4.17.. High Impulse (1000 N) Transfer of 2010 TN4 to DRO insertion.

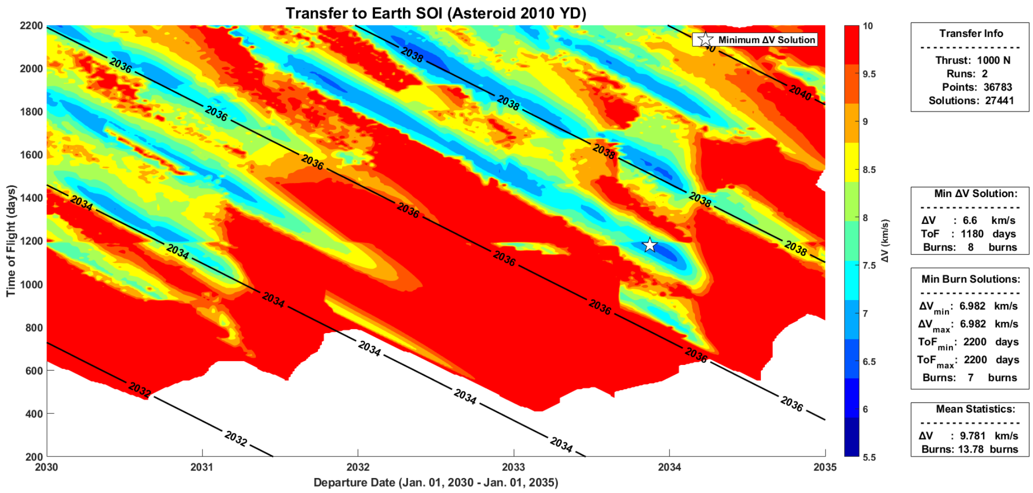

Figure 4.18.. High Impulse (1000 N) Transfer of 2010 YD to DRO insertion.

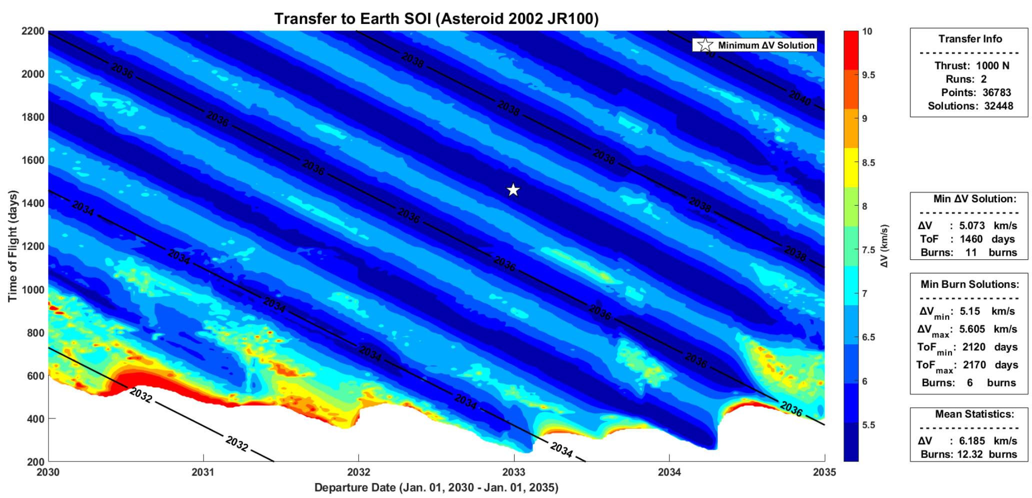

Figure 4.19.. High Impulse (1000 N) Transfer of 2002 JR100 to DRO insertion.

4.2.3 Earth-Moon Transfers to DROs

The transfers from Earth SOI entry conditions to a capture DRO are shown in Figure 4.20. While these results look like bacon plots, they are setup in a marginally different way. Since the initial conditions are fixed and the propagation in this system is done with respect to a rotating frame, there is no point in trying a series of different transfers with different initial epochs. Instead, the angle between the Earth-Moon synodic frame and the entry of the position of the asteroid is established and the transfer is done for a series of different flight times as well as for a series of different arrival locations on the chosen DRO, denoted by the arrival state index. This method avoids many of the complexities of transferring to DROs while still giving a comprehensive view of the solution space for the transfer.

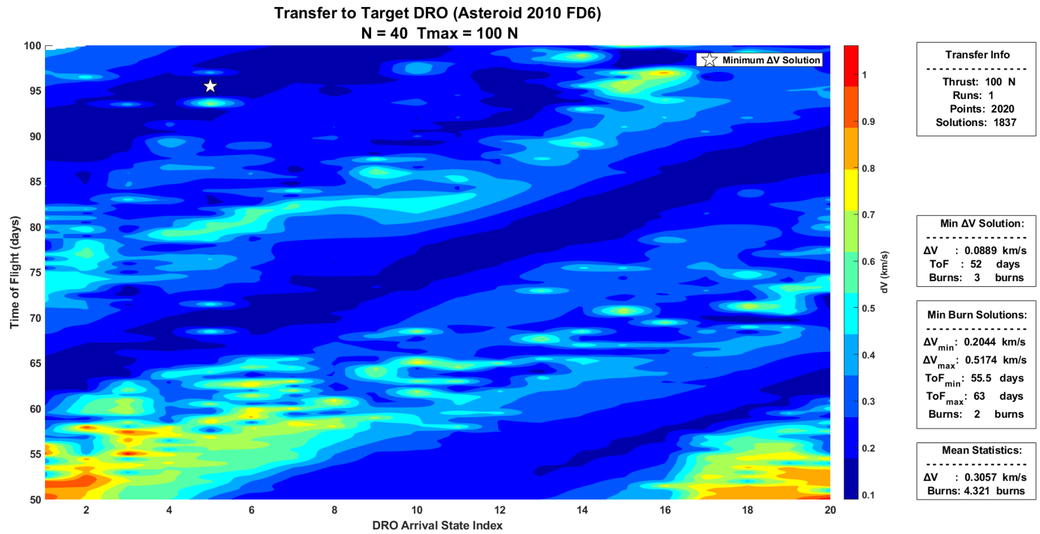

(a) Bacon Plot

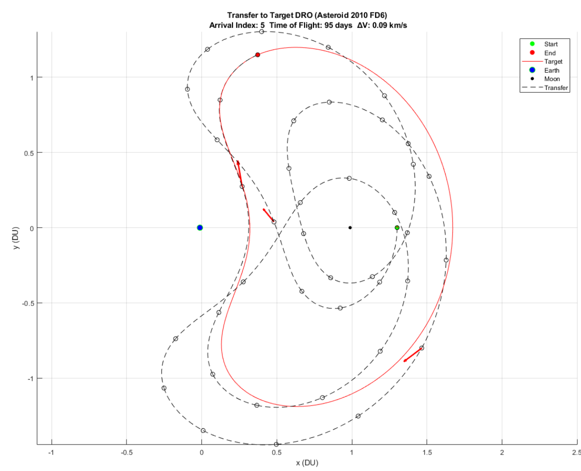

(b) Minimum ΔV solution

Figure 4.20.. Moderate Impulse (100 N) Transfer of 2010 FD6 from Earth Sphere of Influence to Target DRO. Initial solar angle is 0 degrees.

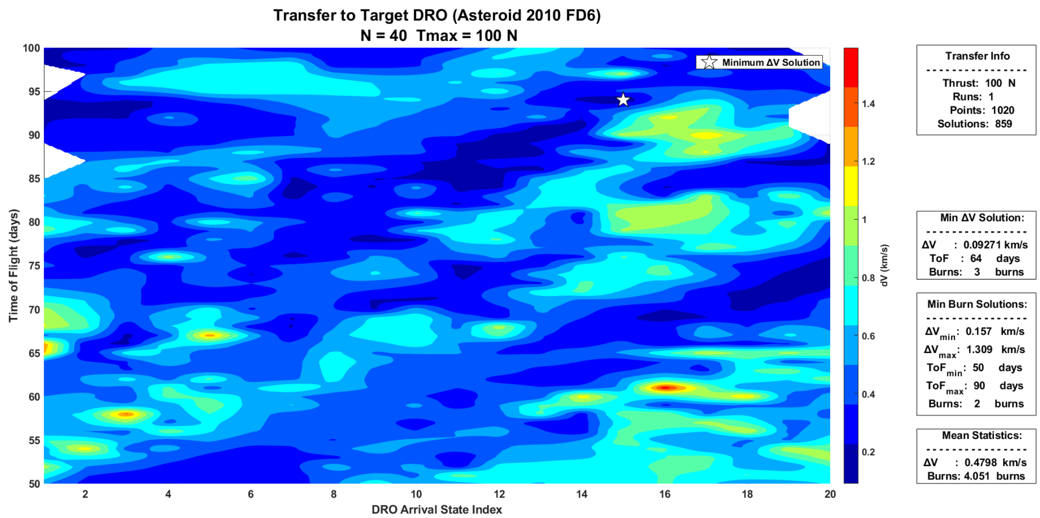

Figure 4.21.. Moderate Impulse (100 N) Transfer of 2010 FD6 from Earth Sphere of Influence to Target DRO. Initial solar angle is 90 degrees.

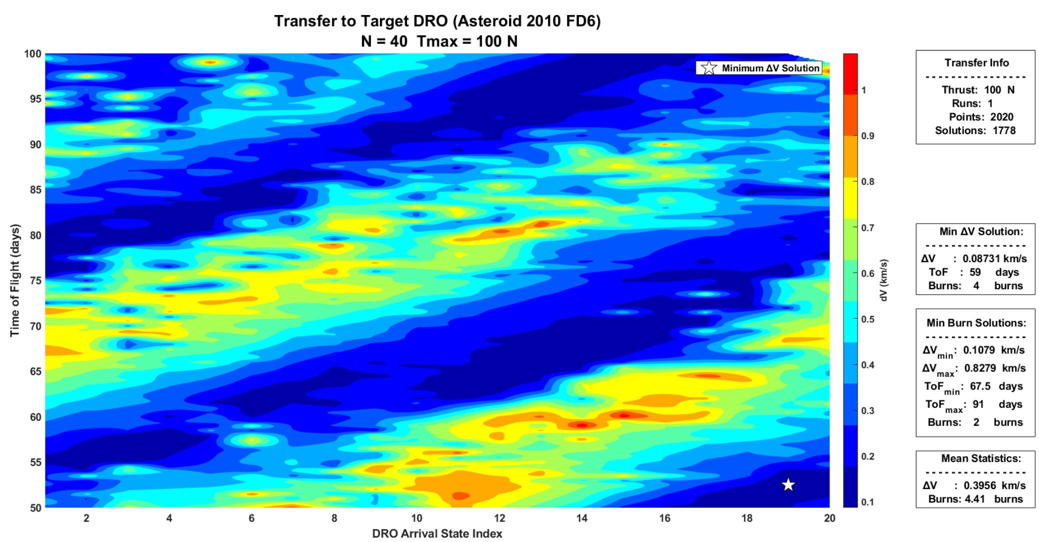

Figure 4.22.. Moderate Impulse (100 N) Transfer of 2010 FD6 from Earth Sphere of Influence to Target DRO. Initial solar angle is 180 degrees.

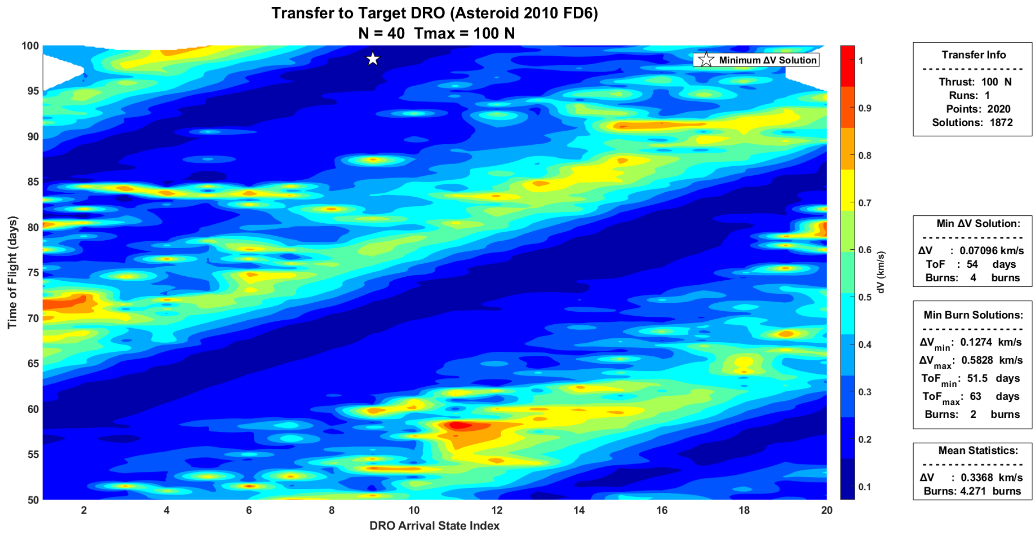

Figure 4.23.. Moderate Impulse (100 N) Transfer of 2010 FD6 from Earth Sphere of Influence to Target DRO. Initial solar angle is 270 degrees.

There are two major trends to pull from the results shown here: 1) The transfer cost does not depend on the arrival location on the DRO, and 2) the transfer cost does not depend on the time-of-flight for the tested range. The first conclusion here is the most important as it shows that any single DRO state could be chosen instead of sampling such a large number. The second is true for the tested data and is confirmed by other runs, but it might not be true for longer transfer times. If this is true in general, then this piece of the optimization could be simplified to a single optimization with an arbitrary time-of-flight and an arbitrary arrival state for the chosen DRO. This would allow for the testing of other interesting variables such as the chosen DRO and the entry excess velocity of the asteroid.

Comparing the same transfer for different levels of thrust shows some of the shortcomings of the optimizer itself. Figure 4.24 shows the same results for the three levels of thrust with an initial solar angle of 180 degrees. Though the 2 major trends just discussed are still true here regardless of thrust, it is evident that there are significant convergence issues. For the low thrust case, 2010 FD6 is the only asteroid to converge on any results, and those results have a converge rate of only 20%. Note that for both low and high thrust cases, the time-of-flight range needed to be increased in order for convergence to be possible.

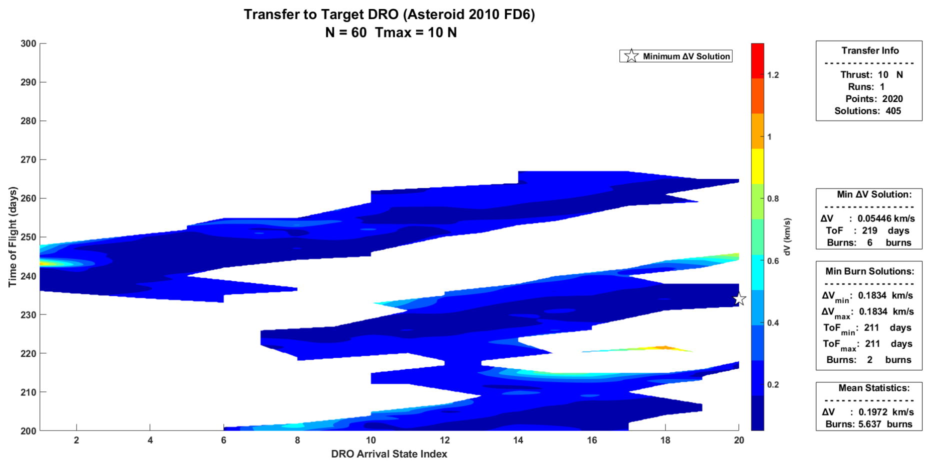

(a) Low Thrust (10 N)

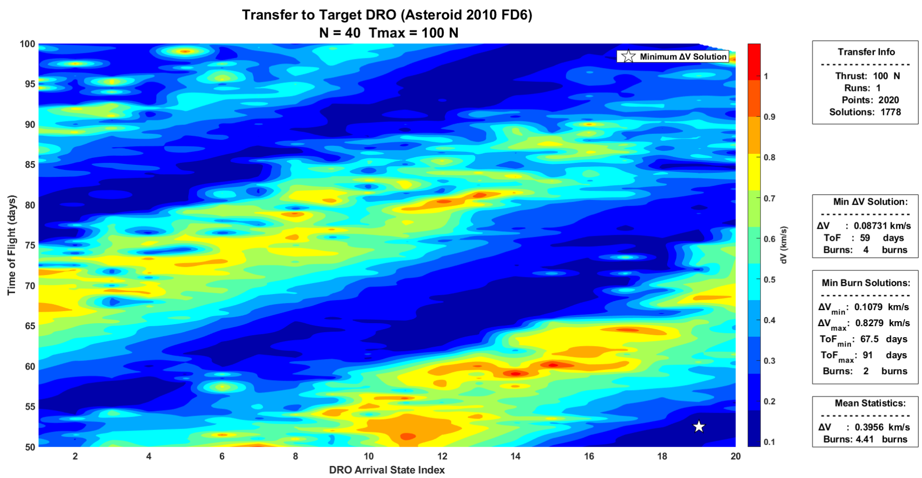

(b) Moderate Thrust (100 N)

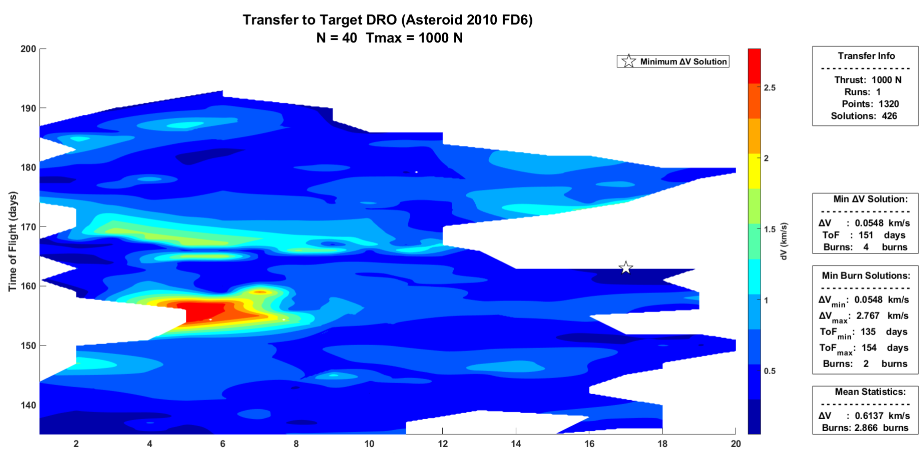

(c) High Thrust (1000 N)

Figure 4.24.. Transfer of 2010 FD6 from Earth Sphere of Influence to Target DRO for various levels of thrust. Initial solar angle is 180 degrees.

With the higher thrust case, there are some interesting improvement over the moderate thrust case. Some issues that made the transfers costly are overcome and the apparent valleys of quality solutions are no longer apparent in the higher thrust case. Nonetheless, there are still some convergence issues with the high thrust case. This could be due to the sensitivity of the Earth-Moon transfers, or possibly the resolution of the genetic algorithm. With such a higher level of thrust, it is possible that the impulses are too powerful, and the optimizer does not have the proper variable resolution to zoom in enough on the thrust magnitudes to properly complete the transfer. More work is needed to discover the exact reason of this behavior.

Although the quality and trending of these results is not nearly as concrete and consistent as those for the interplanetary transfers, it is still clear that the overarching claims made can be trusted. For Earth-Moon transfers to DROs under the given conditions, the chosen target state and time-of-flight do not affect whether or not optimum solutions can be found. Either of these values can be chosen arbitrarily and an equivalently optimal solution will be available.

4.2.4 Comparison of Transfers to DROs for different Asteroids

Transfers for different asteroids suffer similar convergence issues. Only 2010 FD6 is able to converge on solutions at any thrust level, 2010 DL only converges with the highest level of thrust (and with increased flight time), and 2002 JR100 does not converge at every level of thrust, even with the max flight time extended to 250 days. It is not clear from these results whether convergence fails because the optimizer is not robust enough or if the transfers are simply not possible for the given combination of asteroid mass and transfer conditions. Examining this in further detail is left to future work.

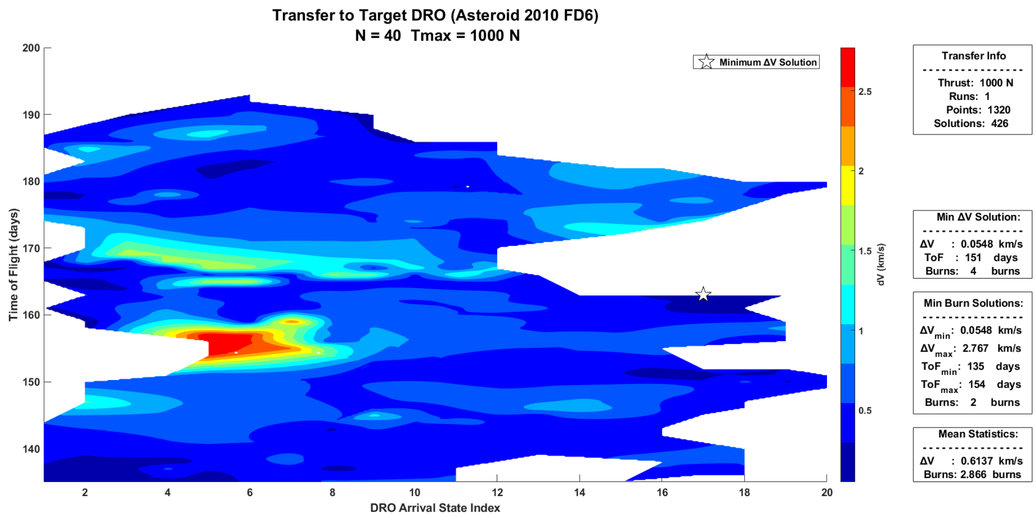

(a) 2010 FD6

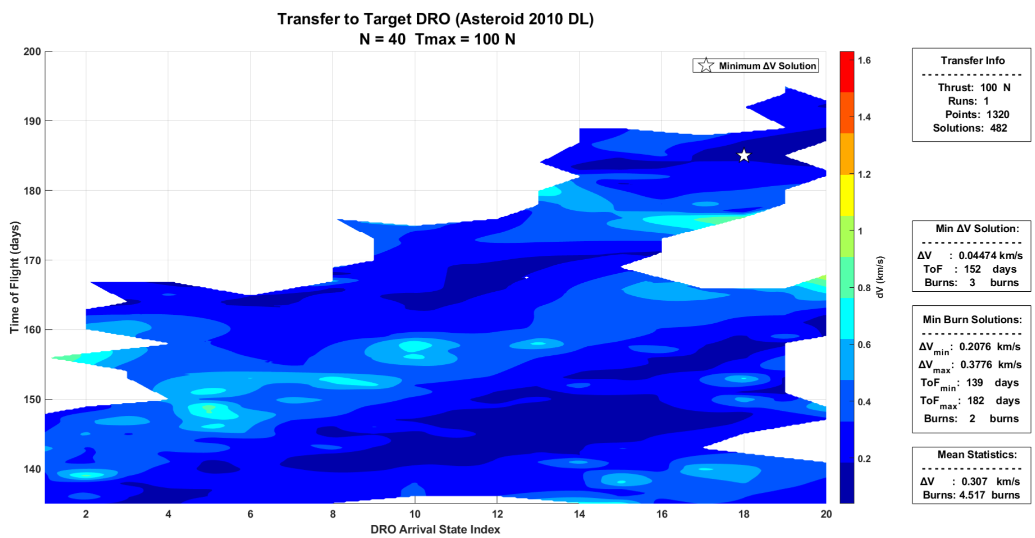

(b) 2010 DL

Figure 4.25.. High Impulse (1000 N) Transfer of 2010 FD6 (a) and 2010 DL (b) from Earth Sphere of Influence to Target DRO.

What can be gleamed from these results does not confirm nor contradict the trends from analysis on Earth-Moon transfers for 2010 FD6. There seems to be some consistency in the solution for 2010 DL that confirms the idea that the arrival state index does not influence the cost of the transfer. There also seems to be some similarly low-cost solutions at any of the flight times that converge. From an energy perspective, these conclusions seem intuitive, however, the fact that the higher and lower thrust solutions for 2010 do not explicitly show these trends, it is possible that some of the deeper underlying mechanics affect these trends. On the other hand, there are obvious and consistent convergence issues due to the optimizer itself and it not unreasonable to attribute these issues to the performance of the optimizer, not the absence of these trends in general. A similar analysis is required for future work to discover the truth of this.

4.3 The Effects of SRP and N-Body Perturbations on Optimal Transfers

This section takes a look at the effects that perturbations have the shape and quality of the transfer optimization results found in this research. In general, the largest interplanetary perturbations are SRP and n-body effects. Asteroids also experience significant perturbations from the Yarkovsky Effects, but more information about the asteroids is required in order to accurately simulate it. For this section, only SRP and n-body perturbations are considered, and only n-body effects from the Earth-Moon system, Venus, and Jupiter. Other bodies may be relevant for different asteroid transfers but since this work looks solely at NEAs, around 1 AU, these planets have the largest gravitational effects.

For each object, the transfers are run in a similar fashion to the previous sections, though only the minimum required time to see trends is tested (usually 200-1200 days flight time). A single run is done with no perturbations, one with only SRP, and one with SRP and n-body effects. Each of these runs is shown as comparison and without the run statistics. First, a comprehensive comparison is done for the asteroid 2010 FD6. This compares the results of perturbations for all levels of thrust and for all transfer targets. Next, interplanetary transfers in general are examined by comparing 1000 N results for transfers to Earth-trailing orbits. Finally, the effects of perturbations are examined in the context of Earth-Moon transfers by comparing the transfer results using CR3BP dynamics and the PBC4BM dynamics.

It is shown in this section that these perturbations ultimately have no significant impact on the transfer optimization space. Neither SRP nor n-body gravitation effect the shape, the trends, nor the quality of the results for any of the tested cases. Some evidence indicates that this might not be true for even lower levels of thrust than indicated, but even the most dramatic differences in results are minimal.

4.3.1 Effects of Perturbations on Transfer with 2010 FD6

The asteroid 2010 FD6 is a good candidate for these lateral comparisons as it is the only asteroid chosen that is light enough to avoid thrust-saturated profiles, even at the lowest tested thrust of 10 N. This means that the transfers for this asteroid will be characteristic of nearly optimum solutions in general and will give good insight into the behavior of these transfers with subtle differences, such as dynamical perturbations.

Both transfers to Earth-Trailing orbits and transfers to DRO insertion are examined, and at each level of thrust tested in this research. Transfer in the Earth-Moon system are examined in a later section. For each of the figures in this and the following section, the first plot shows the results without any perturbations, the second shows the results with only SRP, and the final plot shows the results with both SRP and n-body effects.

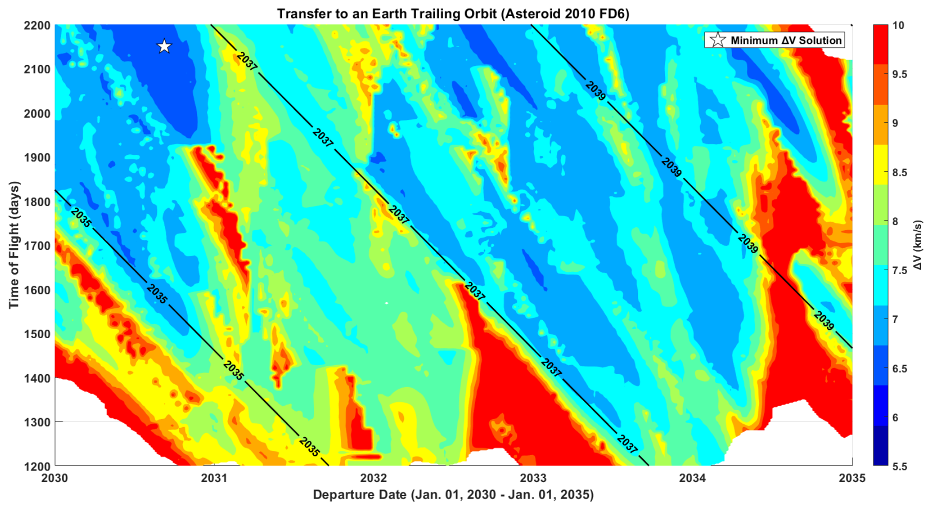

(a) No perturbations

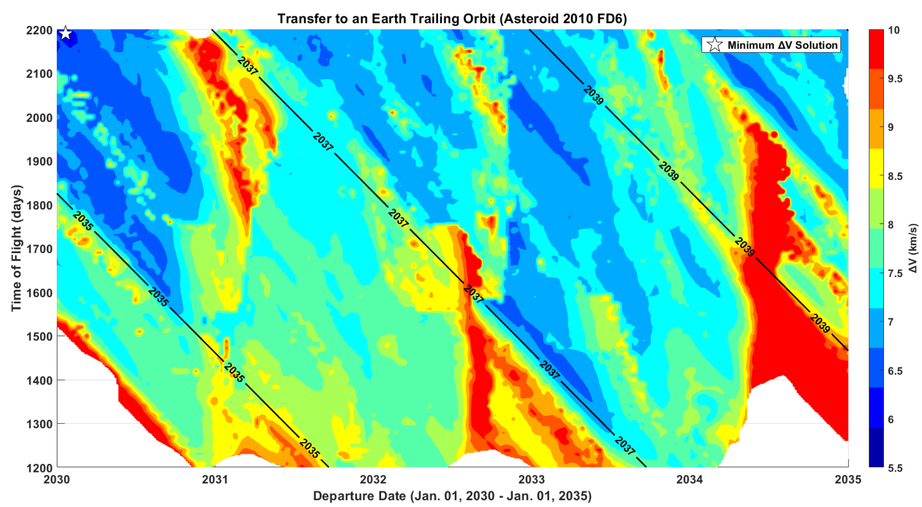

(b) SRP only

Figure 4.26.. Comparison of the effects of perturbations on low impulse (10 N) transfers of 2010 FD6 to an Earth-trailing orbit.

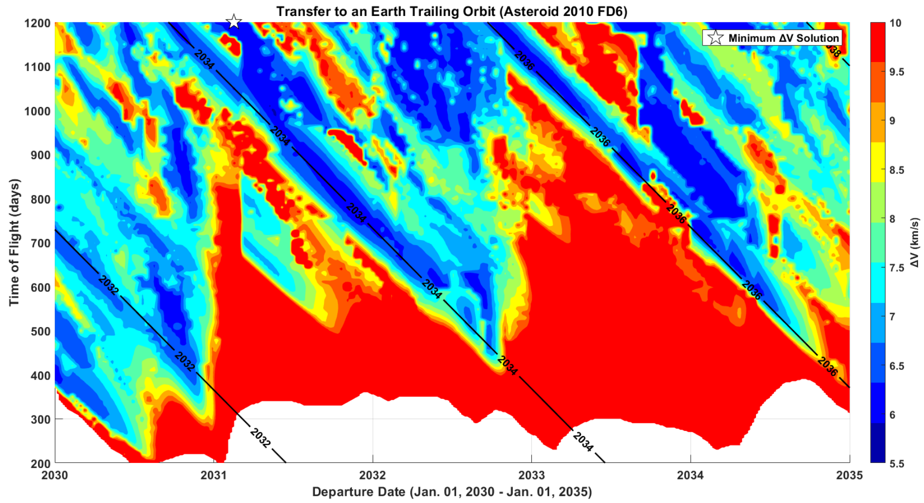

(a) No perturbations

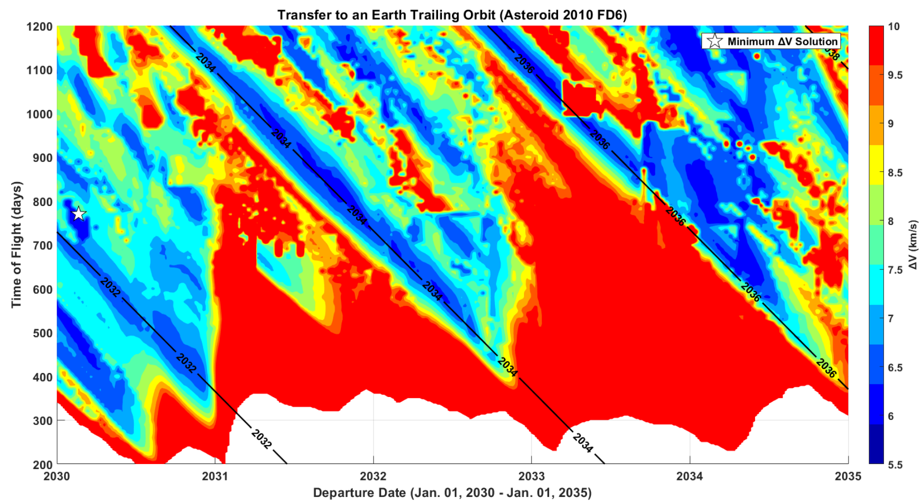

(b) SRP only

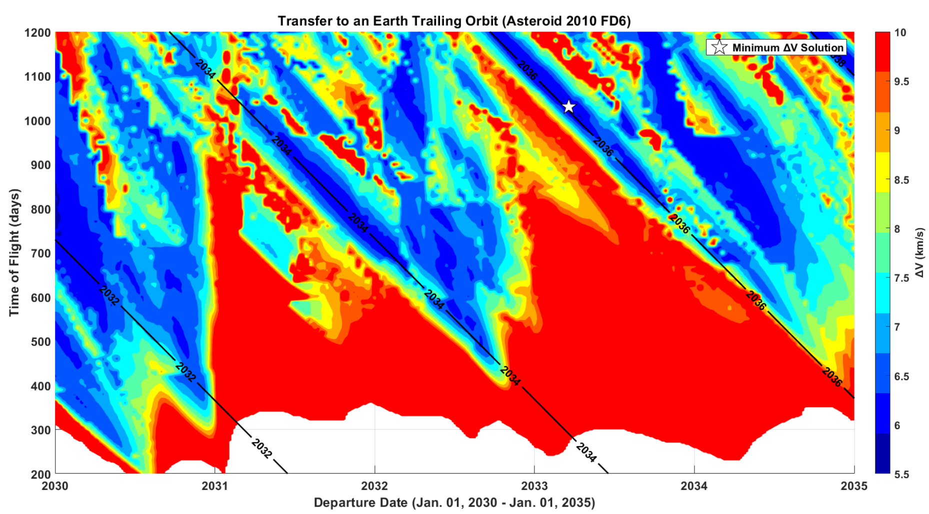

(c) SRP and n-body effects

Figure 4.27.. Comparison of the effects of perturbations on moderate impulse (100 N) transfers of 2010 FD6 to an Earth-trailing orbit.

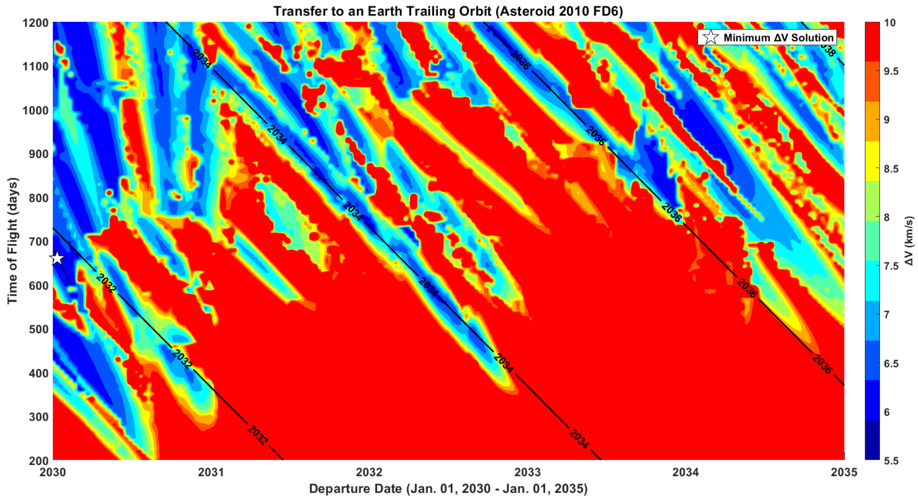

(a) No perturbations

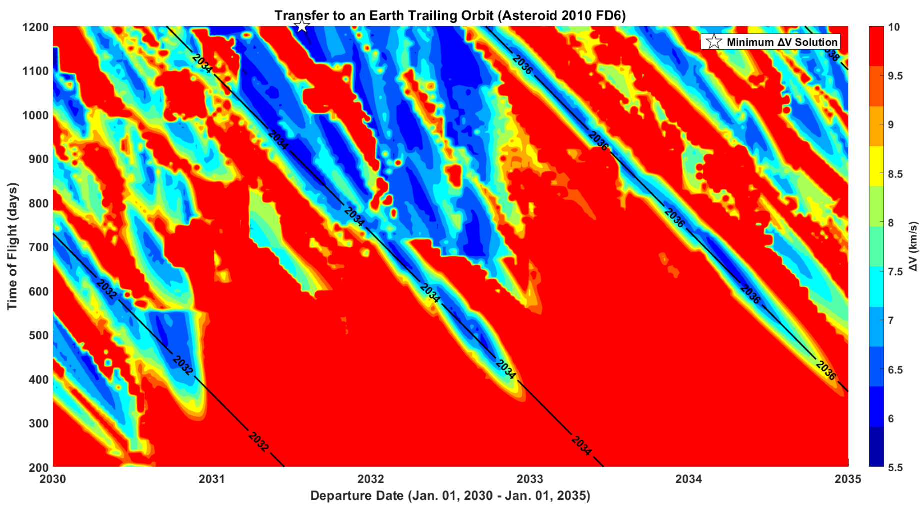

(b) SRP only

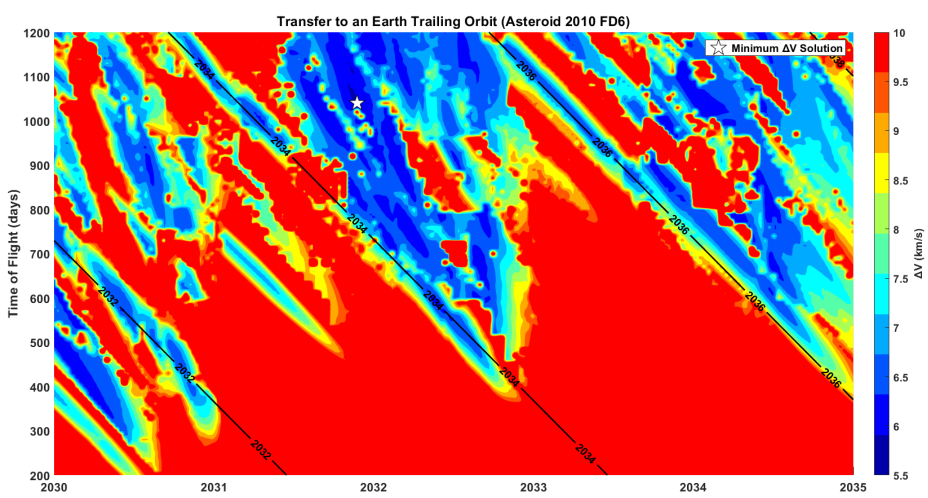

(c) SRP and n-body effects

Figure 4.28.. Comparison of the effects of perturbations on high impulse (1000 N) transfers of 2010 FD6 to an Earth-trailing orbit.

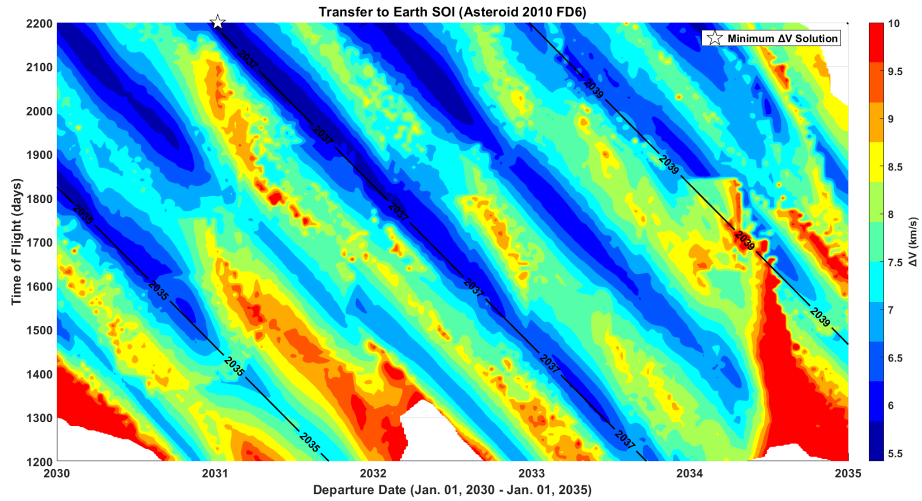

(a) No perturbations

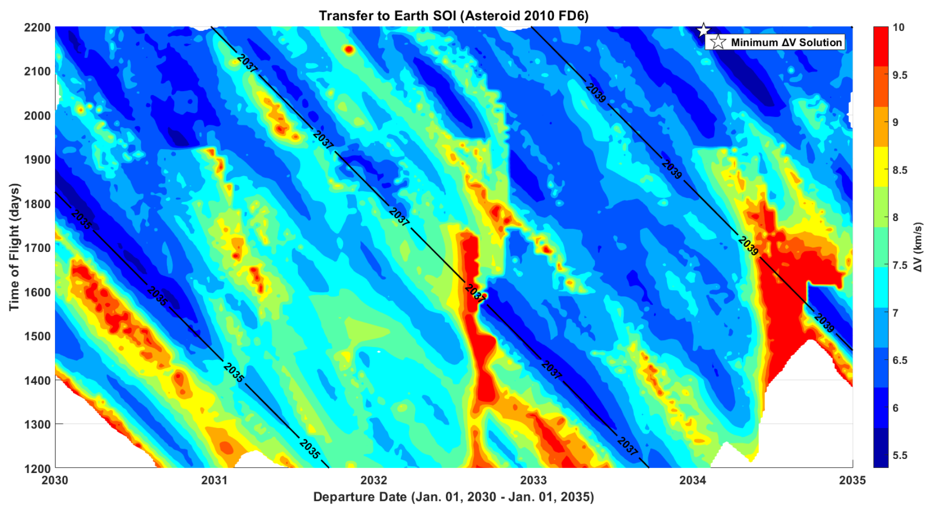

(b) SRP only

Figure 4.29.. Comparison of the effects of perturbations on low impulse (10 N) transfers of 2010 FD6 to Earth Sphere of Influence.

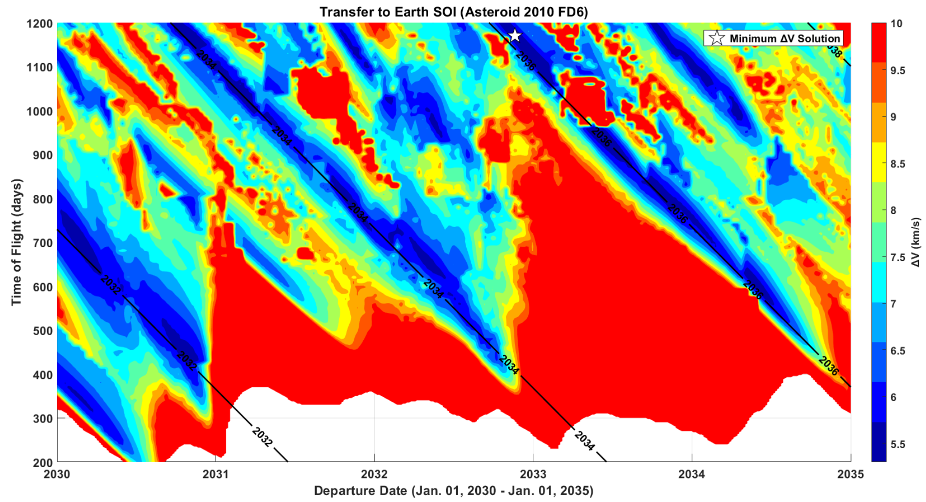

(a) No perturbations

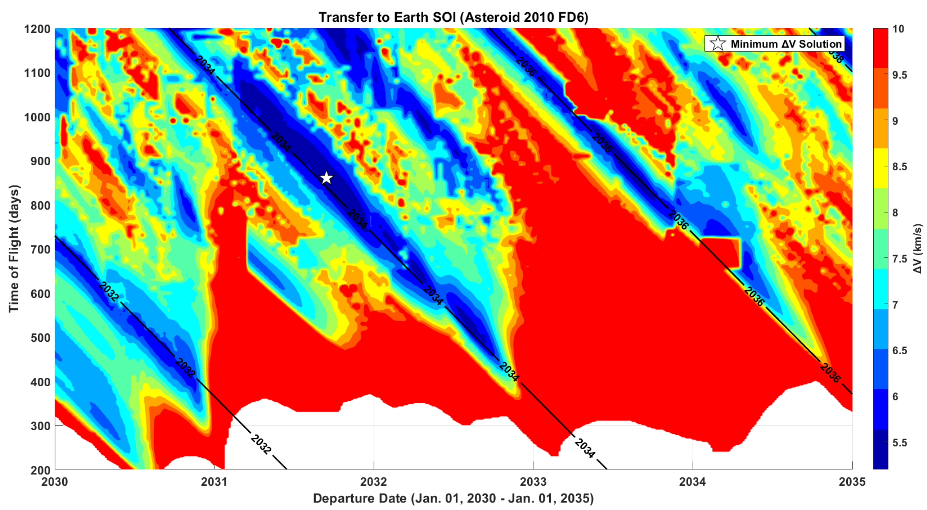

(b) SRP only

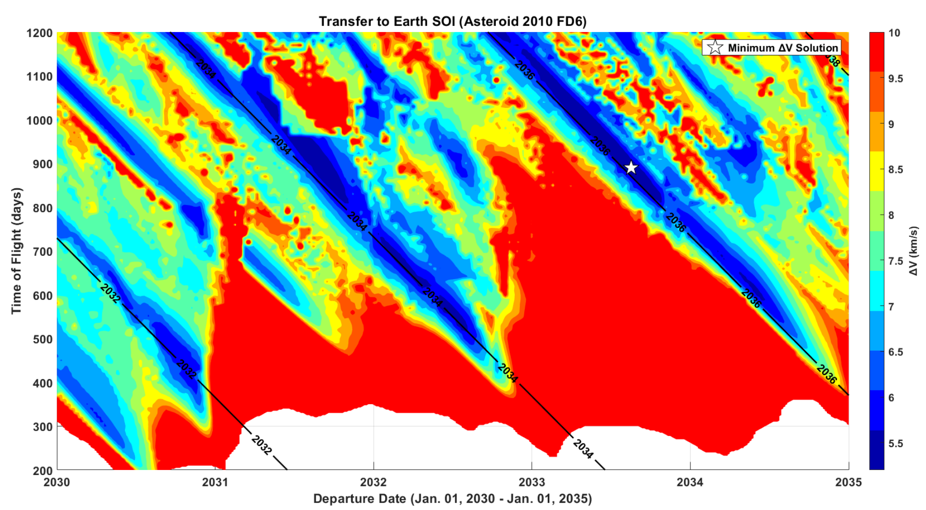

(c) SRP and n-body effects

Figure 4.30.. Comparison of the effects of perturbations on moderate impulse (100 N) transfers of 2010 FD6 to Earth Sphere of Influence.

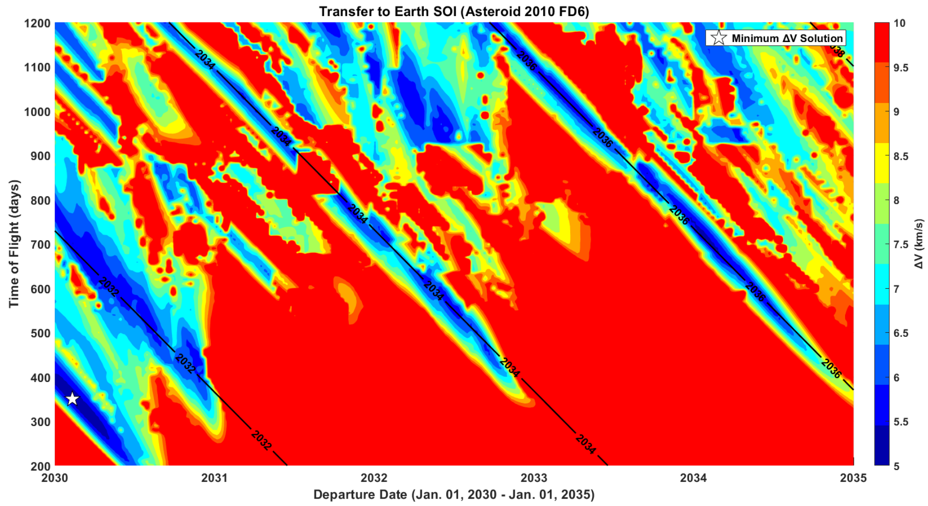

(a) No perturbations

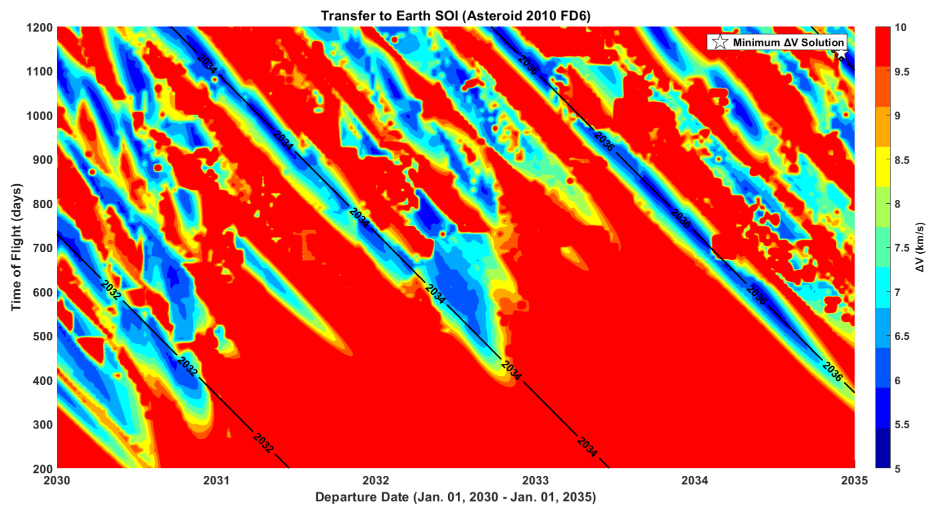

(b) SRP only

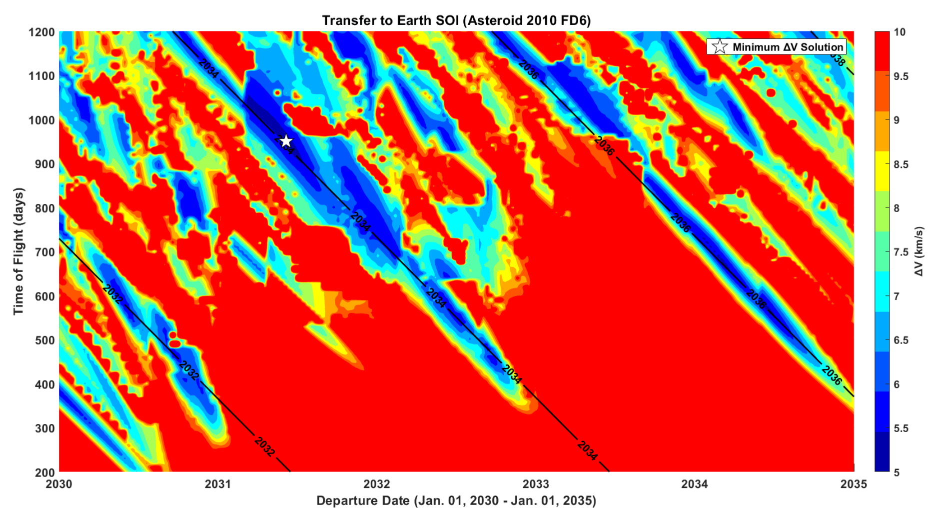

(c) SRP and n-body effects

Figure 4.31.. Comparison of the effects of perturbations on high impulse (1000 N) transfers of 2010 FD6 to Earth Sphere of Influence.

4.3.2 Effects of Perturbations on Transfer to Earth-Trailing Orbits

The effects of perturbations on interplanetary transfers are only examined with respect to transfers to Earth-Trailing orbits. This is because there is no functional difference between the transfers to Earth-Trailing targets and those to DRO insertion. Both will take a similar amount of time so the perturbations will have the same amount of time to affect the transfers. Also, it is evident from the analysis of the effects of perturbations on asteroid 2010 FD6 that there is no significant change observed regardless of the target orbit. It is reasonable to extrapolate this conclusion to other asteroids as well. If any significant differences are observed by the inclusion of perturbations for Earth-Trailing orbits, then an examination of the effects on transfers to DRO insertion would be warranted as well.

In no particular order, the first asteroid examined (barring the already presented discussion on 2010 FD6) is 2012 XB112. The effects of perturbations on these transfers are minimal. With or without any perturbations, the trends for all three cases remain the same, as well as the value of the best solution. There are some minor convergence differences in select regions. The region with the most low-cost solutions changes somewhat between different cases and the small pockets of intermittent high cost solutions appear in different locations.

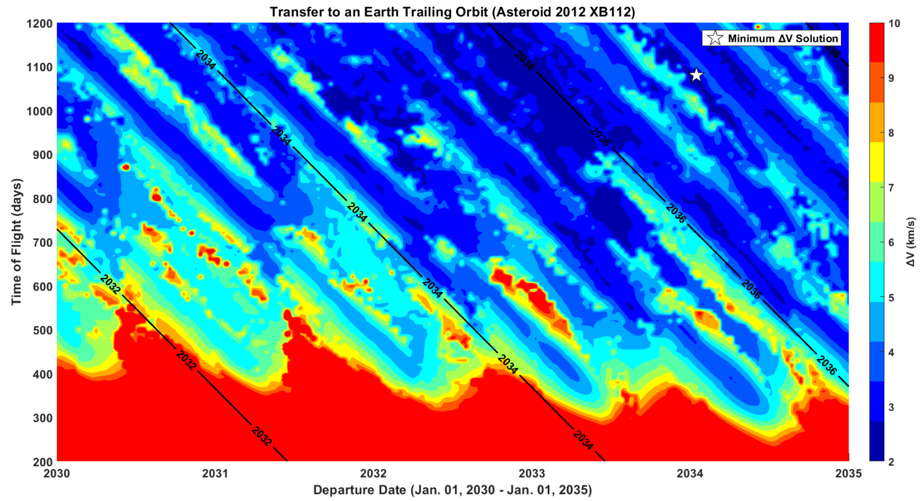

(a) No perturbations

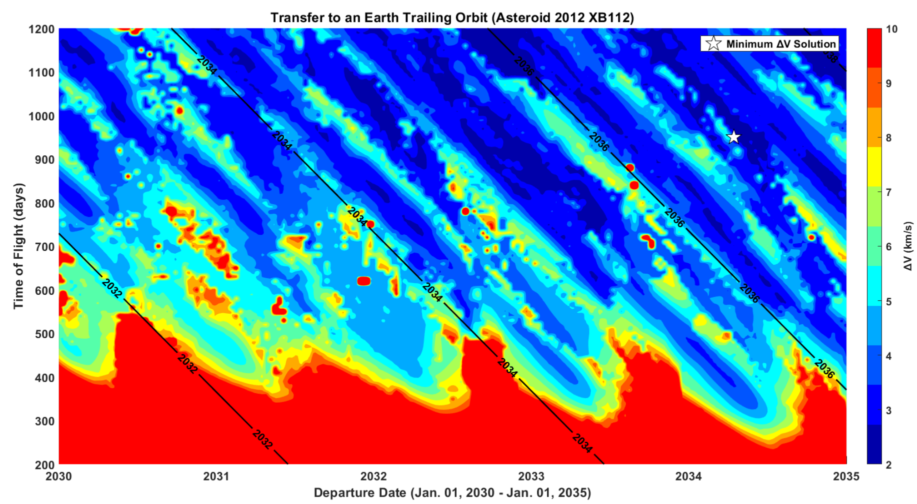

(b) SRP only

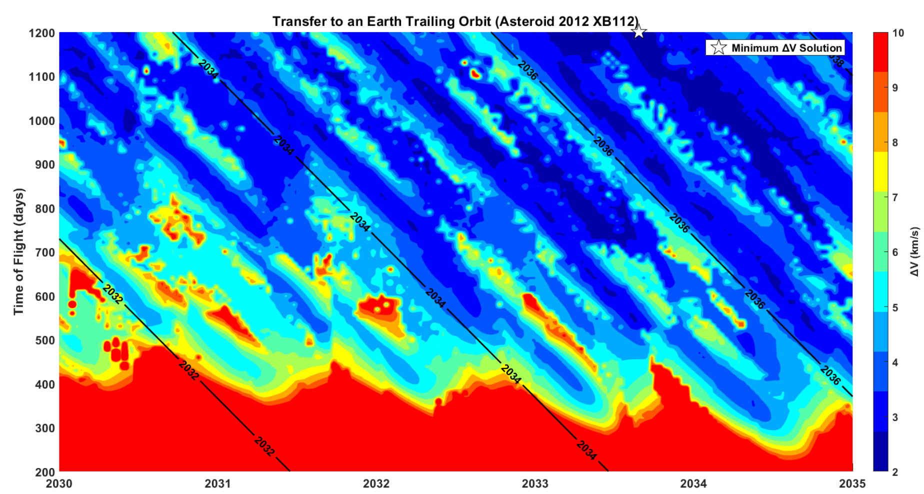

(c) SRP and n-body effects

Figure 4.32.. Comparison of the effects of perturbations on high impulse (1000 N) transfers of 2012 XB112 to an Earth-trailing orbit.

Given the similarity between these results, there is no reason to believe that these differences are a function of the transfers themselves, but the small differences caused by the random aspects of the optimizer itself.

Asteroid 2010 KV7 had some interesting differences. The major trending remained constant, but there are significant differences in the convergence of the different runs. Surprisingly, the run with all perturbations had the most consistent convergence with an almost ideal result. There are not apparent bifurcations in the solutions space and no smatterings of high cost solutions where it is evident that low cost solutions should exist. This improvement on convergence is apparent for the inclusion of just SRP and more so with both SRP and n-body effects.

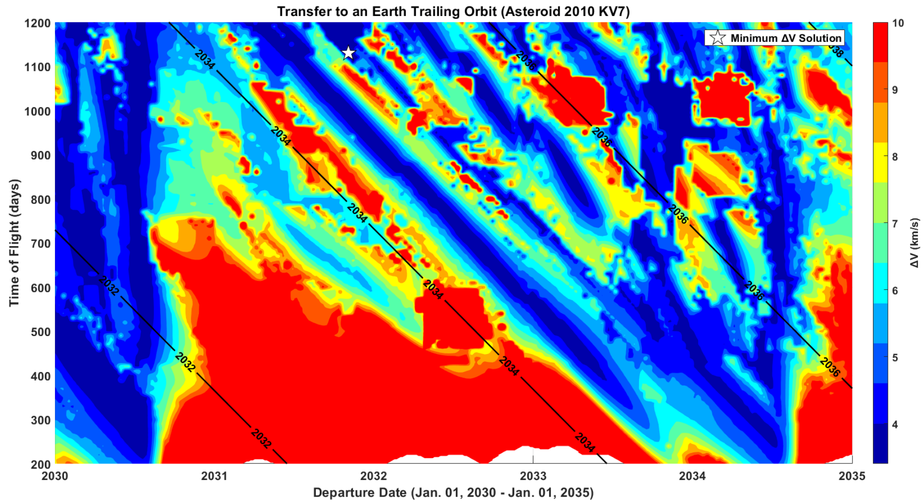

(a) No perturbations

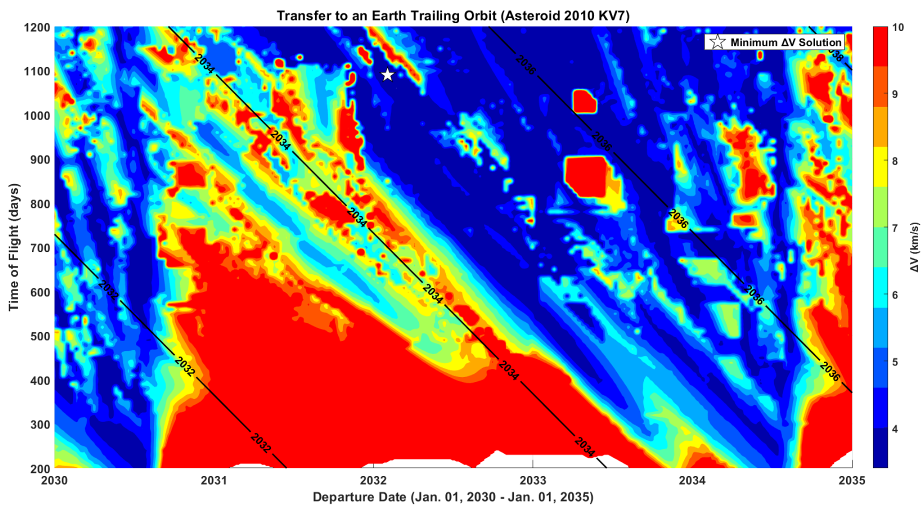

(b) SRP only

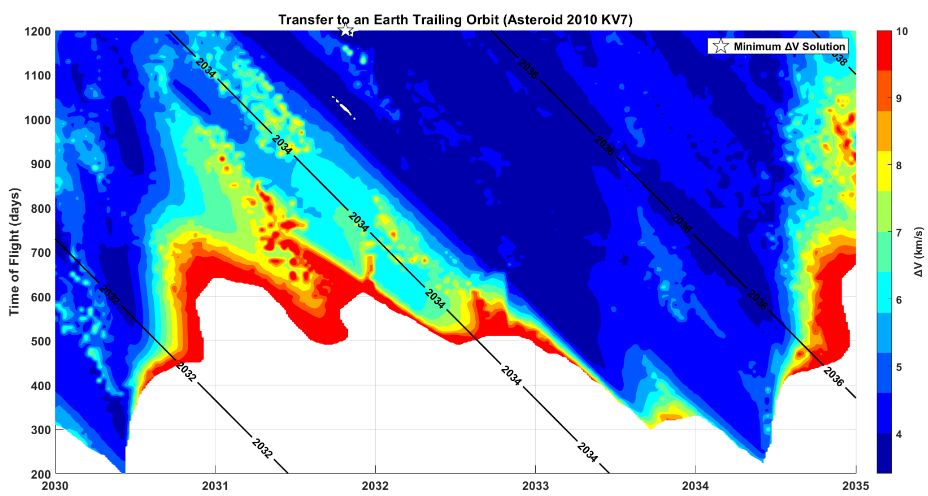

(c) SRP and n-body effects

Figure 4.33.. Comparison of the effects of perturbations on high impulse (1000 N) transfers of 2010 KV7 to an Earth-trailing orbit.

It is difficult to point out the exact reason for this behavior. Since the comparison to MALTO showed similar convergence issues, where high cost solutions appeared where low cost solutions should exist, it is likely that this continues to be the case here. One explanation for the improvement of the solution with the inclusion of perturbations is the increase of the sensitivity of convergence when different effects are added to the dynamics. By adding SRP and n-body effects, the optimizer struggles to meet the constraint (of the forward and backward arcs meetings) unless the solution is more optimal. Small differences in the trajectory cannot be corrected as easily because these perturbations will throw the trajectory off course. By adding more perturbations, it is possible that this inadvertently strains the optimizer enough that is has to produce better solutions at more points in the solution space in order to converge at all. It is important to note that this improvement is only in the overall quality of the results. This inclusion of perturbations does not improve the quality of the best solution found, it only increases the number of solutions that are close to that found minimum.

The next asteroid examined, 2010 TN4, a thrust saturated transfer, even at 1000 N thrust, shows a similar trend as 2010 KV7, though less dramatic There are small differences between all three cases, but there does seem to be more consistent convergence for the case with all perturbations.

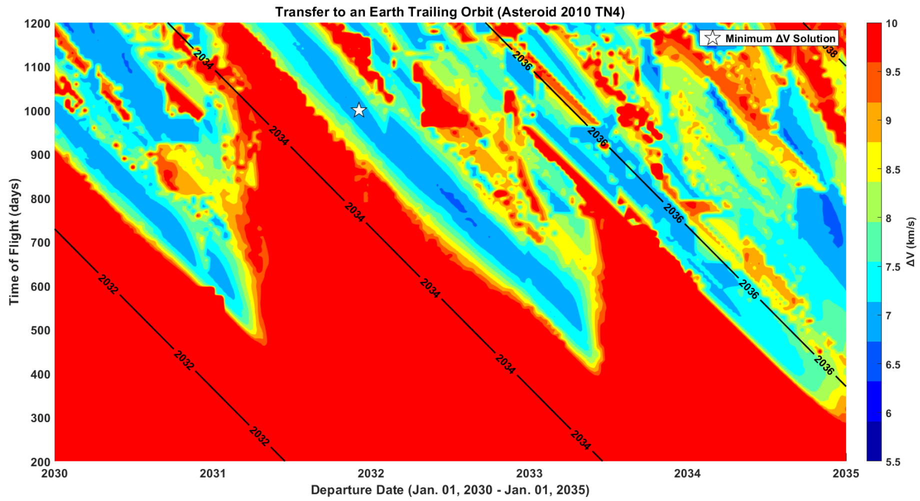

(a) No perturbations

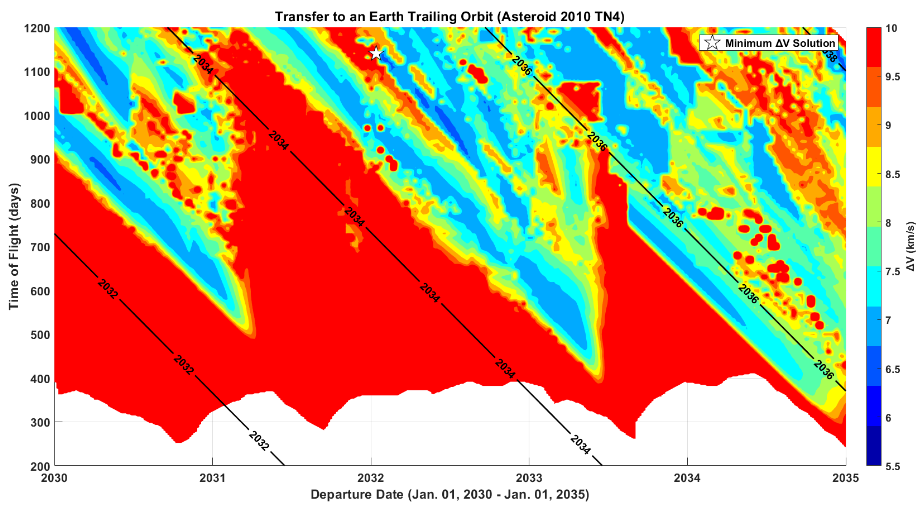

(b) SRP only

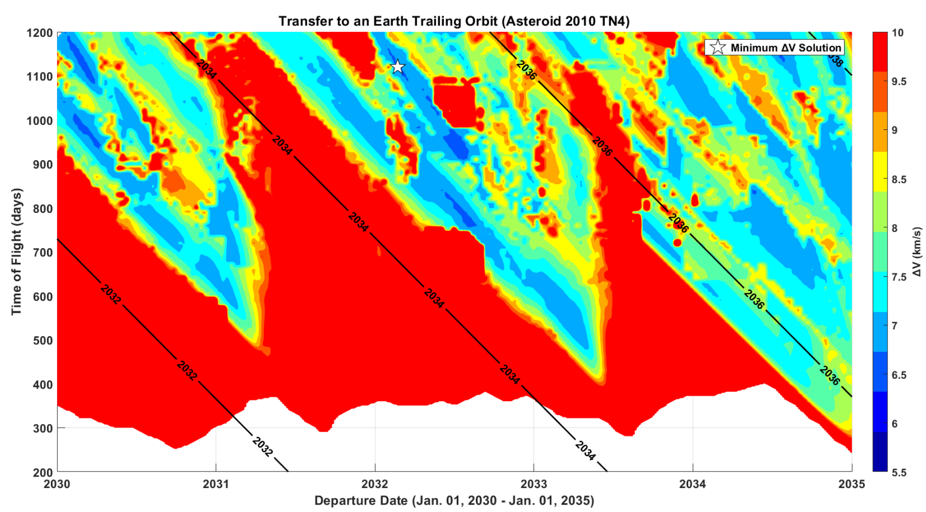

(c) SRP and n-body effects

Figure 4.34.. Comparison of the effects of perturbations on high impulse (1000 N) transfers of 2010 TN4 to an Earth-trailing orbit.

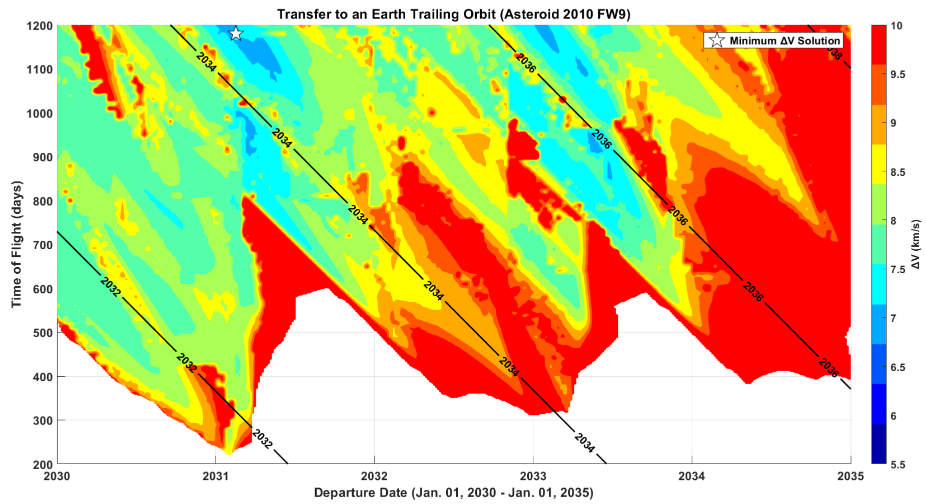

(a) No perturbations

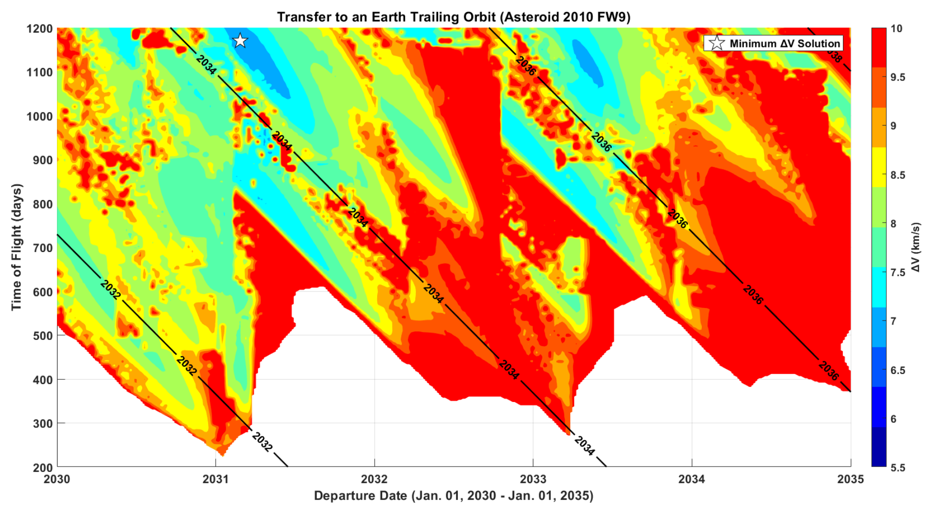

(b) SRP only

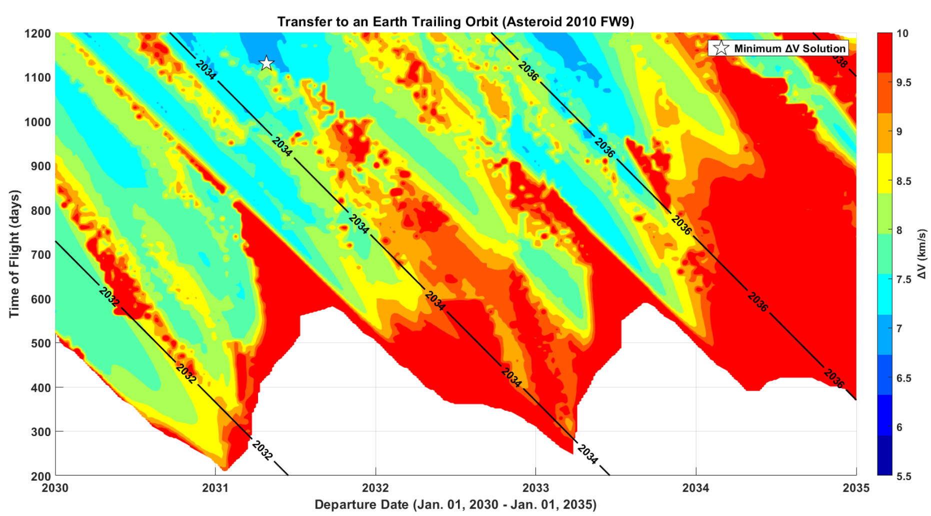

(c) SRP and n-body effects

Figure 4.35.. Comparison of the effects of perturbations on high impulse (1000 N) transfers of 2010 FW9 to an Earth-trailing orbit.

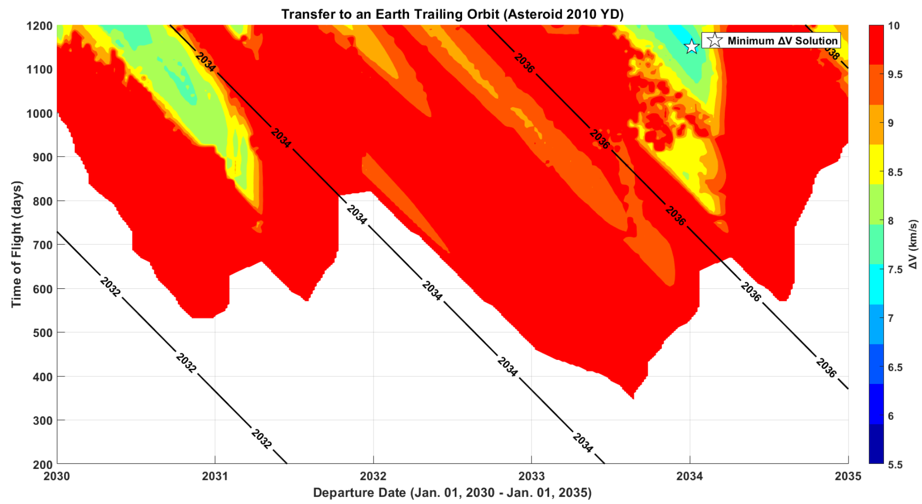

(a) No perturbations

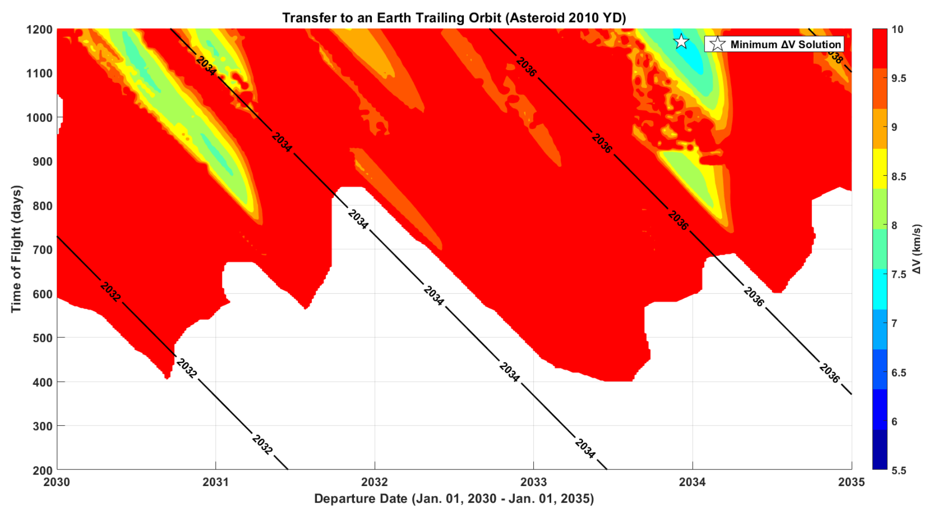

(b) SRP only

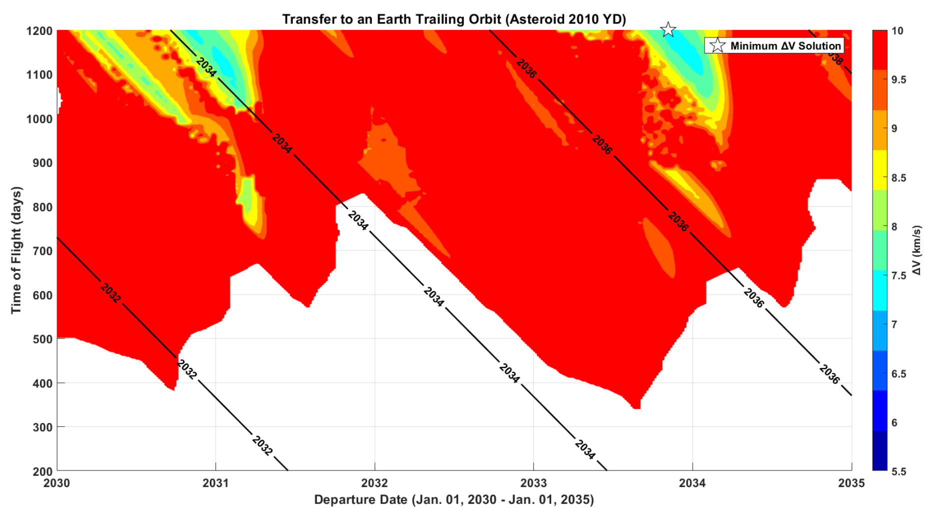

(c) SRP and n-body effects

Figure 4.36.. Comparison of the effects of perturbations on high impulse (1000 N) transfers of 2010 YD to an Earth-trailing orbit.

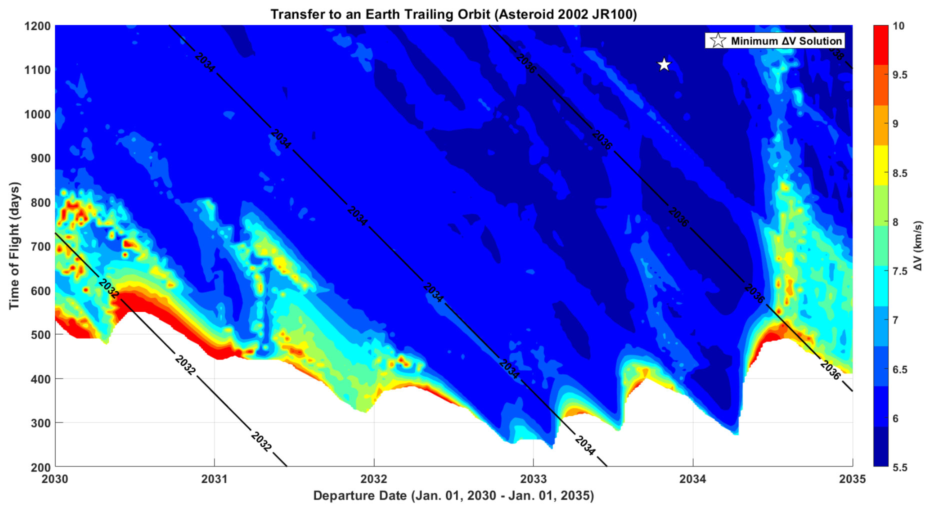

(a) No perturbations

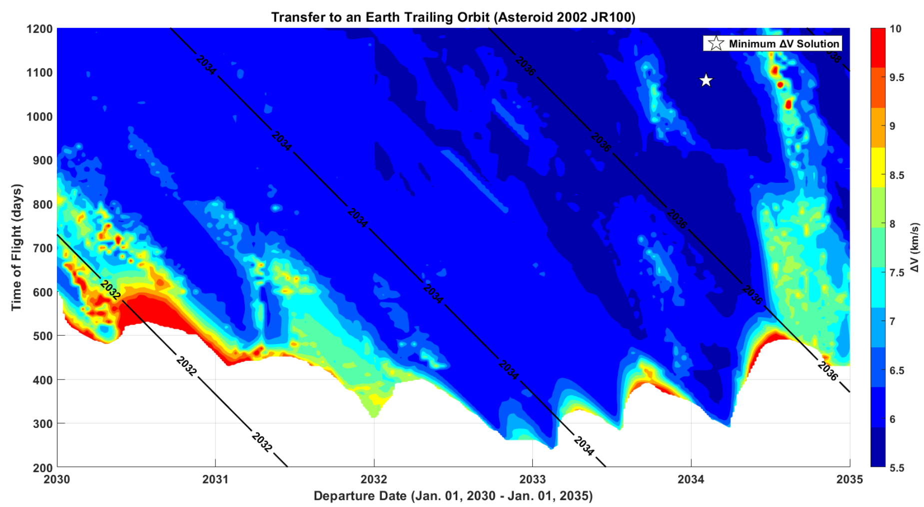

(b) SRP only

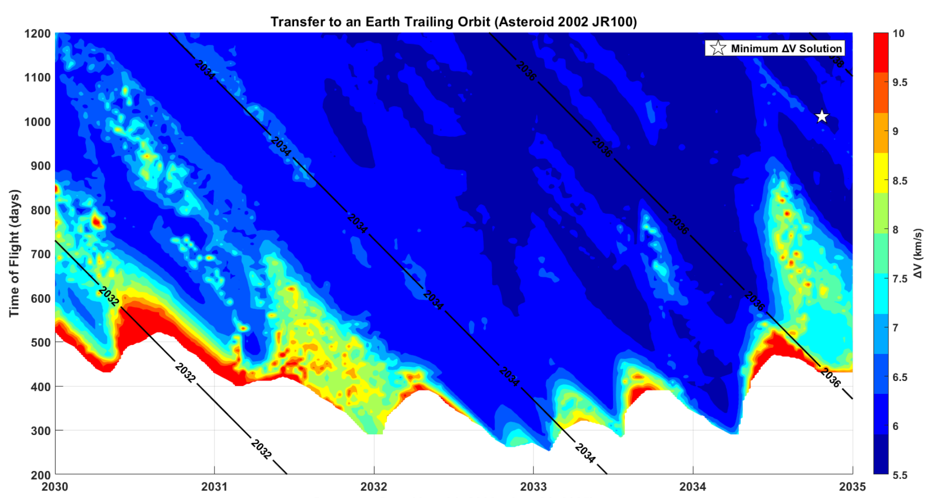

(c) SRP and n-body effects

Figure 4.37.. Comparison of the effects of perturbations on high impulse (1000 N) transfers of 2002 JR100 to an Earth-trailing orbit.

4.3.3 The Effects of SRP and Extra N-Body Perturbations on Earth-Moon Transfers to DROs

Given the evidence thus far that these perturbations do not significantly affect the optimized solution space, a single comparison between the CR3BP and the perturbed BC4BM is enough to confirm the trending. Figure 4.38 shows the comparison of the same transfer from the DRO insertion condition to the target DRO given the two sets of dynamics. As is the case with other results, the addition of the perturbations does not seem to affect the overall trends of the solution space. There is a notable improvement, however, in the convergence of the case with additional perturbations. This is consistent with previous analysis of the effects of perturbations, and, again, a remark on the stability and performance of the optimizer itself. The quality of the best results does not change between these two cases.

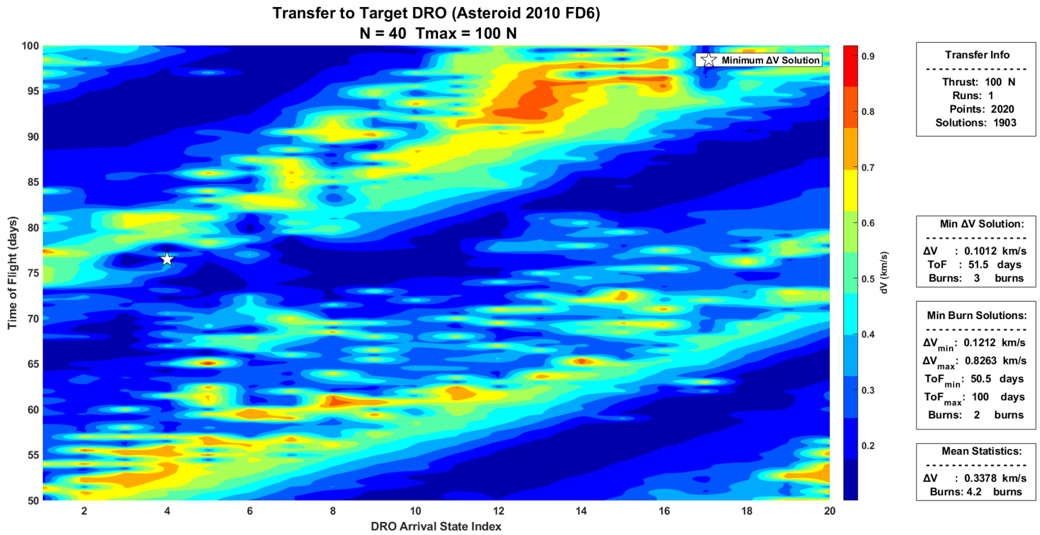

(a) CR3BM

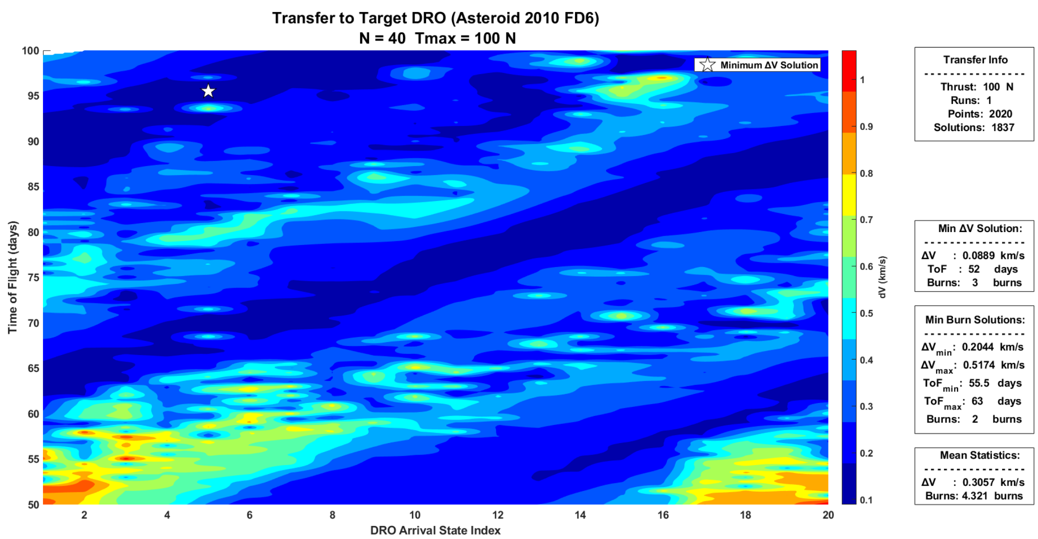

(b) PBC4BM

Figure 4.38.. Comparison of Moderate Impulse (100 N) Transfer of 2010 FD6 from Earth Sphere of Influence to Target DRO with CR3BP dynamics (a) and PBC4BM dynamics (b).

5. SYSTEM CONCEPT EVALUATION

5.1 Estimating Transfers for Mission Design

The transfer optimization done for this work is only one part of the story. Since one of the major goals of this work is to establish a general methodology and framework for designing asteroid capture missions, the optimized transfers cannot be taken merely as standalone data. A more comprehensive view of the transfer solution space can be informed by these optimized results so transfer costs and mission timelines can be constructed from first order estimations, and without the difficulty of optimizing any or all possible candidates under consideration. Asteroid selection is informed by the cost and required transfer time so the ability to find rough estimations of these values quickly is necessary for high-level mission design studies.

This section attempts to develop models for both the transfer cost of fuel-optimized transfers, as well as the time-of-flight of these transfers. These results are then used to establish bounds on the characteristics of asteroids that are viable candidates for capture.

5.1.1 Estimating Transfer Costs for Fuel-Optimum Transfers

The energy-minimum analytic transfer, and the lower bound for the fuel costs of any two-body orbital transfer, is the Hohmann transfer. Hohmann transfers are the most efficient two-burn, impulsive transfers, that give a good first order validation of optimization results and get a quick idea of the actual transfer costs. Hohmann transfers have maneuvers placed at the apogee of the outer orbit and the perigee of the inner orbit, the order depending on whether the starting orbit is larger or smaller. The contrary, using the apogee of the inner orbit and the perigee of the outer orbit has been shown to be less efficient [?]. Thus, the Hohmann transfer orbit is being defined as having the apogee of the outer orbit and the perigee of the inner orbit, making the total ΔV the difference between the velocity at the apogee of the outer orbit and the transfer orbit plus the difference between the velocity at the perigee of the inner orbit and the transfer orbit.

$$\Delta V_{hohmann} = |v_{a\ (outer)} - v_{a\ (hohmann)}| + |v_{p\ (inner)} - v_{p\ (hohmann)}| \tag{5.1}$$

where the velocity at apogee and perigee are given by

$$\begin{aligned} v_a &= \frac{r_a}{h} \\ v_p &= \frac{r_p}{h} \end{aligned} \tag{5.2}$$

where h is the specific orbital angular momentum of the orbit. Since the transfer orbit is based on the apogee and perigee of the initial and final orbit, the entire transfer cost can be formulated in terms of only those values.

$$\begin{aligned} \Delta V_{hohmann} &= |\frac{r_{a\ (outer)}}{h_{(outer)}} - \frac{r_{a\ (outer)}}{h_{(hohmann)}}| + |\frac{r_{p\ (inner)}}{h_{(inner)}} - \frac{r_{p\ (inner)}}{h_{(hohmann)}}| \\ &= \frac{r_{a\ (outer)}}{h_{(hohmann)}}\left|\frac{h_{(hohmann)}}{h_{(outer)}} - 1\right| + \frac{r_{p\ (inner)}}{h_{(hohmann)}}\left|\frac{h_{(hohmann)}}{h_{(inner)}} - 1\right| \end{aligned} \tag{5.3}$$

The h terms can be formulated in terms of the apogee and perigee radii.

$$\begin{aligned} h^2 &= \mu a(1 - e^2) \\ &= \mu\big(\frac{1}{2}(r_a + r_p)\big)\big(1 - (\frac{r_a - r_p}{r_a + r_p})^2\big) \\ &= \frac{\mu}{2}\big(r_a + r_p\big)\big(\frac{(r_a + r_p)^2 - (r_a - r_p)^2}{(r_a + r_p)^2}\big) \\ &= \frac{\mu}{2}\big(\frac{(r_a^2 + 2r_ar_p + r_p^2) - (r_a^2 - 2r_ar_p + r_p^2)}{r_a + r_p}\big) \\ &= \frac{\mu}{2}\big(\frac{4r_ar_p}{r_a + r_p}\big) \\ &= 2\mu\big(\frac{r_ar_p}{r_a + r_p}\big) \end{aligned} \tag{5.4}$$

This formulation for the cost of the Hohmann transfer can be calculated to estimate the cost of transfers. This is what is done for the cost estimations in the previous section. Though this method is commonly used, it is not necessarily the most accurate estimation for fuel-optimized transfers. In order to quantify the effectiveness of this model, the Hohmann transfer is compared with other analytic methods of matching orbital elements. Specifically, the analytic forms for simple inclination matching and apse line matching costs are examined as well.

Inclination matching costs are found using the following equation:

$$\Delta V_{inc} = 2v_{apogee\ (outer)} \sin\left(|i_{outer} - i_{inner}|/2\right) \tag{5.5}$$

This assumes that the node for the outer orbit is at the apogee of the outer orbit. While this will not be true in most cases, it does provide a theoretical minimum cost for inclination matching costs.

The analytic costs for matching the apse line are found on the outer orbit using:

$$\Delta V_{apse} = \sqrt{2v_{burn}(1 - \cos(\eta))} \tag{5.6}$$

where

$$v_{burn} = \sqrt{\mu\left(\frac{2}{r_{burn}} - \frac{1}{a_{outer}}\right)} \tag{5.7}$$

$$r_{burn} = \frac{h_{outer}^2}{\mu(1 + e_{outer}\cos(TA))} \tag{5.8}$$

$$\tan\left(TA - \frac{\pi}{2}\right) = \frac{-\sin(\eta)}{1 - \cos(\eta)} \tag{5.9}$$

$$\eta = \omega_{outer} - \omega_{inner} \tag{5.10}$$

These different analytic costs are used as the basis for an analytic estimation model. The analytic model predicts the transfer cost by adding different combinations of the Hohmann transfer cost, the inclination cost, and the apse line matching costs. Each of these different combinations aree compared to the optimized costs found in the previous chapter to determine the accuracy of each. The results are summarized in the table below. Each of the numbers in the table represents the mean, and standard deviation of the actual results compared to the estimated model according to:

$$Predictive\ Value = \frac{\Delta V_{actual}}{\Delta V_{model}} \tag{5.11}$$

A mean predictive value close to 1 means that the model predicts the actual cost well, while a value lower than one means the model overestimates the cost, over one underestimates the cost. Since the mean of this predictive value in and of itself is arbitrary, a much more important metric for determining the quality of the analytic model is the standard deviation. The standard deviation alone, however, will not necessarily be a useful metric. If the mean predictive value is extremely low compared to a high mean predictive value with equivalent standard deviations, this means that the deviation of the model with the higher mean will be lower on average. There are also cases with extremely low mean values. This arbitrarily lowers the value of the standard deviation, making it seem like model predicts the transfer costs better than it does. As such, the best metric for determining the quality of the model is the standard deviation normalized to the mean.

It is evident that for both transfer to Earth-trailing orbits and to DRO insertion that the best model for predicting the cost of the fuel-optimum transfer is the combination of the Hohmann transfer costs and the inclination matching costs. This is also true when all of the transfer data is considered together as well, just barely outperforming the Hohmann transfer costs alone. An estimation model that uses only the Hohmann transfer costs without considering inclination or apse line matching is an underestimate on average, and adding the apse line correction, in all cases, dramatically overestimates the transfer cost. The predictive values when using Hohmann transfer and inclination matching costs for the tested transfers are shown in Figure 5.1.

If both data sets are combined, the mean predictive value is 1.07483 with a standard deviation of 0.0929282, and the lower 95% confidence interval (LCI) is 1.10409. This model can then be used to predict the fuel-optimal costs of transfers asteroids.

Table 5.1.. Comparison of the different analytic models used to estimate fuel-optimal transfers costs. The mean is given by μ, and the standard deviation by σ

Ratio of Optimized Transfer Costs to Analytic Transfer Costs			
Transfers to Earth-Trailing Orbits			
Analytic Form	μ	σ	σ/μ
Hohmann	1.19107	0.163974	0.13767
Hohmann + Inc	1.06134	0.131192	0.12361
Hohmann + Apse	0.40855	0.09847	0.24102
Inc + Apse	0.603134	0.210848	0.349587
All	0.39167	0.0906779	0.231516

Transfers to DRO Insertion			
Analytic Form	μ	σ	σ/μ
Hohmann	1.26951	0.241122	0.189933
Hohmann + Inc	1.06472	0.0968795	0.090991
Hohmann + Apse	0.350923	0.0747421	0.212987
Inc + Apse	0.479402	0.180614	0.376749
All	0.334917	0.070725	0.211172

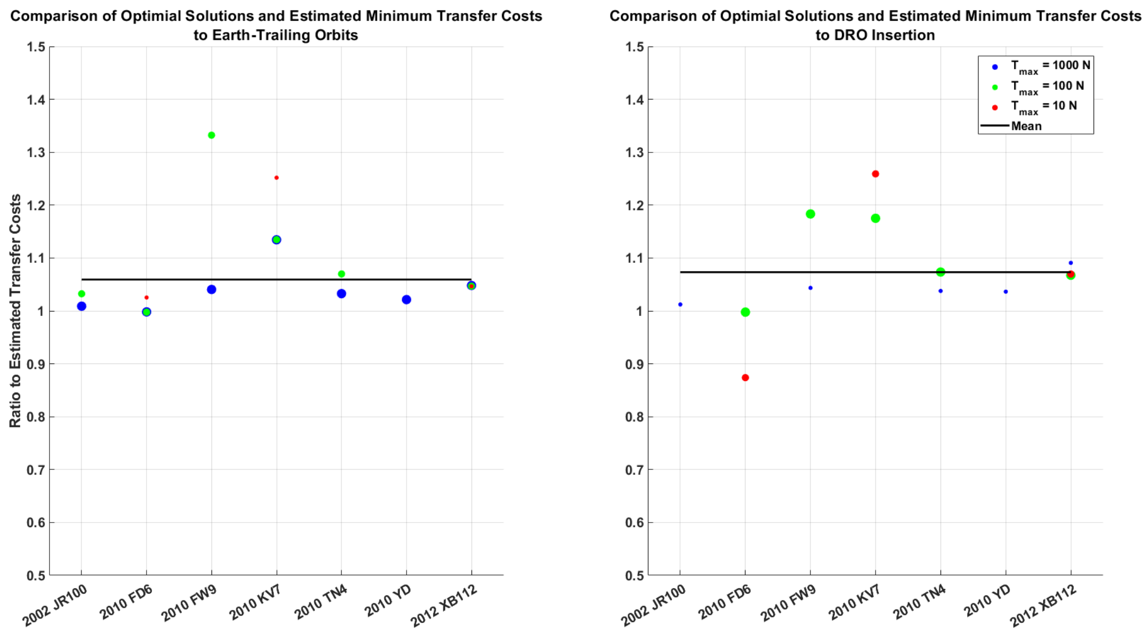

Figure 5.1.. The ratio of the actual to estimated costs for optimized transfers

Assuming the transfer cost can be safely estimated by using the 95% confidence interval as an upper bound and adding a 10% margin for mission design considerations, the total estimated mission cost can be calculated by the following formula.

$$\begin{aligned} \Delta V_{tot} &\leq (\Delta V_{\text{predicted}} * LCI)(1 + \text{margin}) \\ &\leq \big((\Delta V_{\text{hohmann}} + \Delta V_{\text{inc}}) * 1.10409\big)(1 + 0.10) \\ &\lessapprox (\Delta V_{\text{hohmann}} + \Delta V_{\text{inc}}) * 1.21 \end{aligned} \tag{5.12}$$

Using the 99% confidence interval in place of the 95% confidence interval increases this multiplier to approximately 1.23, using the 99.9% confidence interval increases it to approximately 1.25, and using the mean plus the standard deviation increases it to approximately 1.28. Which of these metrics is most appropriate to use as an upper bound depends on the claims being made about the model.

The fact that the standard deviation is greater than the 99% confidence interval is normal. The equation for the lower confidence interval (also called the one-sided confidence interval) is given by:

$$LCI = t^* \frac{\sigma}{\sqrt{N}} \tag{5.13}$$

where t^* is the t-statistic (assumed to be a normal distribution), and N is the number of samples. A one-sided lower confidence interval of 95% has a t^* value of approximately 1.753. This means that the 95% LCI will always be lower than the standard deviation where $\frac{t^*}{\sqrt{N}} < 1$, or $N > 3$. For a 99% confidence interval, the value of t^* for a one-sided confidence interval is 3.733, meaning $N > 9$. Since there are more than ten samples here, both of these models should have a standard deviation greater than the given lower confidence intervals. It is important to note that the confidence interval does not represent a probability that the population lies within the given interval. Confidence intervals are a measure of certainty regarding the estimations of these models. Cox describes 90% confidence intervals in terms of repeated samples: "Were this procedure to be repeated on numerous samples, the fraction of calculated confidence intervals (which would differ for each sample) that encompass the true population parameter would tend toward 90%." [64]. Applying this interpretation to these predictive models, this would mean that the mean value of the transfer cost would tend to fall below the calculted confidence interval in 95% of cases.

For this analysis, the 95% LCI is used. Data points outside this region for the optimized transfers are likely saturated transfers, meaning the true fuel-optimized solution would be underneath this bound. This behavior is evident for 2010 FW9 which, in both ET and DRO cases, has a significantly higher fuel cost for 100 N transfers compared to 1000 N transfers. This suggests that the 100 N case is still a thrust-saturated case, and the 1000 N result is more likely near to the true optimal solution. The asteroid 2010 KV7 also exhibits similar behavior. The one case in which this thrust saturation would not explain the quality of the results in comparison to the model would be for the asteroid 2010 FD6 transfer to DRO insertion. This is the only case where a lower thrust solution found a significantly more efficient transfer than a higher thrust case.

5.1.2 Estimating Transfer Flight Times for Fuel-Optimum Transfers

In the same way that the Hohmann transfer acts as lower bound for transfer costs, a similar lower bound can be constructed for transfer flight times. The minimum possible flight time can be found by taking the minimum required momentum transfer, that required for a Hohmann transfer, and a given level of thrust, and dividing the former by the latter. This is equivalent to the total time required to impart the minimum required momentum into the system if the thrusters burn constantly.

$$t_{min} = \frac{\Delta p_{hohmann}}{T_{max}} \tag{5.14}$$

This is an easy-to-calculate lower bound on the transfer time and gives a quick look at whether or not transferring a given body is even possible. Optimal transfers are not thrust-saturated so this model will not give accurate estimations of fuel-optimal transfer times.

It is also possible to use the estimation of the transfer costs as a more realistic lower bound on the transfer time.

$$\begin{aligned} t_{min\,-\,est} &= \frac{\Delta p_{tot}}{T_{max}} \\ &\leq \frac{m\ \Delta V_{tot}}{T_{max}} \\ &\lessapprox \frac{1.21(\Delta V_{hohmann} + \Delta V_{inc})m}{T_{max}} \end{aligned} \tag{5.15}$$

Developing a more accurate model for estimating transfer times involved several different methods, many of which failed to produce consistent results. Part of the difficulty is that transfer times of optimal solutions are sensitive, and it is common for the optimizer to produce several nearly optimal solutions with very different flight times. There also exists some large flight time at which any transfer could eventually approach the transfer costs of a Hohmann transfer. This implies that the optimizer solutions will get slightly better as the maximum tested flight time is increased more and more. As such, it is difficult to say whether any given model could properly correlate the given data or whether or not the given data displays a consistent type of transfer that could be modeled accurately.

Even with these difficulties, a model is presented here that gives enough of a correlation to create a reasonable bound for flight times. The outline for this model relies on the assumption that the total transfer time can be correlated to a series of walkdown Hohmann transfers. For each transfer, a number of intermediate orbits is established that corresponds to the total number of steps needs to go from the initial to the final orbit. Zero intermediate orbits would correspond to a single Hohmann transfer from the initial orbit to the final orbit.

The other crucial assumption in this model is that there is an optimal amount of momentum exchange each orbit that is directly proportional to the period of that orbit.

$$(\frac{\Delta p}{rev})_{optimal} = \eta P T_{max} \tag{5.16}$$

where η is some proportionality constant. This assumption is based on the principles of Q-Law, which point out that it is only optimal to burn at certain points in the orbit or if the burn location and direction have enough optimality [65, 66]. In Q-Law, each point and burn direction in the orbit is defined as having a certain optimality with respect to changing the current state to the final state. With respect to changing a single variable, semimajor axis for example, this implies that similar parts of the orbit with have similarly optimal conditions and burning at those same locations will result in the most optimal transfer. If each revolution causes a similar change in orbit, it is reasonable to assume that burning will occur at the same range of true anomaly values within each intermediate orbit during the transfer. If this is true, that means that burning occurs for the same percentage of the orbit for each revolution.

The total momentum exchange per revolution is used as an impulsive upper limit that the required ΔV for each intermediate Hohmann transfer cannot exceed. Similar to the Sims-Flanagan approach used for the optimization in the earlier chapters, the idea is that this total accumulated momentum exchange can be approximated by a single impulse.

For each transfer, an initial and final orbit are determined. The number of intermediate orbits is set to 0, and the associated Hohmann transfer is calculated. The required impulse from this Hohmann transfer is found and compared to Eq. 5.16. If the required ΔV to perform this Hohmann transfer is exceeded, the process is repeated with the number of intermediate orbits set to 1, and so on. The total transfer time is then calculated as the sum of the half-periods of all the Hohmann transfers, and the intermediate orbits.

$$P = 2\pi\sqrt{\frac{a^3}{\mu}} \tag{5.17}$$

$$\begin{aligned} t_{tot} &= \sum_{i=0}^{n} \pi\sqrt{\frac{a^3_{i \rightarrow (i+1)}}{\mu}} + \sum_{i=1}^{n} \pi\sqrt{\frac{a^3_i}{\mu}} \\ &= \frac{\pi}{\sqrt{\mu}}\left[\sum_{i=0}^{n} a^{\frac{3}{2}}_{i \rightarrow (i+1)} + \sum_{i=1}^{n} a^{\frac{3}{2}}_i\right] \end{aligned} \tag{5.18}$$

Here, i represents the "ith" intermediate orbit and $i \rightarrow (i+1)$ represents the Hohmann transfer from the "ith" intermediate orbit to the "(i+1)th" intermediate orbit. The initial orbit corresponds to $i = 0$, and the final orbit corresponds to $i = n + 1$. The semimajor axis of each intermediate orbit is determined by evenly spacing the apogee and perigee of intermediate orbits between those of the initial and final orbit. This also corresponds to evenly spacing the semimajor axis of each orbit as well.

$$r_{a\,i} = r_{a\,0} + \frac{(r_{a\,(n+1)} - r_{a\,0})}{n+2}i \tag{5.19}$$

$$r_{p\,i} = r_{p\,0} + \frac{(r_{p\,(n+1)} - r_{p\,0})}{n+2}i \tag{5.20}$$

$$a_i = a_0 + \frac{(a_{(n+1)} - a_0)}{n+2}i \tag{5.21}$$

The semimajor axis of the Hohmann transfers can be determined using the associated apogee and perigee values.

$$\begin{aligned}
a_{i \to (i+1)} &= \frac{1}{2}(r_{a\,i} + r_{p\,(i+1)}) \\
&= \frac{1}{2}\Big[\big(r_{a\,0} + \frac{(r_{a\,(n+1)} - r_{a\,0})}{n+2}i\big) + \big(r_{p\,0} + \frac{(r_{p\,(n+1)} - r_{p\,0})}{n+2}(i+1)\big)\Big] \\
&= a_0 + \frac{(r_{a\,(n+1)} - r_{a\,0})i + (r_{p\,(n+1)} - r_{p\,0})(i+1)}{2(n+2)} \\
&= a_0 + \frac{(a_{(n+1)} - a_0)i + (r_{p\,(n+1)} - r_{p\,0})/2}{(n+2)} \\
&= a_i + \frac{(r_{p\,(n+1)} - r_{p\,0})}{2(n+2)}
\end{aligned} \tag{5.22}$$

This formulation is assuming that the initial orbit is the outer orbit. If the opposite is the case, it can be reformulated in a similar manner by replacing the first line with $a_{i \to (i+1)} = \frac{1}{2}(r_{a\,(i+1)} + r_{p\,i})$ and following a similar process.

In order to bypass the laborious computation required to calculate the total time, equation (5.18) can be reformulated using a Taylor Series. First, the components for the first and last Hohmann transfer are removed from the first sum.

$$t_{tot} = \frac{\pi}{\sqrt{\mu}}\left[a_{0 \to 1}^{\frac{3}{2}} + a_{n \to (n+1)}^{\frac{3}{2}} + \sum_{i=1}^{n} a_{i \to (i+1)}^{\frac{3}{2}} + a_i^{\frac{3}{2}}\right] \tag{5.23}$$

The first two terms can be written explicitly.

$$\begin{aligned}
a_{0 \to 1}^{\frac{3}{2}} &= (a_0 + \frac{\Delta a}{n+2} + \alpha)^{\frac{3}{2}} \\
a_{n \to (n+1)}^{\frac{3}{2}} &= (a_0 + \frac{n\Delta a}{n+2} + \alpha)^{\frac{3}{2}}
\end{aligned} \tag{5.24}$$

In order to simply the sum, first the $a_{i \to (i+1)}$ term is expanded with a Taylor Series.

$$\begin{aligned}
a_{i \to (i+1)}^{\frac{3}{2}} &= (a_i + \alpha)^{\frac{3}{2}} \\
&= a_i^{\frac{3}{2}}(1 + \frac{\alpha}{a_i})^{\frac{3}{2}} \\
&= a_i^{\frac{3}{2}}\left[1 + \frac{3}{2}\frac{\alpha}{a_i} + \frac{3}{8}(\frac{\alpha}{a_i})^2 - \frac{1}{16}(\frac{\alpha}{a_i})^3 + \cdots\right]
\end{aligned} \tag{5.25}$$

The term α is a stand in for $\frac{(r_{p\ (n+1)} - r_{p\ 0})}{2(n+2)}$. Since α is $\mathcal{O}(\Delta r_p)$, $\frac{\alpha}{a_i}$ will always have a magnitude less than one (when going between NEAs and an Earth orbit). The second term in the series is then ignored on the assumption than $(\frac{\alpha}{a_i})^2 << 1$.

$$\begin{aligned} a_{i \to (i+1)}^{\frac{3}{2}} &\approx a_i^{\frac{3}{2}} \left[1 + \frac{3}{2} \frac{\alpha}{a_i} \right] \\ &= a_i^{\frac{3}{2}} + \frac{3}{2} \alpha a_i^{\frac{1}{2}} \end{aligned} \tag{5.26}$$

This can then be plugged back into the sum in equation (5.23).

$$\begin{aligned} \sum_{i=1}^{n} a_{i \to (i+1)}^{\frac{3}{2}} + a_i^{\frac{3}{2}} &\approx \sum_{i=1}^{n} 2a_i^{\frac{3}{2}} + \frac{3}{2} \alpha a_i^{\frac{1}{2}} \\ &= \sum_{i=1}^{n} a_i^{\frac{1}{2}} \left(2a_i + \frac{3}{2} \alpha \right) \end{aligned} \tag{5.27}$$

The goal here is to separate the sum dependent terms and the constants as much as possible. The next step is to expand $a_i^{\frac{1}{2}}$ using a similar process.

$$\begin{aligned} a_i^{\frac{1}{2}} &= (a_0 + \frac{\Delta a}{n+2} i)^{\frac{1}{2}} \\ &= a_0^{\frac{1}{2}} (1 + \frac{\Delta a}{a_0(n+2)} i)^{\frac{1}{2}} \\ &= a_0^{\frac{1}{2}} (1 + \beta_i)^{\frac{1}{2}} \\ &= a_0^{\frac{1}{2}} \left[1 + \frac{1}{2} \beta_i - \frac{1}{8} \beta_i^2 + \cdots \right] \\ &\approx a_0^{\frac{1}{2}} (1 + \frac{1}{2} \beta_i) \end{aligned} \tag{5.28}$$

Here, β_i is dominated by $\frac{\Delta a}{a_0}$ and will also have a magnitude less than one, and, similarly, any terms on $\mathcal{O}(\beta^2)$ or smaller can be assumed to be significantly less than 1 and ignored. Plugging this back into the summation gives:

$$\begin{aligned} \sum_{i=1}^{n} a_{i \to (i+1)}^{\frac{3}{2}} + a_i^{\frac{3}{2}} &\approx \sum_{i=1}^{n} a_0^{\frac{1}{2}} (1 + \frac{1}{2} \beta_i)(2a_i + \frac{3}{2} \alpha) \\ &= \sqrt{a_0} \sum_{i=1}^{n} (2 + \beta_i)(a_i + \frac{3}{4} \alpha) \\ &= \sqrt{a_0} \sum_{i=1}^{n} 2a_i + a_i \beta_i + \frac{3}{2} \alpha + \frac{3}{4} \alpha \beta_i \end{aligned} \tag{5.29}$$

Since the α term is independent of the summation variable, it can be pulled out of the summation.

$$\sum_{i=1}^{n} \frac{3}{2}\alpha = \frac{3n}{2}\alpha \tag{5.30}$$

To isolate the summation variable dependent terms, a_i and β_i are expanded. To simply the expression, $\frac{\Delta a}{n+2}$ is replaced with the variable γ.

$$\begin{aligned}
\sum_{i=1}^{n} 2a_i + a_i\beta_i + \frac{3}{4}\alpha\beta_i &= \sum_{i=1}^{n} 2(a_0 + \gamma i) + (a_0 + \gamma i)(\frac{\gamma}{a_0}i) + \frac{3}{4}\alpha(\frac{\gamma}{a_0}i) \\
&= \sum_{i=1}^{n} 2a_0 + 2\gamma i + \gamma i + \frac{1}{a_0}(\gamma i)^2 + \frac{3\alpha}{4a_0}(\frac{\gamma}{a_0}i) \\
&= 2a_0 n + \sum_{i=1}^{n}(3 + \frac{3\alpha}{4a_0})(\gamma i) + \frac{1}{a_0}(\gamma i)^2 \\
&= 2a_0 n + (3 + \frac{3\alpha}{4a_0})\gamma \sum_{i=1}^{n} i + \frac{1}{a_0}\gamma^2 \sum_{i=1}^{n} i^2
\end{aligned} \tag{5.31}$$

The two remaining summations are well known.

$$\sum_{i=1}^{n} i = \frac{n(n+1)}{2} \tag{5.32}$$

$$\sum_{i=1}^{n} i^2 = \frac{n(n+1)(2n+1)}{6} \tag{5.33}$$

Now equation (5.29) can be fully expanded without summation.

$$\begin{aligned}
\sum_{i=1}^{n} a_{i\,\rightarrow\,(i+1)}^{\frac{3}{2}} + a_i^{\frac{3}{2}} \approx \sqrt{a_0}\Bigg[&\frac{3n}{2}\alpha + 2a_0 n + (3 + \frac{3\alpha}{4a_0})\gamma(\frac{n(n+1)}{2}) \\
&+ \frac{\gamma^2}{a_0}\frac{n(n+1)(2n+1)}{6}\Bigg] \\
= \sqrt{a_0}\Bigg[&(\frac{3\alpha}{2} + 2a_0)n + (3 + \frac{3\alpha}{4a_0})(\frac{n(n+1)\gamma}{2}) \\
&+ \frac{n(n+1)(2n+1)\gamma^2}{6a_0}\Bigg]
\end{aligned} \tag{5.34}$$

Combining equations (5.24) and (5.34) into equation (5.24) gives an analytic form for the approximate total time of the transfers.

$$\begin{aligned}
t_{tot} \approx \frac{\pi}{\sqrt{\mu}}\Bigg[&(a_0 + \gamma + \alpha)^{\frac{3}{2}} + (a_0 + n\gamma + \alpha)^{\frac{3}{2}} \\
&+ \sqrt{a_0}\Bigg((\frac{3\alpha}{2} + 2a_0)n + \frac{3}{2}(1 + \frac{1\alpha}{4a_0})n(n+1)\gamma + \frac{n(n+1)(2n+1)\gamma^2}{6a_0}\Bigg)\Bigg]
\end{aligned} \tag{5.35}$$

A similar process can be followed including second order terms to produce the following equation.

$$
\begin{aligned}
t_{tot}(2^{nd}\ order) \approx \frac{\pi}{\sqrt{\mu}}\Bigg[&(a_0+\gamma+\alpha)^{\frac{3}{2}}+(a_0+n\gamma+\alpha)^{\frac{3}{2}} \\
&+\frac{1}{\sqrt{a_0}}\Bigg((2a_0^2+\frac{3\alpha a_0}{2}+\frac{3\alpha^2}{8})n+\frac{3}{2}(a_0+\frac{\alpha}{4}-\frac{\alpha^2}{16a_0})n(n+1)\gamma \\
&+\frac{1}{8}(1-\frac{\alpha}{4a_0}+\frac{3\alpha^2}{16a_0})n(n+1)(2n+1)\gamma^2+\frac{1}{8a_0}(1+\frac{9\alpha}{8a_0})n^2(n+1)^2\gamma^3 \\
&+\frac{1}{40a_0^2}n(n+1)(2n+1)(3n^2+3n-1)\gamma^4\Bigg)\Bigg]
\end{aligned}
\tag{5.36}
$$

The accuracy of equations (5.35) and (5.36) are compared to the exact form in equation (5.23) over about 14000 asteroids with values of n ranging from 0 to 500. Values of n greater than 500 produces no notable change in the percent error of these analytic forms. The results are shown in Figure 5.2. For values of n less than

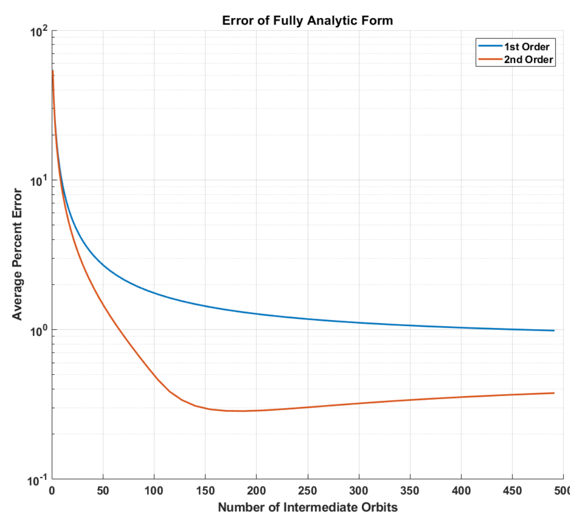

Figure 5.2.. Error of first and second order approximated time-of-flight values.

50, both analytic forms have a significant average error and it is worthwhile to use the exact form of the time estimation. For higher values of n, the analytic version is considerably more computationally efficient, and the error is low enough that it is worth using in place of the exact form. For this work, the exact form is used exclusively to avoid running into error issues for orbits where these approximations are not valid. It is not recommended to do this in general for sampling large numbers of transfers because it takes a significant amount of computational time to both find the exact number of intermediate orbits required for every asteroid and to calculate the time estimate. For single asteroid analyses, the exact model is worth using as the extra computation time is minimal.

It is also possible to speed up the calculations here by initially guessing the value of instead of sequentially increasing n and checking to make sure the thrusters can account for the associated impulses. Since the impulses allowed here are based on the accumulated thrust over a fixed percentage of the orbit, the largest allowable impulse will be that of the largest orbit (the 1st orbit for most cases here). Dividing the total Hohmann transfer by this maximum value gives a rough estimate of the minimum number of intermediate orbits required.

$$n \geq ceil\left(\frac{\Delta V_{hohmann}}{\Delta V_{max}}\right) - 1 = floor\left(\frac{\Delta V_{hohmann} m}{\eta P_0 T_{max}}\right) \tag{5.37}$$

The accuracy of this estimation is not crucial, it is a tool to speed up computation times.

The process for testing the time-of-flight model is the same as that for the fuel cost model in the previous section. The predictive value of the model is determined by taking the ratio of the actual to the estimated value, and those values are deciphered and compared in order to quantify how well the model predicts the transfer flight time.

$$Predictive\ Value = \frac{t_{actual}}{t_{model}} \tag{5.38}$$

Simply guessing the value of η to use for this model proved to be too difficult to get a model that could accurately predict flight times. Arbitrarily modifying the value of η could only produce models that, when compared to the actual flight times, had a standard deviation of approximately 50% of the mean. This model can be improved if the time estimate is given a constant base value, instead of just the summation of the estimated Hohmann transfer times.

$$t_{est} = t_{tot} + t_0 \tag{5.39}$$

This fixed value, t_0, increases the validity of the model, lowering the normalized standard deviation, but choosing this value and the value of η is still difficult. To work through this issue, a genetic algorithm is employed to determine these values.

A genetic algorithm is chosen for this particular issue because the total number of free variables, two, η and t_0, is very small, the cost function is computationally cheap, and it is not clear whether gradient based optimizers would be effective for this type of problem. The cost function is determined based on predictive values (PV) of the model and is given as:

$$J = |\mu - 1| + \frac{\sigma}{\mu} + \frac{CI}{\mu} \tag{5.40}$$

where μ is the mean PV, σ is the standard deviation, and CI is the 95% confidence interval. These values are normalized to the mean to avoid issues where the genetic algorithm will purposefully shrink or grow the model to extreme proportions in order to artificially modify the cost function. This is also handled by the first term in the cost function which tends the model towards the average value of the results.

The results from this optimization yield the value of η to be approximately 0.52, and t_0 to be approximately 1400 days. Using these two values, the mean predicted value is exactly 1, the standard deviation is 0.336249, and the 95% lower confidence interval is 1.11344. The predicted values are shown in the figure below. This model has significantly weaker correlation to the actual results than the cost estimation model. A 35% standard deviation is a poor model, and any correlation from that model is dubious. Nonetheless, this is the best correlation of any of the other models tested. It is clear that there is more room for improvement on this model, but, given that the 95% lower confidence interval is relatively low, this model still gives an idea of the minimum fuel-optimal transfer times.

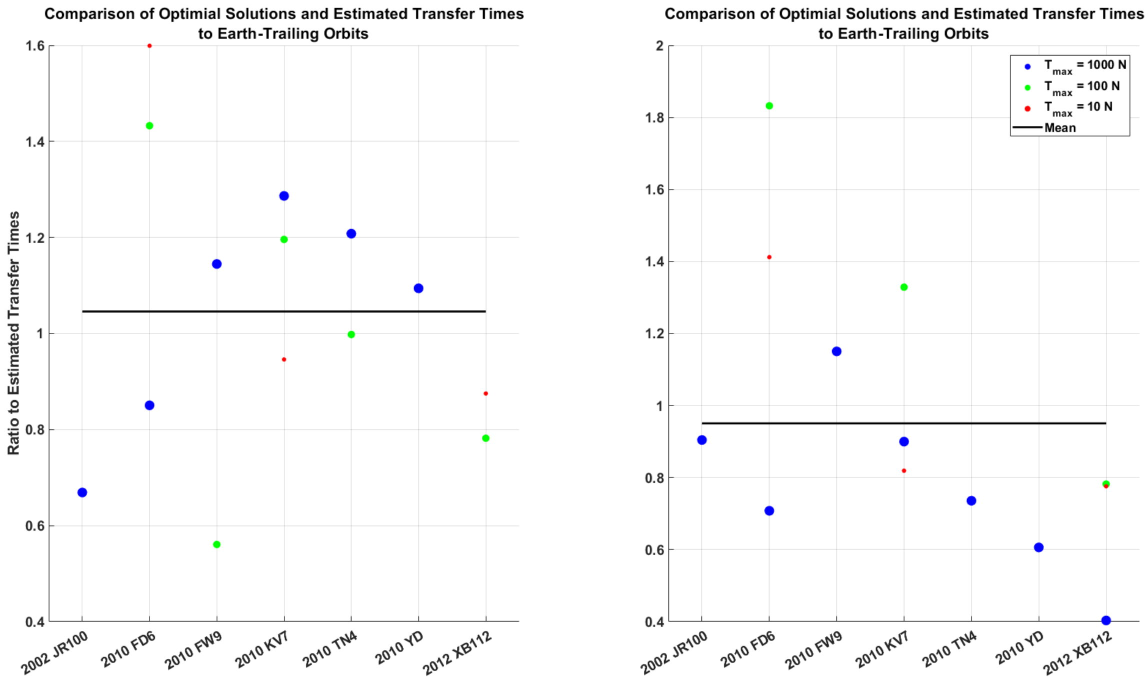

Figure 5.3.. Predicted values for estimating the flight time of fuel-optimum transfers.

5.1.3 Characteristics of Capturable Asteroids

These two models together can give realistic bounds on the size and location of asteroids that possible candidates for capture. By putting reasonable bounds on the possible momentum exchange and flight time for any capture mission, the total number of candidates can be constrained. This can also inform which technologies are feasible.

A preliminary analysis of the energy minimum transfers, Hohmann transfers, gives a concrete bound on the possible technologies for asteroid capture. If a system is incapable of producing the required momentum exchange for even the Hohmann transfer, it certainly will not be able to complete more inefficient lower-thrust transfers. For this analysis, unlike the analysis in the main part of this research, there is no selection criteria. All NEAs listed in the JPL small body database are analyzed, including ones without listed diameters. To estimate these diameters, the following equation is used [53]:

$$d = 10^{3.1236 - 0.5\log_{10}(a) - 0.2H} \tag{5.41}$$

where a is the geometric albedo, and H is the absolute magnitude. For all the asteroids from JPL's Small Body Database, only those without observed albedos do not have an estimated diameter. All of these do, however, have an observed absolute magnitude, H. This means that estimating the diameter is only a function of choosing an appropriate value for the geometric albedo, a. Typically, asteroids have a geometric albedo between 0.30 and 0.05 [53], but more reasonable estimates can be made based on the asteroid's particular compositional classification as shown in Chapter 2 above. Converting these momentum exchange values into ΔV gives a rough idea

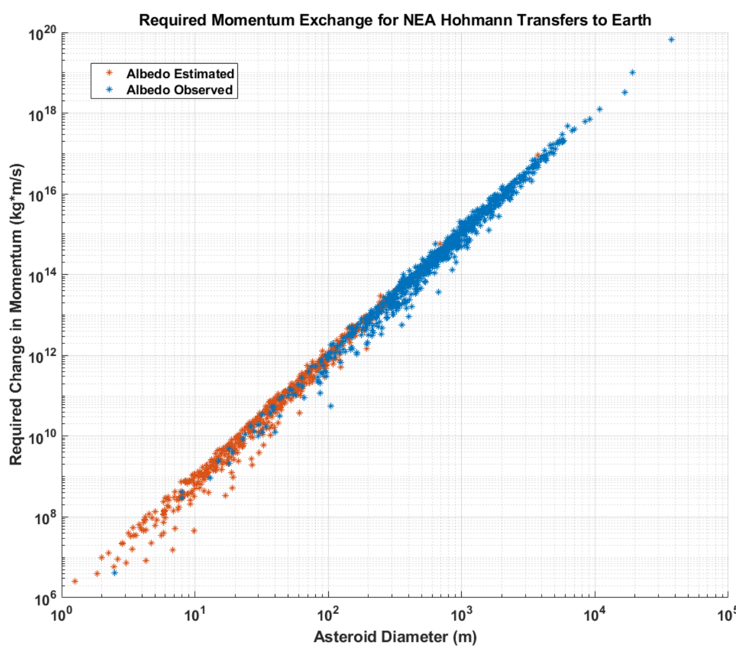

Figure 5.4.. Required change in momentum for Hohmann transfers from NEA initial orbits to an Earth orbit for various NEA diameters. The diameter of the orange points is estimated via an averaged albedo value. The diameter of the blue points is estimated by JPL's observations.

of how difficult these costs are from a mission perspective. While ΔV is a less concrete measurement from a system feasibility perspective, it is a more tractable value from an overall mission design standpoint. Missions that require, say, $15\frac{km}{s}$ change in velocity or more can be discarded as infeasible regardless of which technology will be used. The effect of the capabilities of different technologies will discussed in later sections. Figure 5.5 shows that NEAs are all close enough to Earth that very few of

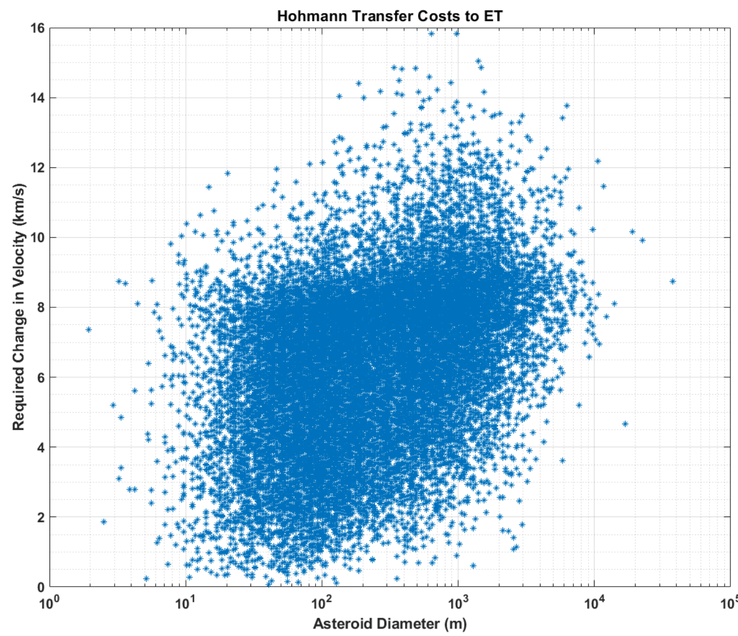

Figure 5.5.. ΔV costs for Hohmann transfers

them violate this ΔV requirement.

To get a more realistic idea of which asteroids are limited by their transfer costs, equation (5.12) can be used on all of the listed bodies. The results are shown in Figure 5.6. This estimation pushes quite a few asteroids past that $15\frac{km}{s}$ bound.

A similar analysis can be performed for the absolute lower bound for transfer times using equation (5.14). This time represents the amount of time required to produce the required momentum exchange for the Hohmann transfer given a certain level of thrust. It is evident from Figure 5.7 that a majority of asteroids are too heavy to transfer in any reasonable amount of time without thrusts on the order of hundreds

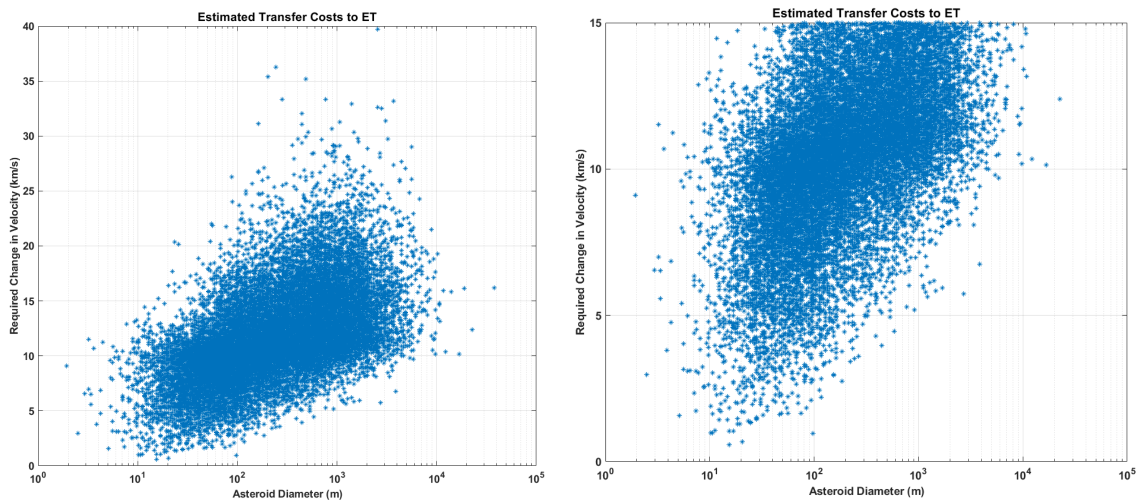

(a) Estimated Transfer Costs (b) Estimated Transfer Costs (zoomed)

Figure 5.6.. Estimated ΔV costs for fuel-optimum transfers.

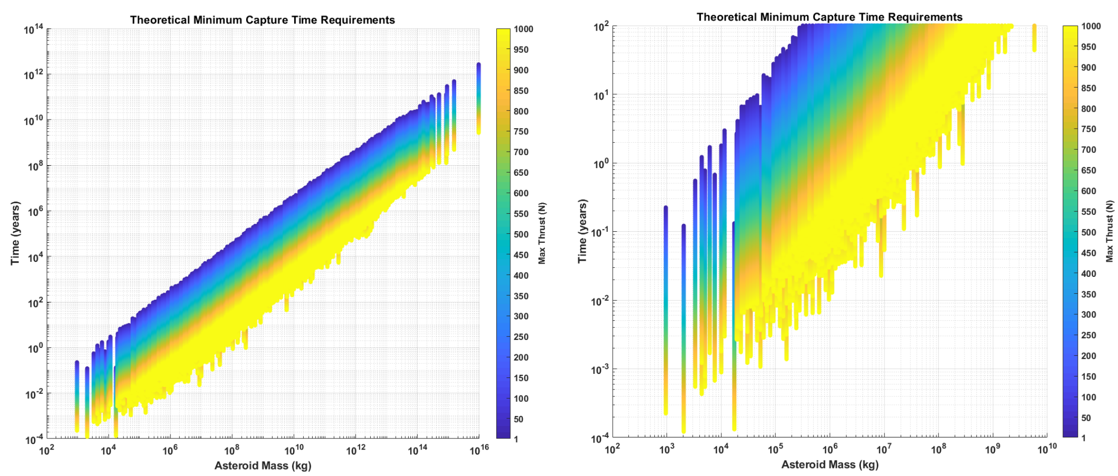

(a) Minimum Transfer Time (b) Minimum Transfer Time (zoomed)

Figure 5.7.. Minimum required time to produce the momentum exchange required for Hohmann transfers for various levels of thrust.

to thousands of kilonewtons. Some of these thrust levels are possible with current technologies but performing these levels of thrust continuously while controlling the thrust direction and maintaining attachment to an asteroid would be a significant challenge.

As with the cost estimations, the flight time estimations can be further extrapolated to the estimation models developed earlier in this work. Figure 5.8 shows the results from applying the flight time model to the listed asteroids. For the sake of computational efficiency, any asteroid larger than 10^{10} kg is ignored, and any estimated transfer times greater than 25 years are ignored as well. This mass is the point at which the minimum possible transfer time is greater than 100 years for all asteroids. The upper bound on the flight time is a simplifying move. Once transfers get much longer than that, calculating all the associated intermediate Hohmann transfers becomes computationally expensive. Twenty-five years is also a reasonable bound on mission flight durations.

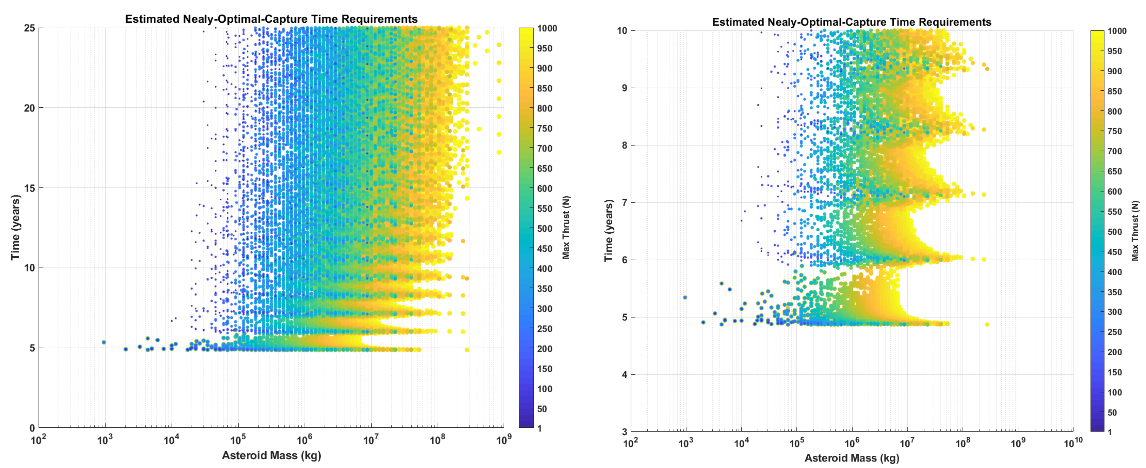

(a) Estimated Transfer Time

(b) Estimated Transfer Time (zoomed)

Figure 5.8.. Estimated minimum transfer time for fuel-optimum transfers.

These two models together give a concrete idea of the asteroids that can be excluded outright from consideration. Asteroids that require more than an estimated $15\frac{km}{s}$ ΔV or take more than 25 years estimated flight time (assuming 1 kN thrust as a best case) can be entirely removed from the selection pool. While ΔV in general is not indicative of the transfer capability of a given technology, the largest projected low thrust ΔV capabilities put the maximum around 15 km/s for spacecraft. Since asteroids are considerably heavier than spacecraft on average, the upper bound is reasonable from both a velocity change perspective and a momentum exchange perspective. These two considerations alone reduce the total population of small bodies from 21806 to a feasible set of 3624 asteroids, only about 16% of the original population. The various physical and orbital properties of these viable candidates are shown in Figures 5.9 and 5.10 below.

There are no viable candidates in the Atiras region, the inner-Earth orbits. This is likely due to the fact that these asteroids are very difficult to observe, not that these asteroids are more difficult in general to transport. This is also true of Atens orbits, orbits that are Earth-crossing but have a semimajor axis less than 1 AU. These are likely just as easy to capture on average as Apollos, they are more difficult to observe with the sun obstructing their view from an Earth viewing perspective. The number of capturable Amors asteroids is small because there are fewer of these types of asteroids classified as NEAs.

The trend in the spectral type is misleading. The reason that there is no clear spectral type for any of the feasible asteroids in not because they have a type that is unclear or difficult to classify, but because all of them are small and small asteroids are more difficult to observe in general. It often takes repeated measurements to confirm the spectral type and asteroids smaller than 100 m in diameter are very difficult to see. This is also in part why there seems to be a spike in asteroids sized from 50-75 m. It stands to reason that there would be significantly more very small asteroids that would be easily capturable. This is true, but those asteroids are also the most difficult to observe. There are likely thousands of tiny NEAs that would be relatively easy to capture, they are not reflected here because they have not been observed yet.

It can be observed from the orbital properties of the feasible set that most easily capturable asteroids are in very Earth-like orbits. The highest percentage of orbits have a semimajor axis close to 1 AU, an aphelion close to 1 AU, and a perihelion close

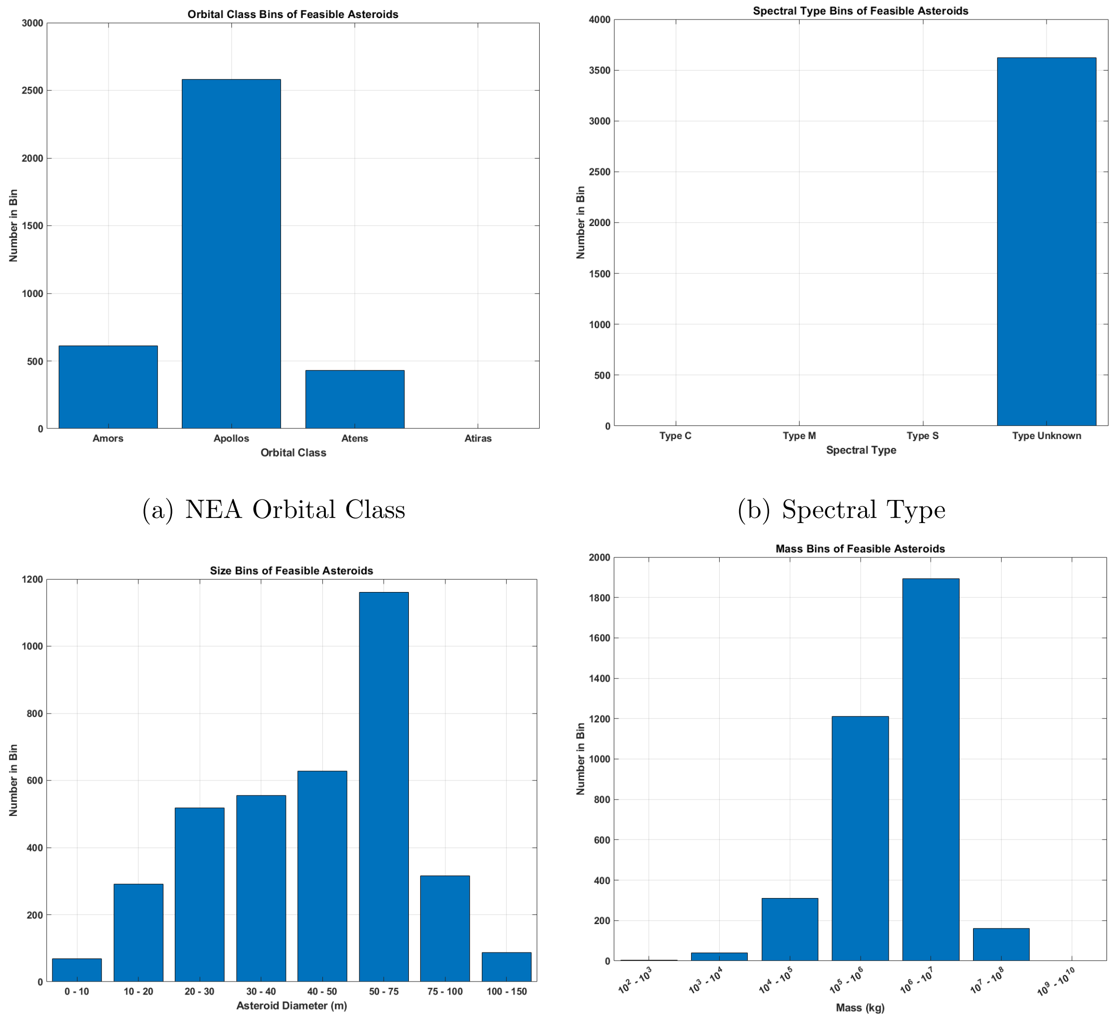

(a) NEA Orbital Class

(b) Spectral Type

(c) Sizes

(d) Mass

Figure 5.9.. Characteristics of feasibly capturable asteroids.

to 1 AU. It is worth noting that that median semimajor axis bin, and the median aphelion bin are slightly greater than 1 AU. The median eccentricity bin is 0.2 to 0.3, with several more eccentric bins being nearly as populous. This suggests that orbits larger and more eccentric than Earth's are actually more viable candidates. It is, again, most likely that this is not the case, but merely a remark on the percentage of regions that have been observed. Asteroids that spend more time on the anti-sun side of Earth are easy to observe. Asteroids in Earth-like orbits could easily be antipodal

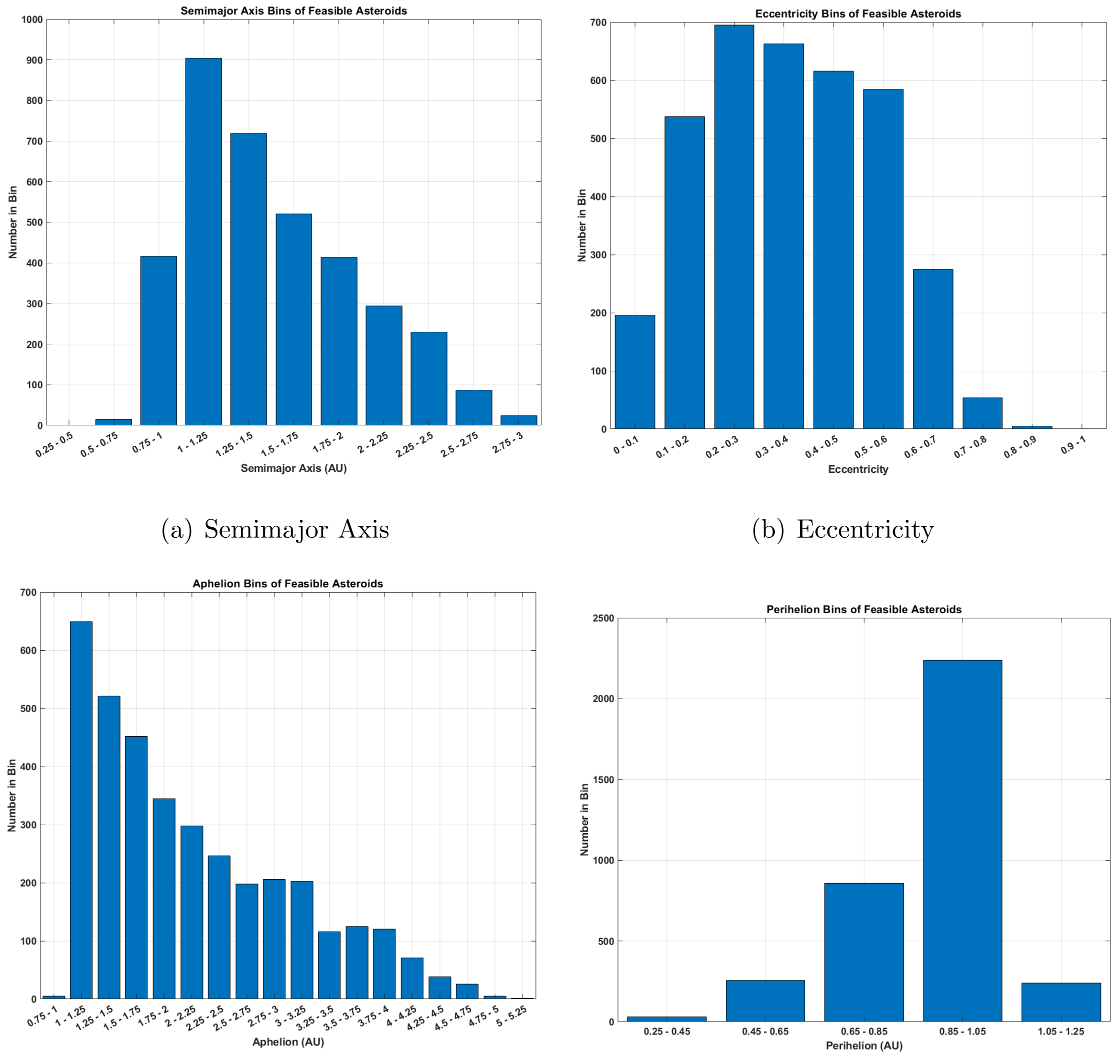

(a) Semimajor Axis (b) Eccentricity

(c) Aphelion (d) Perihelion

Figure 5.10.. Orbital characteristics of feasibly capturable asteroids.

to Earth but would require almost no ΔV to capture. Concerns like these are valid and require an update to these statistics when observations of the NEA population are more complete.

Even with this understanding, the number of Earth-like asteroids is enough to give options to mission designers. If the population of feasible targets is limited to those with an aphelion and perihelion between 0.95 AU and 1.05 AU, there are 8 feasible asteroids in this region. While this is not a necessary condition for a target

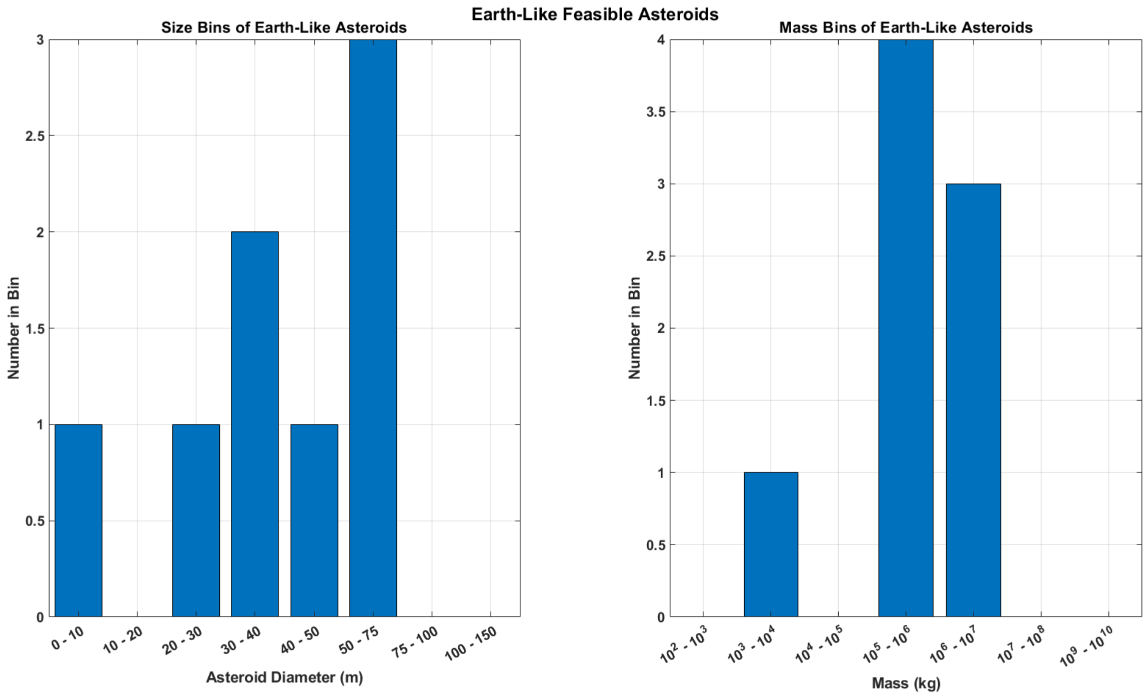

Figure 5.11.. Size and mass bins of asteroids with Earth-like orbits in the feasible set.

asteroid, it significantly reduces the feasible set to objects that are in close-to-Earth orbits. These transfers would likely be very straightforward and take very little time. These 8 asteroids are: 2015 XZ378, 2019 HM, 2018 PN22, 2018 UE1, 2018 DE1, 2013 RZ53, 2014 TW, and 2014 UR.

5.2 Asteroid Transport Technology

The study of different technologies for space transport has gotten more attention in recent years as space has moved more into the commercial sector and the public eye. How to efficiently transport large loads quickly through space is of paramount importance for any human missions and scientific research as journeys get longer and payloads get larger [12]. Asteroids are extremely heavy and moving them is inherently difficult. A large number of creative solutions have been proposed for the movement of large payloads, but few of them are worth considering given their current level of technological readiness. This work will not discuss all relevant technologies in detail. Instead, only the few technologies that might have a significant impact on asteroid transport will be considered.

5.2.1 Qualitative Comparison of Technologies

This section gives a short overview of some of the high level advantages and disadvantages of the different asteroid transfer technologies. Since nearly every possible technology would require some development, and many technologies have not yet been developed in any way, it makes sense to analyze and compare these different choices from a qualitative perspective. Ideas such as maximum possible ΔV, general technological readiness level, and nominal transfer duration all have significant impacts on the mission design and can be compared without reference to specifics. Gravity tractors, for examples, will almost always take longer to capture an asteroid than chemical propulsion systems. How much longer will depend on mission sepcifics, but the comparison gives a first look at the costs and benefits of each technology. This section gives an initial look at such comparisons before calculating the particular differences between each technology.

Considerations such as TRL, attachment requirements, and number of launches are important when choosing a technology for asteroid transfer. In general, mission considerations can be made in order to deal with systems of different levels of thrust, or different requirements for system support. Mission success becomes much more difficult when it is dependent on the use of undeveloped technologies. Asteroid tethers, for example, have never been made and present a number of interesting and difficult problems. Gravity tractors, ion beams, impactors, etc., bypass the need for such systems, simplifying the overall spacecraft design. This is not to suggest that other difficulties are not associated with these technologies. Gravity tractors take significant

Table 5.2.. Qualitative comparison of asteroid transfer technologies. Note that the TRL listed is for the technology itself. Any technology that requires attachment would have a lower overall TRL since attachment to an asteroid has not yet been attempted.

Slow Technologies				
Technology	TRL	Max ΔV	ToF	Attachment
Electric Prop.	High	Very High	Med-Long	✓
Solar Sail	Med	Med-High	Long	✓
Gravity Tractor	High	Low-Med	Long	✗
Ion Beam	Low	Low	Long	✗
Enhanced Yarkovsky	Low	Low	Long	✗
Laser Ablation	Low	Low	Long	✗

Fast Technologies				
Technology	TRL	Max ΔV	ToF	Attachment
Kinetic Impactor	High	Low-Med	Low-Med	✗
Chemical Prop.	High	Med	Any	✓
Mass Driver	Low	High	Any	✓

Explosives				
Technology	TRL	Max ΔV	ToF	Attachment
Nuclear (Standoff)	Med	Med	Med-Long	✗
Nuclear (Surface)	Med	Med-High	Med-Long	✓
Nuclear (Subsurface)	Med	Med-High	Med-Long	✓
Conventional (Surface)	Med-High	Low	Long	✓
Conventional (Subsurface)	Med-High	Low	Long	✓

amounts of time and precise orbital maneuvering in order to transport anything, let alone something of the considerable mass of asteroids. Impactors, mass drivers, and explosives all have nice energy transfer properties, but they require damaging the transported material which is far from ideal.

These considerations show that the asteroid transport problem is implicitly more complex than previously attempted spacecraft transfers. If the technology has a high TRL for spacecraft, it requires attachment; if the momentum transfer is highly efficient, the transfer either takes a significant amount of time or the technology will damage the asteroid. It is fair to assume that early attempts to transport and asteroid should discount destructive options outright. Much of the interest for asteroid capture comes from a scientific perspective and returning as much the material intact as possible is critical for scientific analysis. Some scientists have also encouraged mission designers to push for gravity tractors specifically because this is the only option available right now that does not change the form, composition, or surface properties of the asteroid whatsoever. Ablative technologies such as enhanced Yarkovsky systems and laser systems require removing the top layer of dust from the asteroid, and well understood propulsive technologies require attachment which can also alter or potentially destroy parts of the asteroid. At the very least, attachment will disturb the surface properties.

From a qualitative perspective, gravity tractors are the best option currently available. They have the highest TRL, and require limited technological development. The most difficult part of using a gravity tractor is find a trajectory that efficiently transfers the object back to a desired orbit. Based on the optimization analysis done in this work, it is likely that this is not an issue of whether such a trajectory can be found, simply how much time it will take to create, verify, refine, and output with realistic mission design considerations and high-fidelity simulations.

5.2.2 Quantitative Comparison of Technologies

These technologies cannot be boiled down to a single characteristic. The applicability of each technology is based on mission parameters and certain sets of assumptions that will not be uniformly valid. Simple examples of this would be launch capabilities. The chosen launch vehicle and the chosen asteroid's initial orbit play in tandem to dictate the total possible launch mass. Even so, it is still useful to estimate the capabilities of each of these technologies in a way that can be compared. In this section, technologies will be assessed by their total momentum exchange capabilities, each taking on the necessary assumptions to calculate such a range, so that each can be compared to the number of asteroids that can be captured with that amount of momentum exchange.

Momentum exchange can be given in two simple forms:

$$\Delta p = \Delta V m = F \delta t \tag{5.42}$$

Usually, the latter is simpler to calculate, but in some systems, it is more convenient to formulate that momentum exchange in terms of the available ΔV.

The capabilities of gravity tractors have been studied at length [15, 17, 34, 35]. A gravity tractor of mass m, hovering an asteroid of density ρ and diameter D, will produce the given momentum exchange, Δp, over a time period, Δt, if it hovers at the recommended safe distance of 1.5 asteroid radii.

$$\Delta p_{GT} = \frac{8\pi}{27} G \rho D m \Delta t \tag{5.43}$$

To get ranges for the various technological capabilities, it is assumed that there is a ten-year flight time, and that the launch mass ranges from 1000 kg to 10,000 kg. For gravity tractors, it is also assumed that the target asteroid is 10 m in diameter. The efficacy of gravity tractors when compared to other sizes of asteroids is discussed at length further below. The calculated Δp for gravity tractors is $3.9212 * 10^5 - 3.9212 * 10^6 \ \frac{kg*m}{s}$ and this value increases linearly in proportion to the diameter of the asteroid being pulled. As shown in equation (5.43), the momentum exchange scales linearly with the diameter of the asteroid. While this seems counterintuitive since it implies that a gravity tractor can more easily transfer larger asteroids, this is not the case. The caveat is that as diameter increases linearly, the mass increases cubically, so the required momentum exchange to transfer larger asteroids increases faster than the diameter. So, while the spacecraft can affect more momentum change for a larger asteroid, the larger asteroid will still be more difficult to transfer.

Calculating the momentum exchange capabilities of electric propulsion systems and ion beams is very similar since ion beams are functionally two EP systems - one to push the spacecraft and one to push the asteroid [39, 40].

$$\Delta p_{EP} = \eta_p \sqrt{\frac{\eta_{EP} \Delta t}{8\alpha}} m \tag{5.44}$$

$$\Delta p_{IB} = \eta_B \sqrt{\frac{\eta_{EP} \Delta t}{8\alpha}} \beta m \tag{5.45}$$

where α is the inverse specific power of the spacecraft (given in $\frac{kg}{kW}$), η_p is the pointing efficiency for the attached EP system, η_{EP} is the thrust or power efficiency of the EP system itself, η_B is the beam efficiency of the ion beam system - essentially how much of the beam actually hits the asteroid, and β is the percentage of the mass of the ion beam system that is dedicated to pushing the asteroid. For these systems, the power efficiency is much more important than the system mass. Assuming a power efficiency of 0.7, a pointing efficiency equivalent to a spacecraft angle offset of 30% for the tug, a beam efficiency of 0.9 for the ion beam, and an inverse specific power of 20 kg/kW we can obtain a range of capabilities for these two technologies. The value of β could vary significantly depending on the spacecraft. For this analysis, it is assumed that the ion beam used to push the asteroid has equivalent system mass to that used to maintain the spacecraft pointing and distance. This is likely an overestimation since the force generated to push the asteroid forward will also push the spacecraft backwards and must be counteracted while maintaining pointing. With some system mass added in the value of β is assumed to be 0.45.

Using these values, the momentum exchange range is found to be $3.2179 * 10^7 - 3.2179 * 10^8$ $\frac{kg*m}{s}$ for EP tugs and $1.5049 * 10^7 - 1.5049 * 10^8$ $\frac{kg*m}{s}$ for ion beam systems.

To calculate the capabilities of a solar sail, the equations for the effects of SRP are used as a baseline.

$$a_{srp} = p_{srp} C_r (\frac{1AU}{R})^2 \frac{A_{sun}}{m_{tot}} \tag{5.46}$$

In this equation, the mass, m_{tot}, will be the total mass pulled by the sail, which is the mass of the asteroid and spacecraft combined. Converting this to momentum exchange yields the following:

$$\Delta p_{ss} = a_{srp} m_{tot} \Delta t = p_{srp} C_r (\frac{1AU}{R})^2 A_{sun} \Delta t \tag{5.47}$$

The sun-facing area, A_{sun}, can be calculated using the following expression.

$$A_{sun} = (\frac{A}{m})_{ss} \beta m \eta_{ss} \tag{5.48}$$

where $(\frac{A}{m})_{ss}$ represents the expected area to mass ratio of the solar sail itself, β represents the mass fraction of the spacecraft that the sail itself takes up, and η_{ss} represents the percentage of the sail that is effectively pulling the spacecraft. The value of η_{ss} would be determined by a number of different factors such as the angle to the sun, and the amount of the sail that is occulted by the asteroid.

$$\Delta p_{ss} = p_{srp} C_r (\frac{1AU}{R})^2 (\frac{A}{m})_{ss} \beta m \eta_{ss} \tag{5.49}$$

Assuming a typical value for p_{srp} of $4.5565 * 10^{-6} \frac{N}{m^2}$, a C_r of 1.1, an average radial distance of 0.9 AU, a solar sail area to mass ratio of $156.5 \frac{m^2}{kg}$ (a proposed value for a helio gyro [38]), a mass percentage, β, of 10%, and an η_{ss} value of 0.9, the ranges for the momentum exchange of the solar sail can be calculated to be $1.1460 * 10^7 - 1.1460 * 10^8 \; \frac{kg*m}{s}$.

The next technology to estimate is chemical propulsion. The capabilities of chemical propulsion systems are highly variable. They are dependent on the percentage of system mass allowed, the exhaust velocity of the system, and the propellant used. Instead of trying to assume all of these different parameters, for chemical systems, this work simply takes the values from a characteristic set of thrusters and uses those. Doing a full spectrum summary of the capabilities of different chemical propulsion systems is beyond the scope of this work. The characteristic thrusters chosen are the Ariane Group 400 N monopropellant thrusters [68]. These thrusters output a force between 120 and 420 N, with the steady state full throttle thrust averaging to approximately 400 N. The specific impulse of these thrusters has an average value of about 2118 Ns/kg, and a mass flow rate of approximately 180 g/s at the 400 N of thrust level. These values can be used to determine the approximate exhaust velocity via:

$$v_e = \frac{F}{\dot{m}} \tag{5.50}$$

Doing so for these thrusters yields an approximate exhaust velocity of 2222 m/s.

If an extreme mass fuel percentage of 98% is assumed as an upper limit, then the rocket equation, equation (5.51), can be used to determine the amount of possible ΔV.

$$\Delta V = v_e \ln(\frac{M+P}{M}) = v_e \ln(1+\eta) \tag{5.51}$$

where M is the system mass excluding propellant, P is the propellant mass, and η is the propellant mass percentage, $\frac{P}{M}$. Using these values and the calculated exhaust velocity gives a total ΔV of $8.6934\frac{km}{s}$. This is an upper limit and is not feasible given most real mission considerations. Nonetheless, it is not unreasonable to assume that chemical systems will be able to produce these levels of ΔV in the near future. Using these values with the momentum equation gives upper bounds on the possible exchange capabilities of chemical systems. This range is $8.6934*10^6 - 8.6934*10^7 \frac{kg*m}{s}$.

Ranges for possible amount of total momentum exchange for kinetic impactors, explosive technologies, and mass drivers are taken from JPL's report to Congress, the 2006 Near-Earth Object Survey and Deflection Study [11] and mapped onto Figure 5.4. The results are shown in Figure 5.12. It is important to note that the ranges shown are calculated for both the Delta IV Heavy and Ares V launch vehicles. For most of the technologies, these two launch vehicles give a range of possible momentum exchange capability for each technology (the lower value of the range from one of the launch vehicles and the upper from the other), but for kinetic impactors, the available momentum exchange is dependent on a constant, β. This constant represents how much the asteroid will break up on impact. A low β value means that asteroid is more solid and is less likely to break apart, and the momentum exchange with an impactor will be more efficient. The ranges shown for the momentum exchange capabilities of kinetic impactors in the figure is based on a series of tests for a large range of β values, with the tests repeated for each launch vehicle. This is in contrast to the ranges for the other technologies, which come solely from the analysis of the separate launch vehicles.

These ranges can be used as concrete bounds for the different costs of asteroid transfers. Using the same process as before, the feasible set of asteroids can be narrowed down now by the capabilities of each technology, instead of choosing reasonable bounds in general. These estimations can also work in closer conjunction with the estimated flight times and the approximate level of equivalent thrust of each technology. Using the technological limits of momentum exchange is a much more reasonable bound than assuming an upper bound on ΔV and can give a more realistic assessment of the feasible set of target asteroids. Figure 5.12 shows these ranges overtop the estimated transfer costs to give an idea of the capabilities of each. The gravity tractors capabilities increase with the asteroid size, so this range increases linearly as asteroid diameter does. Other than electric propulsion, ion beams, impactors, and explosives, these ranges increase linearly with time. Electric propulsion and ion beams increase proportional to the square root of the increase in time. Impactors and explosives increase proportionally to the number of additional launches allowed. The ranges shown for these impulsive technologies assumes two launches - one to hit the asteroid out of its initial orbit and another to capture it.

This analysis can be extended to include the statistics presented earlier such as asteroid sizes, orbital characteristics, etc. Since there are no feasible asteroids for conventional contact explosives, they are ignored from here on out. Figures 5.22 through 5.25 show some of the characteristics of the feasible set of asteroids from before reduced by which asteroids are capturable by each given technology. For these figures, the statistics shown are asteroids that can be captured in less than 25

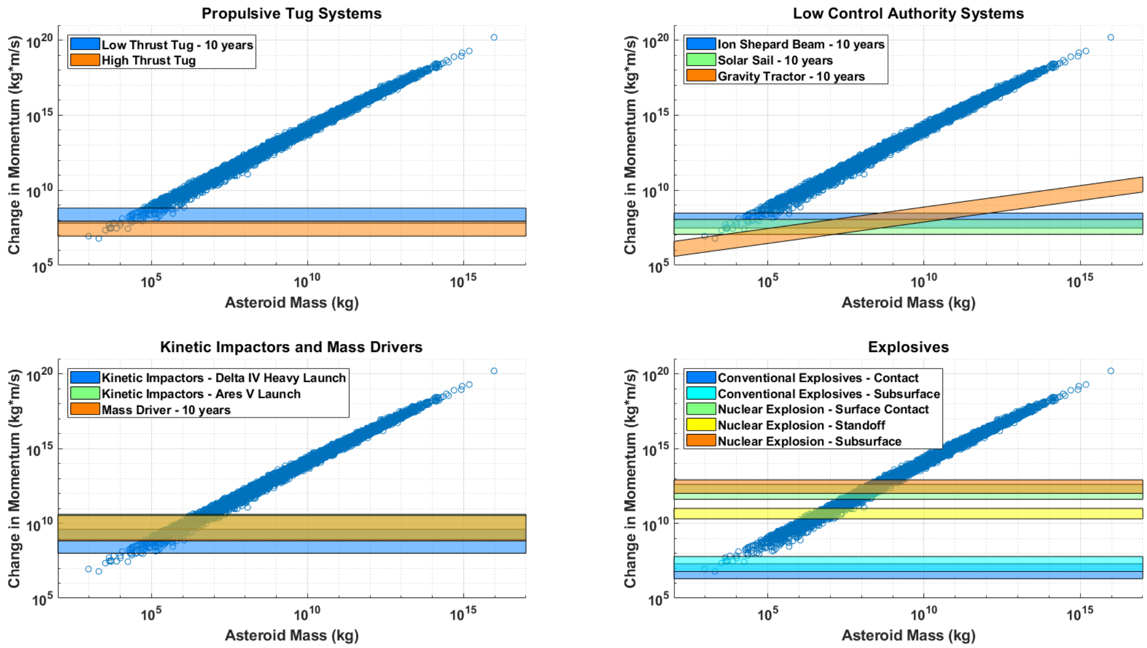

Figure 5.12.. Required change in momentum for Hohmann transfers from NEA initial orbits to an Earth orbit for various NEA diameters with asteroid transfer technologies mapped over top.

years and have estimated transfer costs less than the average amount of expected momentum exchange for the transfer. The estimated transfer costs are determined using equation (5.12).

Other characteristics shown in these plots tend towards those already discussed in previous sections. The most populated bins are associated with the most easily observed characteristics, not with the characteristics that have theoretically optimal transfer characteristics such as small size, and Earth-like orbital properties. Once the observations of NEAs are more complete, a repeat of this analysis will be required to get a more complete understanding of the characteristics of feasible target asteroids. This information would be paramount for repeated asteroid capture campaigns, commercial efforts for example.

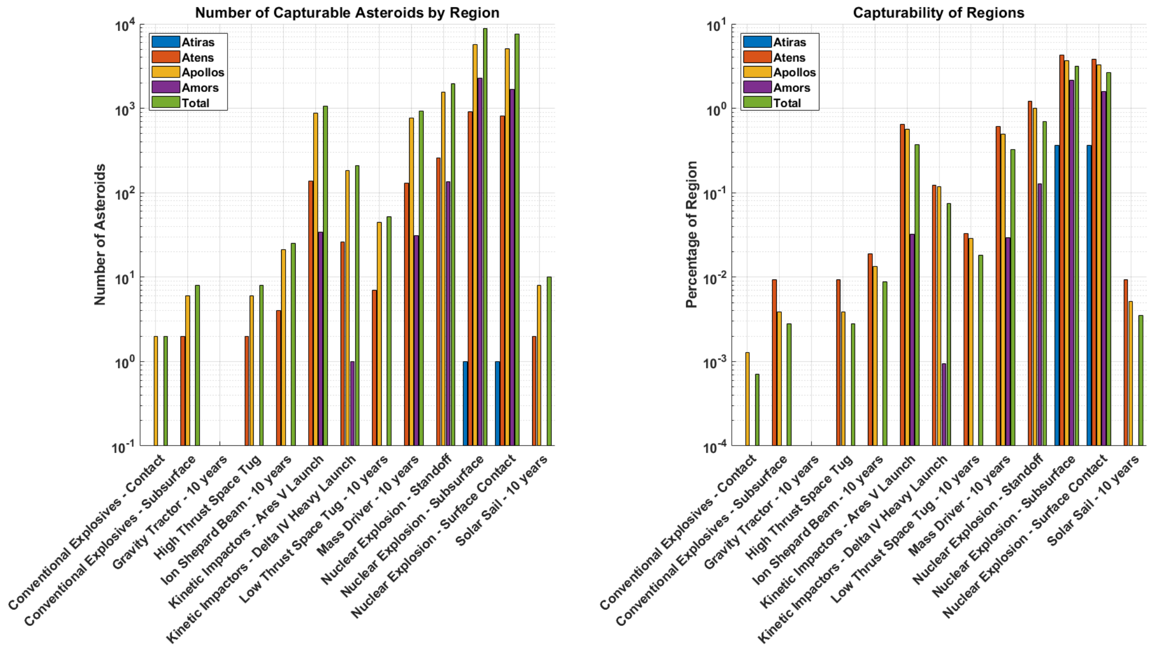

Figure 5.13.. Capturable population for each orbital regime listed by technology.

One important note is that gravity tractors are ineffectual for the estimated requirements of momentum exchange given the 10-year timeframe and maximum launch mass. This relationship is shown in figure 5.26(a). A gravity tractor that has 10,000 kg mass cannot transfer any of the listed NEAs in a 10-year timeframe. A 100,000 kg gravity tractor can transfer around 100 targets given 10 years. Since the momentum exchange capabilities of gravity tractors are linear in both time and spacecraft mass, these two numbers can be reciprocated to produce the same result. For example, if 100 targets can be transferred for a 100,000 kg spacecraft given 10 years, the same number can be transferred with a 10,000 kg spacecraft given 100 years. This reciprocity can be metricized via the product of spacecraft mass and flight time and compared to the number of capturable targets. This analysis is shown in figure 5.26(b). A minimum of 667 ton-years is required to transfer a single asteroid using a gravity tractor. A 10-ton spacecraft pulling an asteroid for 10 years would be a 100

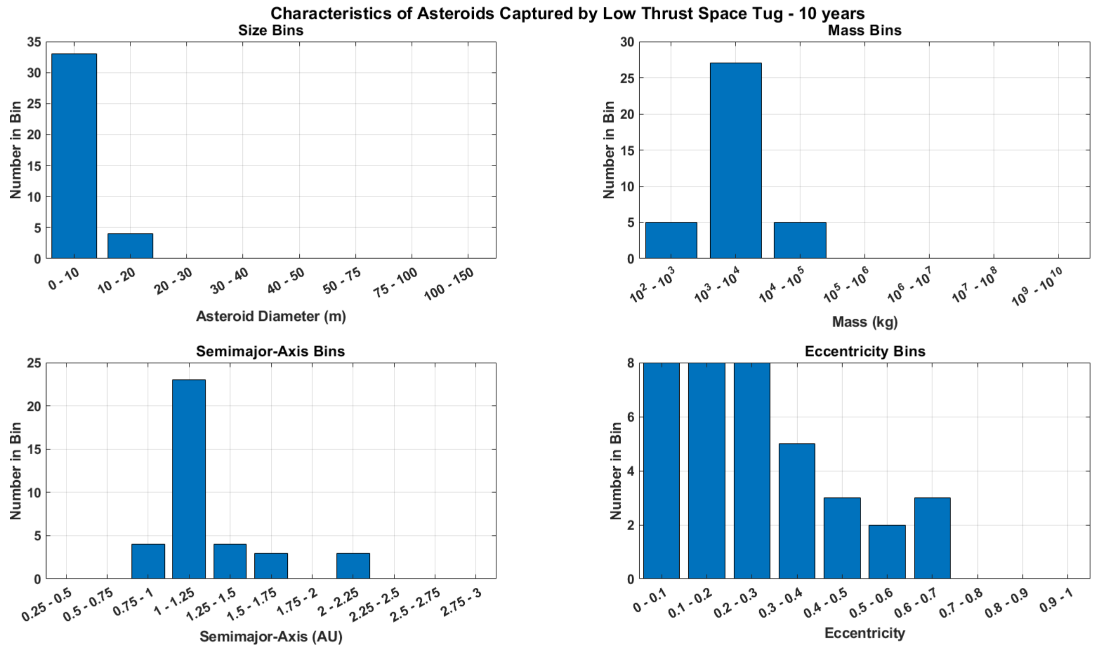

Figure 5.14.. Characteristics of asteroids capturable by a low thrust tug in 10 years.

ton-year gravity tractor. Almost an order of magnitude more mass-time is required for gravity tractors to be feasible. Given current launch capabilities, this is not yet feasible for asteroid capture, but it is feasible for asteroid deflection.

It is also worthwhile to look at the efficiency and feasible target population characteristics of theoretical technologies. While the figures produced give insight into existing technologies, they do not map concretely onto mission with different assumptions such as available launch vehicles, system thrust, system efficiency, and so forth. To give a more concrete idea how this can affect the population of potential target asteroids, this analysis is generalized to a given level of momentum exchange which mission designers can then reference irrespective of the chosen technology. Figure 5.27 shows the characteristics of capturable asteroids for any given level of available momentum exchange. It is worth noting that this figure is presented such that the lowest possible level of momentum exchange to capture targets in the given bin is shown.

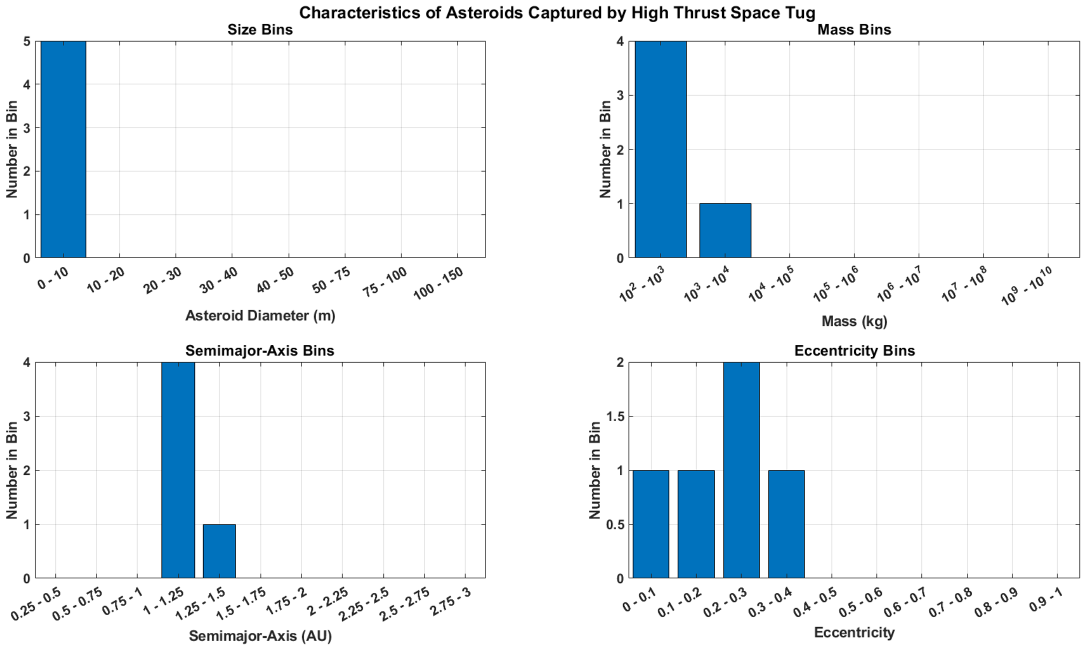

Figure 5.15.. Characteristics of asteroids capturable by a high thrust tug.

This means that anything at or above the shown level of momentum exchange can capture the targets in the given bin.

This information gives a quick, easy overview of the types of asteroid that are feasible for a given technology. The lower the available momentum exchange, the smaller the asteroids, the lower their mass, and the closer their orbit is to Earth's.

5.3 Mission Design Concepts for Asteroid Capture

Mission design in general is a complex process that requires a tremendous amount of mission and system specific information. This section does not attempt to make suggestions for all missions, it only attempts to make general claims about the mission design space and to make suggestions therefrom. These suggestions are meant to provide a framework that mission designers can use as a starting point and move outward from there.

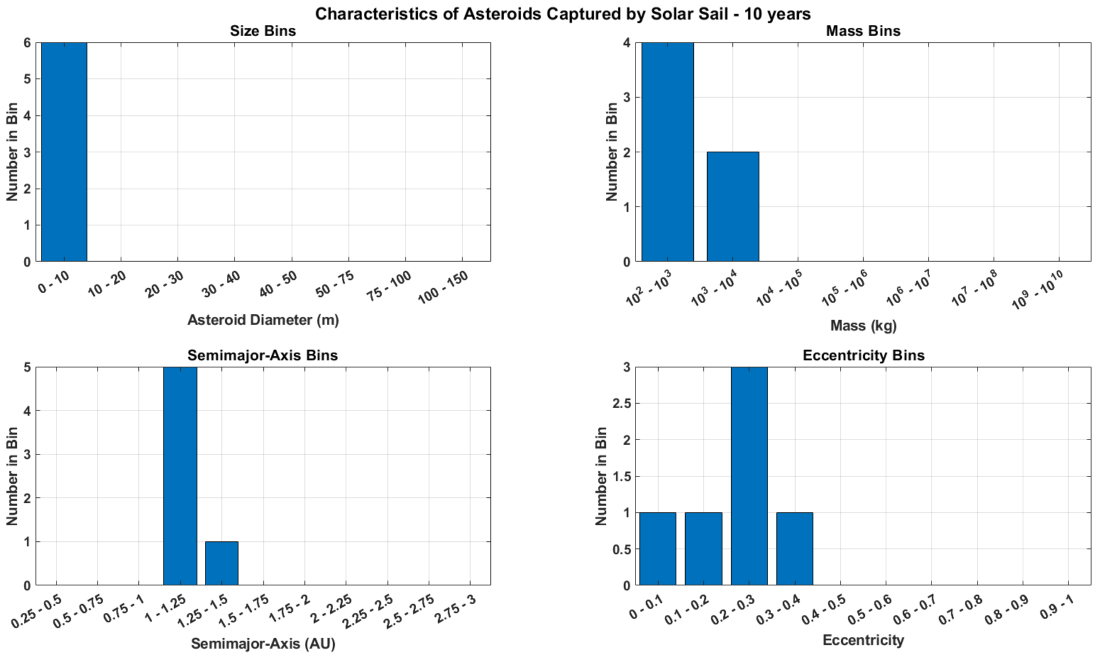

Figure 5.16.. Characteristics of asteroids capturable by a solar sail tug in 10 years.

This section begins by outlining the decision process for an asteroid if a technology is already chosen, and an order of magnitude for the mission timeline is decided. Using these two limiting mission parameters, suggestions are made and statistics for the types of asteroids available are outlined. Finally, specific asteroids are suggested for each of listed technologies. The second part of this section follows a similar process but instead focuses on how to choose a technology based on key asteroid choices and a range of mission timescales. Finally, these two analyses are combined to produce an overall roadmap for mission designers. The goal of this roadmap is to summarize and simplify the process and results of the first two sections and to provide a visual guide for the process of selecting these mission criteria.

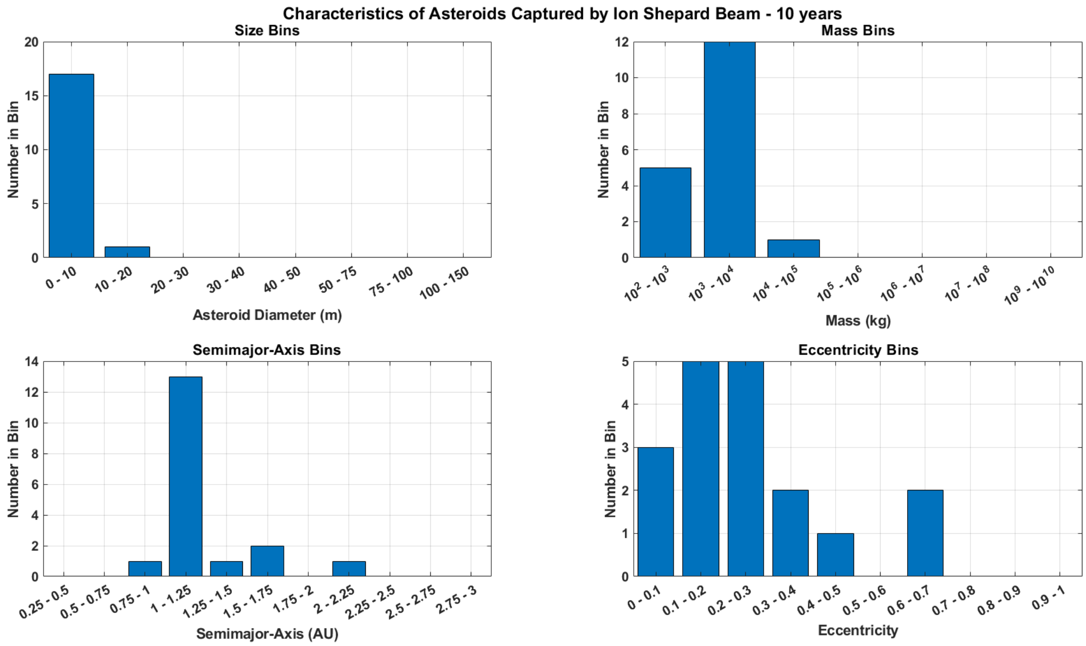

Figure 5.17.. Characteristics of asteroids capturable by an ion beam in 10 years.

5.3.1 Choosing an Asteroid

There are a number of considerations to address when choosing a target asteroid. Important considerations include the size, content, and scientific significance of the asteroid. The latter is still an easy requirement for the decision process as no asteroid has been captured thus far and any asteroid would have significant scientific significance. A similar argument could be made for the content of the asteroid. Commercial asteroid mining missions would like to target asteroids high in precious elements - S-type and M-type asteroids - but, again, since no asteroid capture has ever been performed, these remain secondary considerations until the process of bringing these objects back to Earth becomes more vetted. The remaining major consideration is the size of the chosen asteroid.

The asteroid's size affects almost every aspect of the mission. A larger asteroid requires more momentum exchange to move, it will increase the mission time for low-

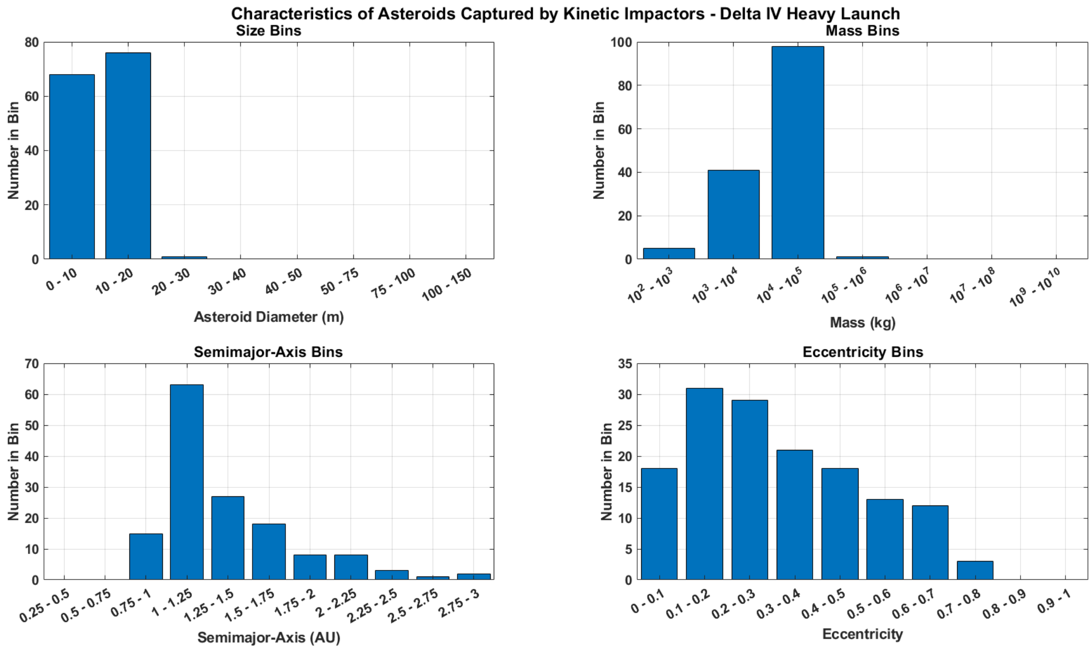

Figure 5.18.. Characteristics of asteroids capturable by kinetic impactors launched from a Delta IV Heavy.

thrust technologies, it will make attachment more difficult for propulsive technologies, the probability of the asteroid breaking up during the transfer will increase, and the potential damage that the asteroid could cause if the mission were to lose control, would be much higher. Nonetheless, a bigger asteroid significantly increases the scientific and engineering value of the mission and it worth capturing the largest asteroid possible. There is also a notable lower bound for capture candidates. Bringing back a 10 cm diameter boulder would be relatively easy, but it would be less significant than returning larger objects. While the relationship between size and mission cost would change for each mission, it is reasonable to assume that there is some nominal lower bound for the size of desirable capture targets.

Ultimately, the upper and lower bounds on the size of the asteroid are subject to a significant study. From a safety perspective, assuming a 90 degree impact angle and an impact velocity of $20\frac{km}{s}$ (the average of asteroids impacting Earth is considered

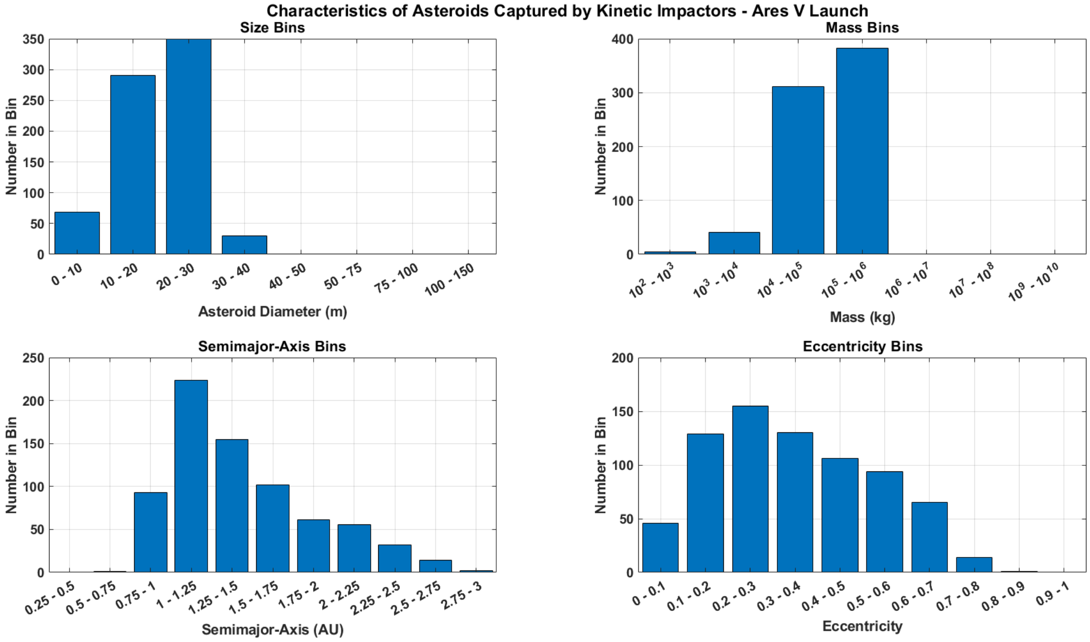

Figure 5.19.. Characteristics of asteroids capturable by kinetic impactors launched from an Ares V.

to be $17\frac{km}{s}$), an asteroid can have a diameter of 35 meters before causing significant damage if it were to go off course and enter the Earth's atmosphere [67]. This worst case is a good upper bound for asteroid size. A full mission analysis of probabilities of impact, impact angles, and so forth could be produced for a specific mission and a more accurate upper bound could be made. It is also fair to point out that a 35 m diameter asteroid is unwieldy and would be difficult to transport regardless. To give some perspective, 35 m is just over 8 stories tall. Transporting anything of this size would be no small effort.

Without safety considerations, the lower bound for asteroid size should be considered from a scientific and engineering perspective. Part of the interest of asteroid capture missions is to set a precedent for future missions. Capturing an extremely small asteroid (a diameter of only a few centimeters, for example) has significantly less scientific and engineering value compared to the capturing asteroids on the order of several meters in diameter or larger. A framework for moving small bodies

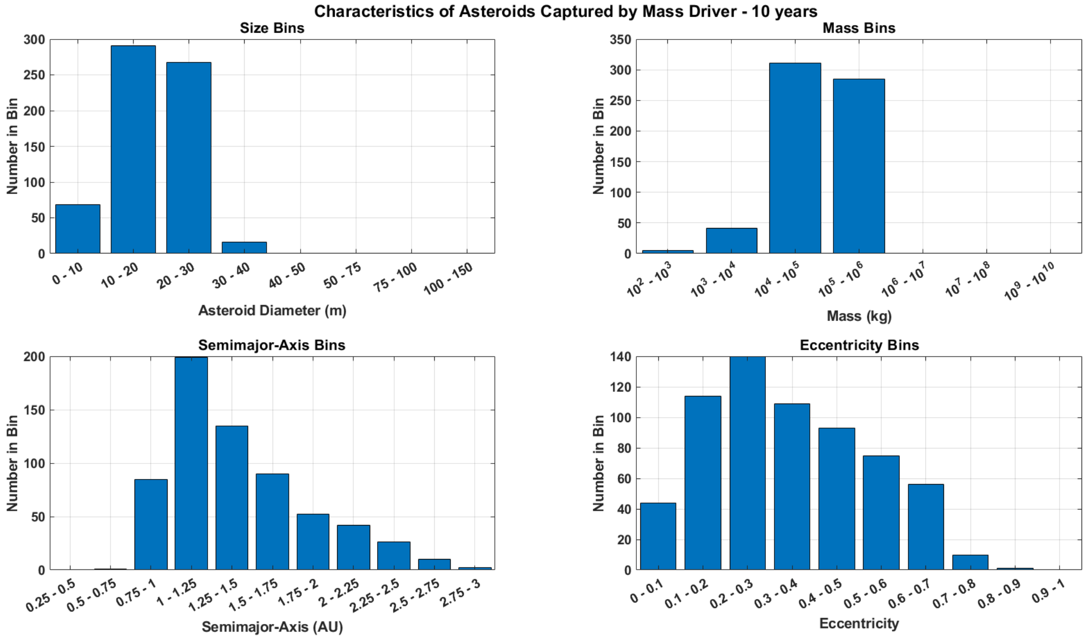

Figure 5.20.. Characteristics of asteroids capturable by a mass driver in 10 years.

in the Earth-vicinity has important implications not only for commercial efforts but for human journeys as well. Showing that a large asteroid can be safely placed in cis-lunar space would help to qualify claims about journey to Mars and other places in the solar system, it would be a form of safe practice for ferrying large crew or cargo payloads, and it would validate the need for cis-lunar initiatives such as the Lunar Gateway. With these considerations in mind, the lower bound for asteroid diameter is set at 1 meter for this work. Asteroids with diameters from 5 m to 10 m would be ideal targets.

Other size considerations come from the specifics of a given technology. Attachment becomes more difficult with larger asteroids, but systems that do not require attachment will take significantly longer flight times as the asteroid size increases. Estimating the technology-specific upper bounds is difficult. Since no asteroid attachment systems have ever been put to use, it is highly speculative to estimate the difficulties associated with increasing the size of the attachments system. Perspec-

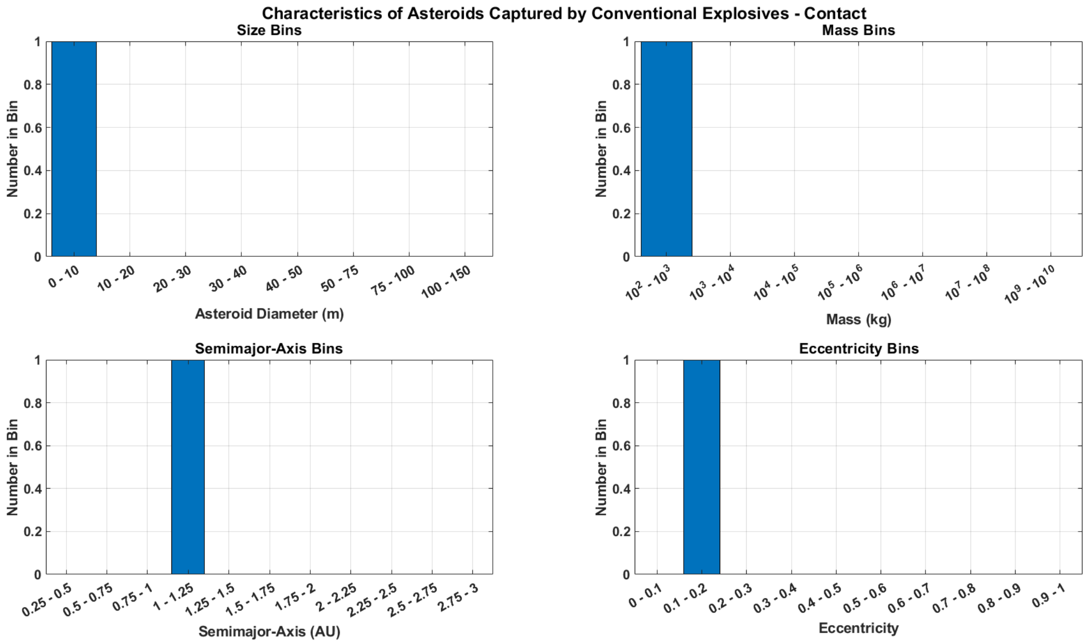

Figure 5.21.. Characteristics of asteroids capturable by surface conventional explosives.

tive for the time requirements for non-attachment systems is also difficult. From the trajectory analysis in this work, it evident that low-thrust systems have a higher minimum flight time before producing nearly optimal solutions. This minimum time is not consistent between asteroids as it is a function of both the asteroid size, the exact level of thrust of the chosen technology, and the asteroid's orbit. The smallest asteroid analyzed in this work, 2012 XB112, has an effective spherical diameter of 2.5 m and can be captured with 10 N of thrust in 1-2 years, only a marginal increase over the flight time for an optimal transfer with 100 N or 1000 N of thrust. The asteroid 2010 FD6, an 8 m diameter asteroid, however, requires 4-5 years to transfer optimally with 10 N of thrust over the 1 year required for 100 N of thrust. The best method found so far is the time estimation model proposed in earlier sections of this work. This model can at least give an estimation of the upper limit on the minimum flight time required for transfers using systems with 1 N of thrust or less.

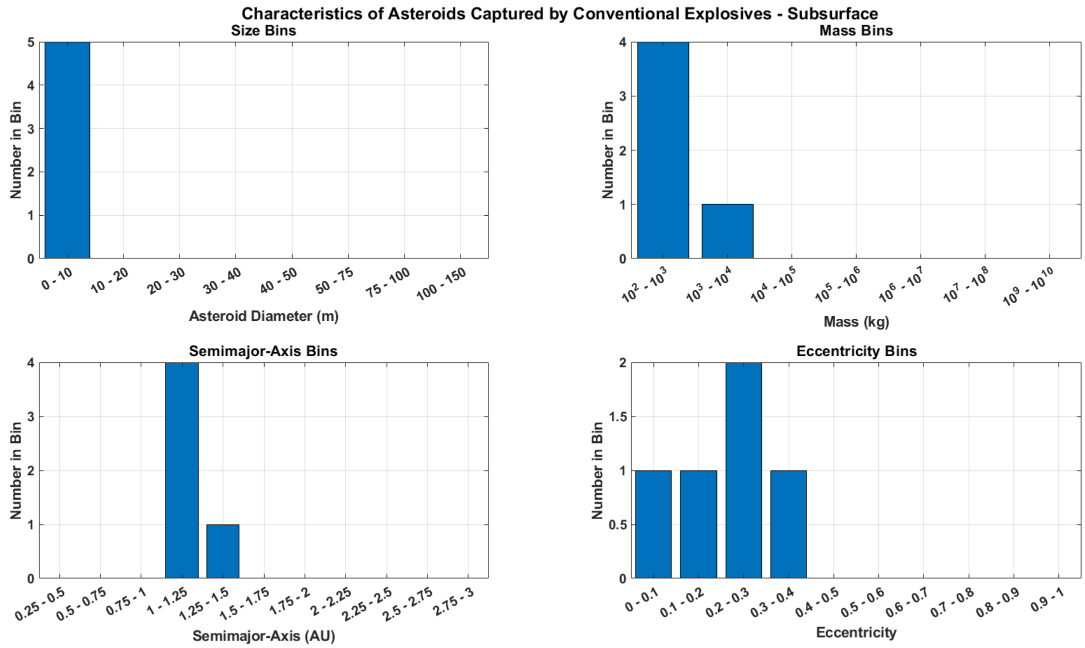

Figure 5.22.. Characteristics of asteroids capturable by subsurface conventional explosives.

With size limits established, the next focus for selecting an asteroid should be on the orbital properties of the asteroid. The closer the asteroid is to an Earth orbit, the lower the transfer cost will be and the more room for extra launch mass there will be. However, since observability is still a key factor in understanding the NEA population, choosing an asteroid that is solely Earth-like may pose issues without an observation mission beforehand. For example, if a different target needs to be chosen during the design process, it would be very difficult to modify the asteroid selection for NEAs with Earth-like orbits because we have not observed many of them. Apollos orbits, which spend time above the Earth, are much easier to observe and would offer a multitude of different, but similar options should the need arise. This is just one consideration. With a full observational set, Earth-like orbits would likely be the cheapest option in most instances.

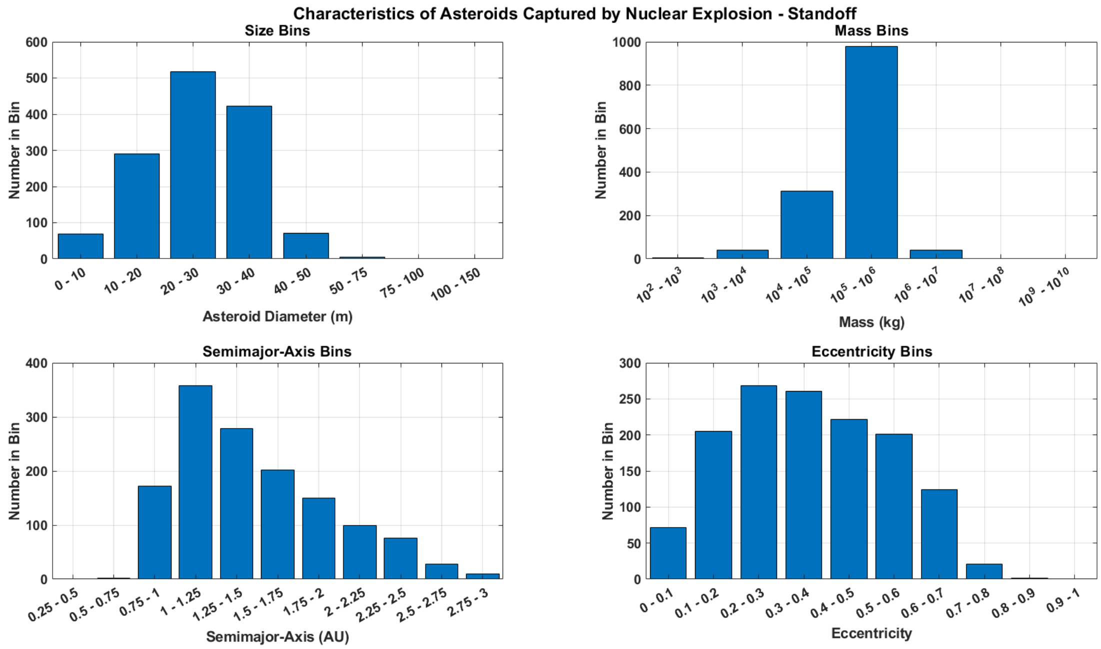

Figure 5.23.. Characteristics of asteroids capturable by standoff nuclear explosives.

For an early mission in the history of asteroid capture, choosing an Earth-like orbit is ideal. Making every detail of the mission as simple as possible increases mission feasibility and likelihood of success. An Earth-like orbit can be defined as having an aphelion and perihelion between 0.95 and 1.05 AU. Restricting the set of feasible targets by their diameter leaves just over 1100 possible asteroids. Doing so for the orbital properties leaves eight possible choices. Combining the restrictions on orbit and mass, the population of feasible NEAs is reduced to three possible candidates: 2015 XZ378, 2018 PN22, and 2013 RZ53. The properties of these asteroids are listed in the Table 5.4. This limited selection makes the choice much more straightforward. Through analysis of optimal transfers and intelligent filtering of desirable asteroid properties, the population of over 22,000 NEAs is reduced to three top candidates. Of these three, 2018 PN22 is the least viable. It requires the largest inclination change for the transfer, it has the highest estimated transfer cost, and it is neither

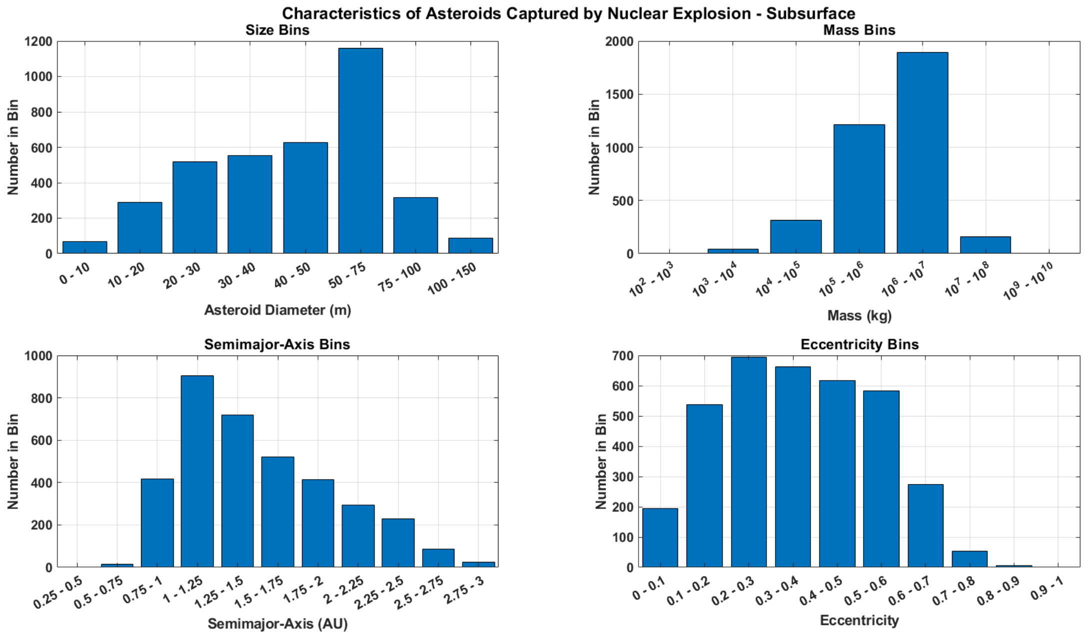

Figure 5.24.. Characteristics of asteroids capturable by sub-surface nuclear explosives.

Table 5.3.. Properties of candidate asteroids with Earth-like orbits and diameters between 5 m and 35 m. The transfer cost is calculated using the estimation model developed earlier in this work. Transfers are assumed to be to an Earth-trailing orbit.

Name	Diameter (m)	Semimajor (AU)	Ecc.	Inc. (deg)	Transfer Cost (km/s)
2013 RZ53	5.109	1.016	0.0284	2.108	1.564
2018 PN22	28.166	0.997	0.0392	4.385	3.058
2015 XZ378	30.784	1.014	0.0348	2.719	1.962

the smallest asteroid (easiest to tether, and maneuver), nor is it the largest (most material for study). The two ideal candidates are 2013 RZ53, and 2015 XZ378. These two asteroids are both in Earth-crossing orbits and require less $2\frac{km}{s}$ to transfer into an Earth-trailing orbit. This much propulsion has been achieved by chemical

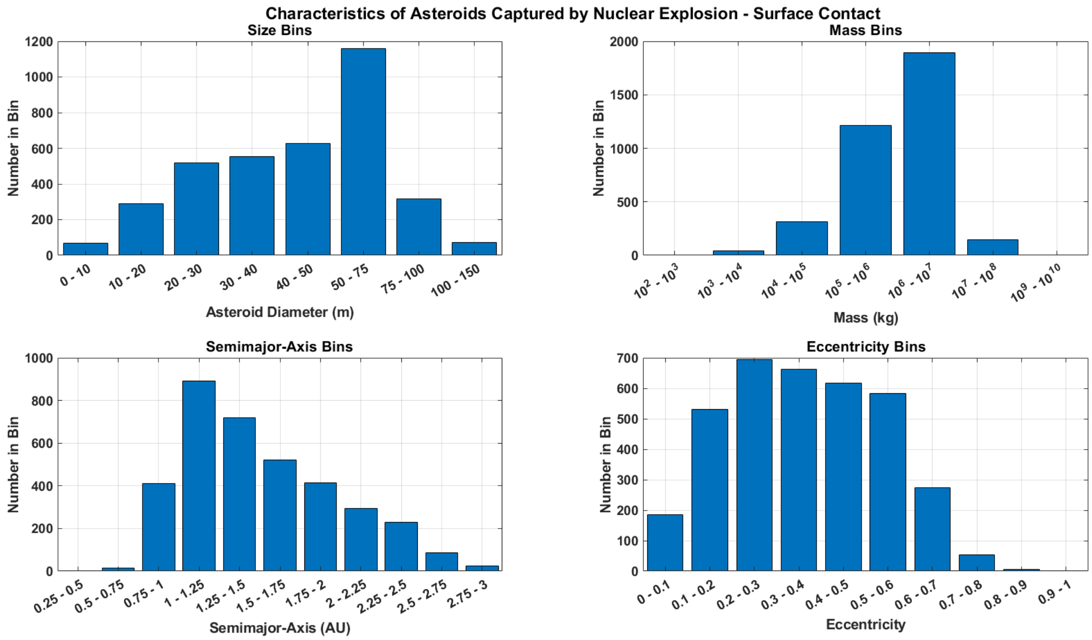

Figure 5.25.. Characteristics of asteroids capturable by surface nuclear explosives.

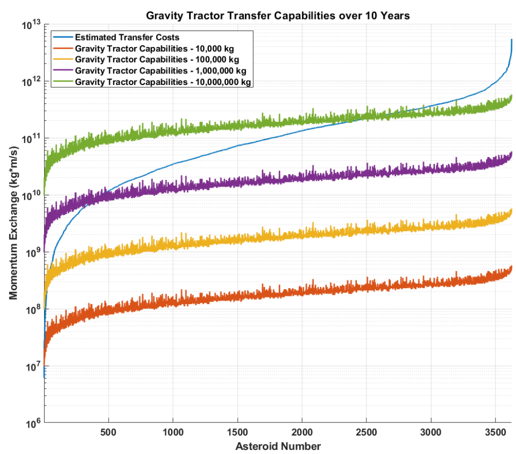

(a) Capabilities of gravity tractors given different masses.

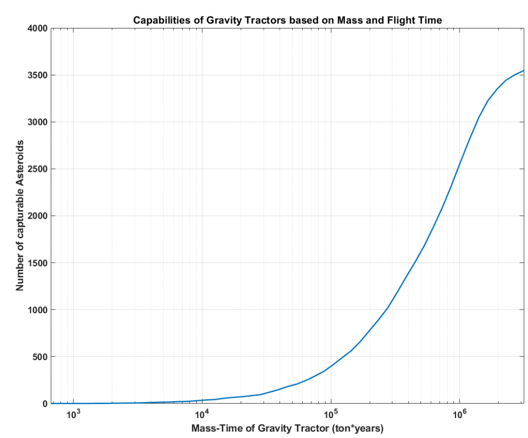

(b) Number of capturable asteroids compared to the mass-time of the gravity tractor.

Figure 5.26.. Capture capabilities of gravity tractors.

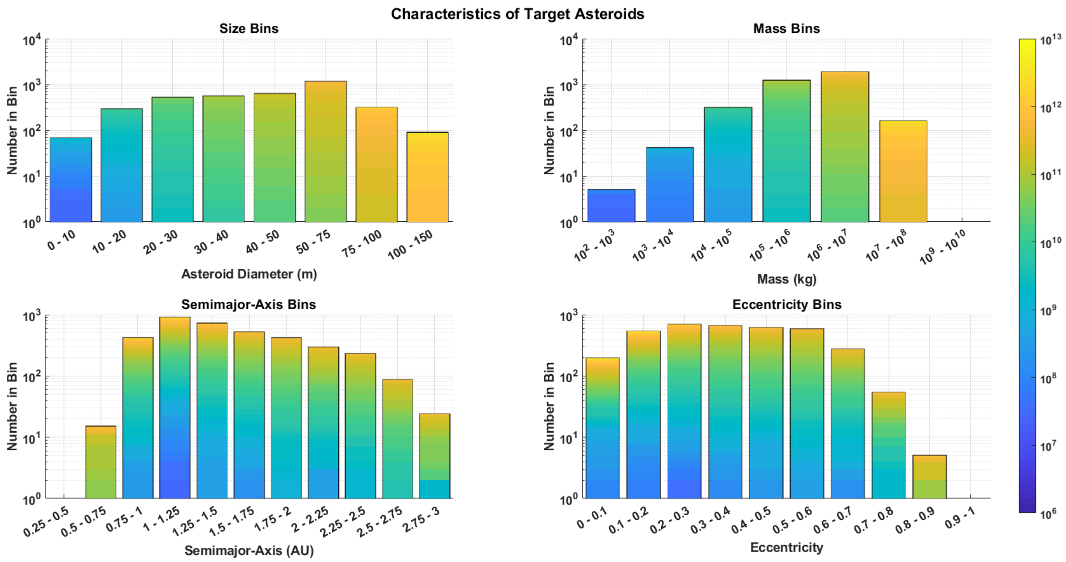

Figure 5.27.. Characteristics of asteroids capturable by any technology, generalized to available level of momentum exchange. Unlike previous plots, those shown in this figure are given on a logarithmic scale.

propulsion in the past and has been surpassed significantly by low-thrust systems, making it a reasonable mission benchmark. It is also possible that with different transfer methods, this value could shrink even further.

A mission with any technology that could produce the required momentum exchange could feasibly transport 2013 RZ53 within 10 years or less. Asteroid 2015 XZ378 would be a feasible target for higher thrust technologies but would be more difficult for low-thrust systems. For this reason, for all systems that cannot sustain an average thrust on the order of 100 N or more, the smaller asteroid of these two, 2013 RZ53 is the recommended target. This is also the ideal target for missions with more conservative mission requirements and is the choice recommended for early attempts at asteroid capture. For larger asteroids, if the technology chosen can sustain 100 N of thrust or greater, and the mission can allow for the capture of a larger asteroid, 2015 XZ378 is the recommended target.

These recommendations are for early asteroid missions. The orbital and mass constraints are intentionally over-restrictive in order to reduce the feasible population as much as possible. For example, if the Earth-like condition is loosened from being within 5% to being within 10% of Earth's aphelion and perihelion, the number of asteroids in the feasible set that meets the requirements goes from 8 to 57. Reducing it further to 15% increases this number to 139. The relationship is shown in Figure 5.28. This relationship gives a more concrete bound for mission design and allows a tuning of this parameters for a more or less restrictive asteroid set.

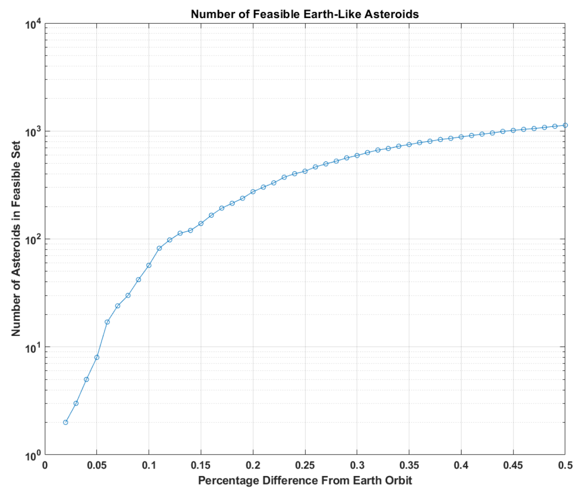

Figure 5.28.. Relationship between the percentage difference in aphelion and perihelion and the number of asteroids in the feasible set within that range.

Another reasonable way to limit the asteroid selection process is by estimated transfer cost. While ΔV is a typical metric for mission transfer costs, the efficacy of this metric is reliant on the fact that most spacecraft have a mass of a similar order. A more concrete metric for the comparison of transfer costs is the amount of momentum exchange required. Figure 5.29 shows the relationship between the required momentum exchange and the required change in velocity for the estimated asteroid captures into Earth-trailing orbits. It is clear that, while the trending is similar, the two plots are different enough that choosing a bound on one would not be equivalent to choosing a bound on the other. For typical missions, where the mass of spacecraft is relatively small, these differences are minimal and either gives a concrete comparison, but since the mass range is so large for asteroids, momentum exchange is a more tractable assessment of the feasibility.

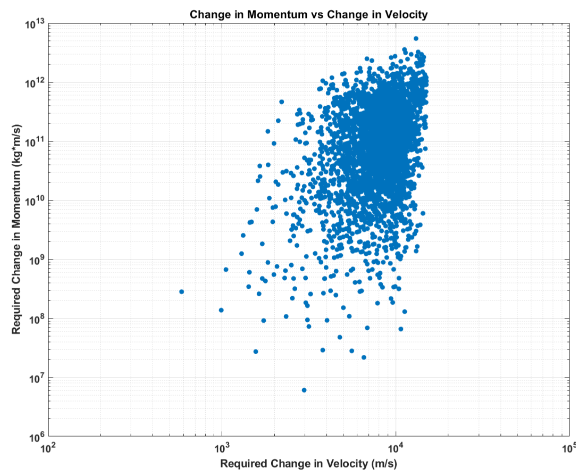

Figure 5.29.. Comparison between the required momentum exchange and the required change in velocity to capture asteroids into Earth-trailing orbits.

The 10 asteroids with the smallest momentum exchange requirements are shown in the table below. It is clear from the transfer costs shown here that strictly limiting the ΔV is not a useful metric. The asteroid that requires the lowest amount of momentum exchange has a transfer ΔV requirement of over 11 km/s. Choosing between these asteroids comes down to mission preferences. In general, having a more Earth-like orbit simplifies the transfer and would require less control authority to complete. A transfer that requires a large inclination change, for example, would be very difficult for systems that do not have strong thrust vectoring. Asteroids in orbits with low inclination, a semimajor axis near 1 AU and an eccentricity close to zero will require the least effort to transfer efficiently and should be among the first selected for capture.

Table 5.4.. Properties of candidate asteroids with the smallest momentum exchange requirements, listed in ascending order by the required amount of momentum exchange. The transfer cost is calculated using the estimation model developed earlier in this work and are assumed to be to an Earth-trailing orbit. The first column labeled 'Transfer Cost' represents the required momentum exchange and the second, the required change in velocity.

Name	Diam. (m)	Semimajor (AU)	Ecc.	Inc. (deg)	Δp Cost (10^7 kg*m/s)	ΔV Cost (km/s)
2008 US	4.450	1.611	0.6134	5.963	0.608	11.253
2019 VBS	3.875	1.067	0.2092	0.875	2.178	3.798
2019 YS	4.249	1.089	0.2104	2.853	2.731	4.763
2019 SS2	6.142	1.065	0.2651	1.408	2.809	4.991
2018 WV1	7.385	1.040	0.0603	1.653	2.894	1.736
2019 AS5	2.940	1.348	0.3925	0.701	4.784	6.550
2018 VP1	5.602	1.588	0.4298	3.242	6.583	7.844
2017 UJ2	5.602	1.122	0.1836	0.525	6.883	3.161
2018 UL6	3.375	1.101	0.2544	3.151	7.272	5.580
2017 WE30	3.610	2.123	0.6728	1.019	9.151	10.688

From this list, the only asteroids that have significant differences from an Earth-like orbit are 2008 US, 2018 UL6, 2019 YS, and 2017 WE30. The former three have relatively large inclinations in comparison to the others, and the latter has a large semimajor axis. Both 2008 US and 2017 WE30 also are highly eccentric orbits, as is 2018 VP1. With these characteristics in mind, the best candidates are 2019 VBS, and 2018 WV1. Asteroid 2019 VBS is the number one candidate because it is the lowest required momentum exchange cost on this list that maintains Earth-like orbital properties. The other asteroid, 2019 WV1, is also a great choice because it has similar transfer properties, is in an Earth-like orbit and is the largest asteroid on this list.

5.3.2 Choosing a Technology

Choosing a technology is more complex than deciding on the asteroid. There are feasibly many asteroids for any given technology to choose from, the differences between which could easily have little to no impact on the mission. The technology, on the other hand, completely determines almost every part of the mission from the timeline to the supporting subsystems to the launch and so forth.

From a pure transfer perspective, there are attractive qualities to destructive technologies, nuclear blasts, kinetic impactors, and mass drivers, for example. These technologies have high momentum exchange efficiencies for a given launch mass. However, the prospect of destroying or damaging asteroids, in any way, early in the process of capture is not ideal. Any damage can significantly change the surface properties and since these technologies have never been tested, it is difficult to predict the extent of the damage on the internal or even chemical properties of the asteroids. While they remain interesting and viable options in the asteroid capture conversation, for early missions, highly destructive technologies should be bypassed.

Another important consideration for choosing a technology is whether or not it requires direct attachment to the asteroid. The process of attachment can damage the surface of the asteroid. This likely would be insignificant - it is insignificant compared to the damage of explosive technologies, for example - but it still would affect the overall quality of the scientific output from the capture. This minor surface damage is also possible for any technology that directly affects the asteroid. For example, laser ablation systems will burn off the top layers of parts of the asteroid, and Yarkovsky systems would require changing the surface properties intentionally. Any of these things could disturb scientific analysis. If the goal of the mission is purely scientific, the only technologies that could transport the technology with no notable damage would be ion beams, which would only place charged particles on the surface and would not have a significant impact on surface properties, and gravity tractors, which have no contact with the asteroid whatsoever and would leave it physically unchanged.

Ion beams are highly efficient and have been shown to be more mass efficient than gravity tractors [40] but they require high efficiency power systems (on the order of 5-20 kW/kg). These systems also have beneficial vectoring properties, being able to easily modify the net thrust vector on the asteroid. The major downside of ion beams, besides their large power requirements, is the requirement of two propulsion systems - one to push the asteroid and one to maintain the spacecraft's proper position behind the asteroid. These systems should be given serious consideration if they drawbacks are not considered an issue. Otherwise, gravity tractors are currently the most feasible entirely non-destructive asteroid transfer option.

On top of the 'clean' properties of gravity tractors, they are also very mass efficient. Theoretically, any gravity tractor could pull any asteroid back to Earth given enough time. Functionally, this is limited by the cost of the transfer for the tractor itself and is dependent not on the time it can spend near the asteroid, but on how long the gravity tractor can maintain efficient proximity operations maneuvers that pull the asteroid optimally. Launch mass is the most restrictive factor for the design of gravity tractors since they need no new systems in order to operate in an asteroid capture mission. Any other technology, even propulsive technologies that have been used in missions for decades require the development of attachment systems for capture missions. Gravity tractors also have a distinct advantage over technologies that require attachment in that spinning targets are feasible. Systems that require attachment must either find asteroid with almost no rotational momentum or they must slow that rotation manually. Neither of these are trivial considerations, but a gravity tractor could pull any asteroid regardless of its spin rate. For these reasons, gravity tractors are very attractive technologies in general. The major downside of gravity tractors is their time requirements. It takes a considerable amount of time to transfer any object using the small gravitational perturbations from a launched spacecraft. The equivalent force on an asteroid is on the order of 0.01 N to 0.10 N. This is evident in Figure 5.26. With multiple launches and longer allowed mission times, this number could be improved significantly, but the overall number of potential targets would still be relatively low compared to other technologies given equivalent considerations.

With current levels of technological development, propulsive technologies show promise for asteroid capture. Propulsive systems are well understood and offer missions with much lower flight times than very-low thrust technologies. The transfer can also be continuously vectored, which is much more difficult for other systems. Discounting the need to develop attachment technologies, one major issue with propulsive systems is the momentum exchange efficiency properties. While propulsive systems can maneuver spacecraft very efficiently, the process of pulling an object means that multiple spacecraft are required to maintain efficient thrust vectoring. A single tug will have to carefully maneuver in order to avoid ejecting material onto the asteroid, both potentially contaminating the surface and reducing the effective thrust of the system. Multiple spacecraft help bypass this issue, but this requires launching multiple launches and attaching both spacecraft to the same tether. If the propulsive system is designed to push the asteroid instead, this can bypass the blowback onto the asteroid, but it requires that the system be firmly connected to the body, and connected at the center of mass on average to avoid spinning the asteroid during transit. This is possible, but it requires a surveillance mission beforehand or that the spacecraft spends a significant amount of time beforehand in order to determine these properties itself. Another issue with push-style propulsion is that the surface of asteroids is rocky, but not necessarily firm enough to support a system clamping tightly into it and thrusting. A thorough preliminary survey of the surface properties would be required to determine if the target asteroid is feasible.

All of these things in mind, propulsive systems are still good options. The issues presented are just a few that mission designers should consider, but none of them make the mission infeasible. Adding multiple launches, for example, is expensive and can add some complications, but it has been done before. The majority of the required development for these systems would be the attachment technology and otherwise, these systems have a high TRL. Many of the other proposed technologies such as mass drivers, Yarkovsky systems, laser ablations systems, etc., all require ground-up technological development. This not only makes them more expensive and increases the build time before launch, it also incurs the risks of unforeseen technological complications. Propulsion has been so thoroughly used in missions that the chances of a completely unexpected failure are much lower. Another major advantage of propulsive systems is that they allow for larger corrective maneuvers during the transfer. If something goes wrong with the return trajectory, the higher the thrust of the system, the more direct continuous control the system has, and the more easily it can account for unpredicted perturbations.

Of the types of propulsive technologies, low-thrust systems, and chemical systems, both have merits in different contexts. Chemical systems require more launch mass and more complex piping, pressurants, etc., and these systems cannot provide total Δv equivalents on the same order of magnitude as low-thrust systems. Chemical propulsion can, however, deliver very high and sustained levels thrust. As seen in the trajectory analysis presented in this work, the higher thrust transfers are equivalently costly from a transfer perspective, but they often require much less time. Lower mission times mean there is less time for things to go wrong and the spacecraft suffers fewer environmental effects. The longer the mission time, the more difficult and costly it becomes to protect against interplanetary radiation, for example. Low-thrust systems have the advantage of significantly higher ΔV caps and fundamentally more simple systems. The shock from thrusting for low-thrust systems would also be significantly less, reducing the probability of inadvertently damaging the asteroid. Ultimately, the choice of using chemical thrust or low-thrust systems is a matter of preference for the asteroid capture problem. If long mission times are a potential issue, using chemical systems are ideal for reducing the flight time. If higher ΔV is needed for other parts of the mission, including the transfer there, the observational period, etc., then low-thrust systems would be a more appropriate choice.

These two technologies, gravity tractors, and propulsive options, are currently the best candidates for asteroid transport. The TRL of gravity tractors is high enough that one could be launched as soon as it is built. Gravity tractors do not directly or indirectly affect the properties of the asteroid in any way and would be ideal choices for scientific missions. Propulsive options offer higher thrust levels, vectored control, and a litany of experience. For missions interested in capturing larger asteroids, or asteroids that are farther away from Earth, these technologies are the best choice.

5.3.3 A Preliminary Roadmap for Asteroid Capture Missions

The roadmap for this section is given in two parts. The first is a preliminary technology roadmap. The goal is to compare the technologies from a mission design perspective by presenting a simple decision flowchart. The goal of these flowcharts is to allow an initial comparison of different key characteristics in the mission and how they impact the technology and asteroid choices specifically.

The first part of this analysis takes a look at choosing a technology based on mission design considerations. The considerations examined here are development, attachment, damage, launches, and control authority. These are just a few of the many different metrics you could use to qualify the validity of different missions and transport technologies. Tables 5.5 and 5.6 show how the examined technologies fall into these different categories.

Using these qualities, an initial decision flowchart is created and shown in Figure 5.30. This chart is not a full-proof way of deciding on a technology. There are many different, important mission considerations that might force one technology or another and enumerating and discussing every possible one of them would be overwhelming and would not lend itself to a coherent analysis. The choices shown here are meant to be high level decisions that can guide mission designers and are not meant to be rules of the decision-making process.

The flowchart characterizes decisions into independent and dependent decision chains. A dependent decision chain, shown in red, represents a choice that must be followed if the answer to the associated question is what the chart displays. An

Table 5.5.. Mission design considerations for asteroid transfer technologies. Systems with an asterisk under the 'Multiple Launches' category do not require multiple launches but could benefit from them.

Slow Technologies							
Technology	Required Development	Attachment	Damage to Asteroid	Breakup Liklihood	Multiple Launches	Control Authority	Versatility
Electric Prop.	Low - Med.	✓	Attachment	Very Low	✗*	High	High
Solar Sail	Med.	✓	Attachment	Very Low	✗	Low	Med.
Gravity Tractor	None	✗	None	None	✗*	Low	Low
Ion Beam	Low - Med.	✗	None	None	✗*	Med.	High
Enh. Yarkovsky	High	✗	Surface	None	✗	None	Very Low
Laser Ablation	High	✗	Surface	None	✗*	Low	Med.

Fast Technologies							
Technology	Required Development	Attachment	Damage to Asteroid	Breakup Liklihood	Multiple Launches	Control Authority	Versatility
Kinetic Impactor	Low	✗	Impact	Med.	✓	Low	Low
Chemical Prop.	Low - Med.	✓	Attachment	Very Low	✗*	High	High
Mass Driver	High	✓	Digging	Low	✗*	Med.	Very Low

Table 5.6.. Mission design considerations for explosive asteroid transfer technologies. Systems with an asterisk under the ‘Multiple Launches’ category do not require multiple launches but could benefit from them.

Explosives							
Technology	Required Development	Attachment	Damage to Asteroid	Breakup Liklihood	Multiple Launches	Control Authority	Versatility
Nuclear (Standoff)	High	✗	Surface	Med.	✓	Low	Low
Nuclear (Surface)	High	✓	Nuc. Blast	High	✓	Low	Low
Nuclear (Subsurface)	High	✓	Nuc. Blast	Very High	✓	Low	Low
Conv. (Surface)	Med.	✓	Blast	High	✓	Low	Low
Conv. (Subsurface)	Med.	✓	Blast	Very High	✓	Low	Low

independent choice, shown in black, represents a suggestion to the decision flow. An example of this relationship is given by the first decision point in the tree. If technological development is not feasible, then the only viable option for asteroid capture is gravity tractors. However, if technological development is feasible, gravity tractors may still be a viable choice, but it is recommended that first the rest of the decision tree is examined before deciding on gravity tractors. Further into the decision tree, the red choices represent the confluence of all the previous choices. The second decision point, whether surface damage is acceptable or not, for example, is reached already assuming that technological development is feasible. Given that, if surface damage is not acceptable, the only options are ion beams and gravity tractors. This means that the tree following the second decision point must only lead to those two technologies, but the decision between those two is based on a suggestion from the third decision point, the total mission time. By another example, if one reaches the decision point 'Is the asteroid sun-side?', and the answer is 'Yes', solar sails are the suggested technology, but they are not the only feasible technology given this decision chain. Ultimately, there is no way to dilute the decision process in light of all possible mission considerations. This flowchart pulls out what requirements can reduce the technological choices and otherwise is a series of informed suggestions.

There are also other preliminary mission considerations that could directly affect the outcome of this decision-making process. Properties of the asteroid, for example, could have a big impact on the choice of technology. This decision flow is meant to be representative of the process for early asteroid capture missions. Certain decisions are not necessarily ideal given any context, including the following of the decision tree, the choices are meant to reflect reasonable reflections on the previous decisions. If core damage to the asteroid is allowed, and no control authority is required, then the mission likely does not have a high-fidelity capture target and is not concerned for the end status of the asteroid. In this case, any technology is possible, but kinetic impactors and nuclear options are the recommended choices due to their high momentum exchange capabilities and their relatively simple development.

Some of the most limiting choices in the tree, besides the allowed development, are the amount of damage allowed to the asteroid, and the amount of control authority required. In this case, ion beams are predicted to be more efficient than gravity tractors with equivalent launch masses given sufficiently efficient power systems [40]. If surface damage is allowed, but core damage is not, then impacts and explosives are no longer viable. For missions with precise target orbits, high control authority is required, which leaves propulsive options and mass drivers. Lower control authority systems that are still viable include solar sails, laser ablation systems, ion beams, and gravity tractors.

The availability of launches can also constrain the problem considerably. Impactors and explosives require a minimum of two impacts to change the asteroid to an Earth-like orbit. While this is technically possible with one launch, it would be a feat of mission design to do so and it would be considerably more effort than simply choosing a different technology. This can also impact the choice of non-destructive technologies. Propulsive systems can improve their average efficiency with multiple tugs working simultaneously as could ion beams, laser ablation systems, and anything with implicit pointing inefficiencies. If the asteroid is large enough, multiple launches could be mandated in order to properly maneuver it into a capture orbit.

Once these considerations are addressed and a technology is chosen, Table 5.7 outlines the remaining suggestions for mission design considerations. This table is independent of the previous decision tree and thus, will contain some recommendations that are contradictory to certain progressions through the decision tree. These will not, however, ever violate the dependent decisions in the tree and will not create fundamentally contradictory mission requirements. Certain technologies are also removed from the table, namely conventional explosives since they have been shown to be undesirable choices for asteroid capture.

Another important perspective to add to the technology decision making process is the versatility of the technology. Choosing to spend considerable time and money to develop mass drivers, for example, might be the best option when considering the asteroid capture problem in a vacuum. However, mass drivers do not have many potential uses outside of asteroid capture. While the investment might be worthwhile, spending the same amount of time and effort to improve electric propulsion, as one example, would have value for many other missions and mission types. Similarly, the advancement of certain technologies for other missions could improve the technologies usability for asteroid capture scenarios. Electric propulsion will continue to be a subject of intense interest and development over the next several years so it reasonable to assume a natural progression in ability of these systems early on in a mission design phase. Technologies that require ground-up development will have no independent advancement outside specific asteroid capture missions willing to invest into that particular technology. Ultimately, ubiquity and adaptability become a much more important technological consideration than many other straight-forward considerations such as momentum exchange capabilities or required flight times. Chemical and low-thrust propulsion systems, solar sails, and ion beams all have a wide array of potential mission uses and this makes them more reasonable and safer options, especially early on in mission design. Laser ablation systems, gravity tractors, kinetic impactors, and explosives have some other proposed uses, but few. Enhanced Yarkovsky and mass driver systems have essentially no uses outside of asteroid capture and thus become more difficult options to justify.

This table is meant to give high level suggestions to consider once the transport technology has been chosen. The maximum asteroid diameter is obtained from the asteroids in the feasible set that require less than the predicted maximum amount of momentum exchange required to transfer them, with the transfer cost calculated using the models developed in this work. The suggested asteroid target varies, but in general, it is either the ideal candidate given from the previous sections or, for destructive technologies, it is the largest possible asteroid that can be feasibly transferred. This is because the multiple hits from the destructive techs will likely cause the target to become significantly smaller as it breaks up. The largest feasible target allows the most asteroid to be returned to the Earth while still using utilizing these options. The survey mission column represents a suggestion for an entirely separate precursor mission to survey the asteroid. For kinetic impactors and mass drivers, surveying beforehand is essential since the physical properties of the asteroid have a large impact on their efficacy. For all technologies, a survey period is required so technologies where a survey mission is not suggested are such that they could support an effective survey phase and still properly perform their maneuvers. All missions could benefit from an additional precursor survey mission, but it simply not necessary for most. Finally, as was mentioned before, the multiple spacecraft column is a suggestion and not a declaration. Ion beams, for example, could greatly increase their capabilities by having multiple spacecraft simultaneously pushing the asteroid, but it not recommended at this stage in asteroid capture. This also the case for chemical propulsion and mass drivers.

Table 5.7.. Mission design suggestions given a chosen transport technology.

Chosen Technology	Max Asteroid Diameter (m)	Suggested Target Asteroid	Multiple Spacecraft
Slow Technologies			
Electric Prop.	15.43	2018 WV1	✓
Solar Sail	5.11	2019 VBS	✗
Ion Beam	10.19	2019 VBS	✗

Chosen Technology	Max Asteroid Diameter (m)	Suggested Target Asteroid	Multiple Spacecraft
Fast Technologies			
Kinetic Impactor	40.58	2018 FM2	✓
Chemical Prop.	5.11	2013 RZ53	✗
Mass Driver	35.34	2014 WA366	✗

Chosen Technology	Max Asteroid Diameter (m)	Suggested Target Asteroid	Multiple Spacecraft
Explosives			
Nuclear (Standoff)	56.02	2013 BS45	✓
Nuclear (Surface)	128.33	2012 MD7	✓
Nuclear (Subsurface)	140.71	2015 SO2	✓

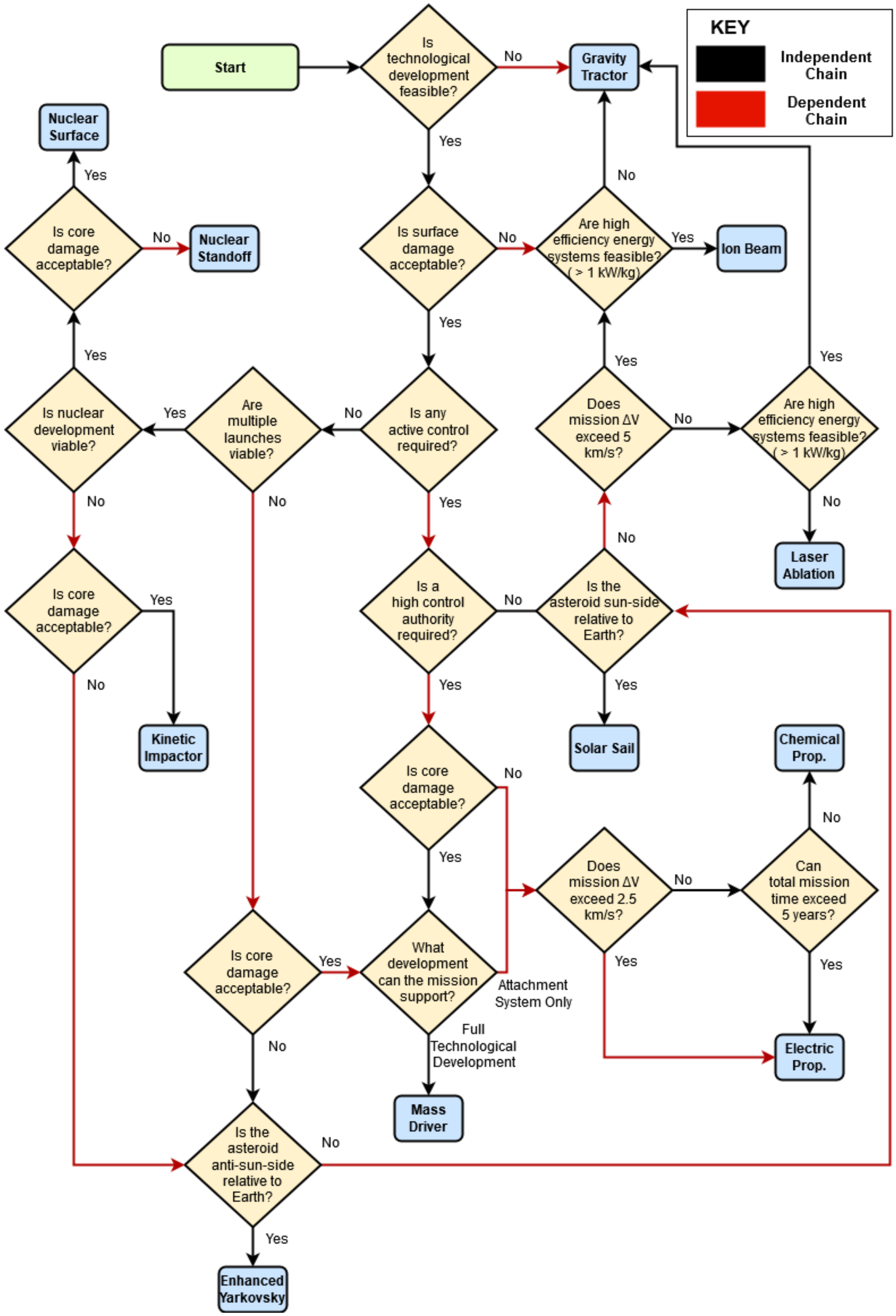

Figure 5.30.. Preliminary asteroid capture technology flowchart. Red lines represent dependent choices while black ones represent independent choices.

6. CONCLUSIONS AND FUTURE WORK

6.1 Future Work

The first goal of this research was to setup a generalized optimizer in an effort to discover the overall shapes and trends of the optimized transfer solutions for asteroid capture missions. This was done for several asteroids with a large epoch and time-of-flight range and in the presence of several different perturbations. While these efforts were largely successful, they suffered some shortcomings.

The optimizer developed in this work is robust and fast but it's speed is limited to the language it was written in, MATLAB, and would see a significant increase in performance if it were written in a more efficient language such as C or Fortran. The optimizer also suffered from performance issues regarding the choices of the genetic algorithm and its movement through the solution space. Since runs were done in time-of-flight blocks based on the number of impulses required to maintain a low-thrust approximation, there was notable bifurcation of the solutions on the edges between these run blocks. This could be solved by doing a single run for the entire time-of-flight range, or a method could be developed for translating solutions with N impulses into approximations of solutions with N+1 or N-1 impulses. There is also a possibility of developing a method similar to the Sims and Flanagan approach whereby nodes can be moved along the trajectory. This would dramatically decrease the number of nodes for any solution and could help settle these discrete node issues. Similarly, the optimizer suffered when certain solutions propagated too far through the solutions space. This was partially solved by the seeding and searching algorithms developed, but there were still issues with solutions from low ΔV valleys being unable to spread out efficiently and consistently despite the fact that those low-cost solutions should exist. MALTO deals with these issues by constraining the number of allowed revolutions for each solution and it is possible that a similar solution could be employed here to improve the overall quality of the results.

Despite these failings of the optimizer, the results were largely successful. It was found that perturbations do not significantly affect the optimized transfers of asteroids. It was also found for all of the tested asteroids that neither epoch nor time-of-flight directly affected the quality of the results. For any chosen epoch, there was a certain flight time that corresponded to the minimum time at which nearly optimal solutions could be found and any flight times greater than that would only marginally improve the cost of the transfers. Functionally, any time-of-flight above some minimum that depends on the initial orbit and the thrust of the spacecraft, there exists nearly optimal transfer solutions. This greatly simplifies the transfer problem from a mission design perspective because it eliminates the need to find an optimal flight time. So long as the time-of-flight is long enough, the transfer time can be fixed, and the transfer optimized otherwise. In a similar context, the fact that the additional perturbations did not significantly impact the solution space means that mission designers can confidently assess the transfer optimization problem without concern for the effects of these perturbations. Using simple two-body dynamics or Lambert solvers is enough to find the costs of transferring asteroids to a given orbit.

Outside of the work necessary to update the optimizer itself, any conclusions drawn therefrom would require an update in the future as well. As more asteroids are discovered, as the NEA population becomes more observed, and as technologies develop enough to allow missions to consider returning asteroid farther from Earth, the results found here will need to be redone. Any ideas developed from the examination of the currently known population of capturable asteroids will have to done in the context of these new developments. This will also allow for these trends to analyzed with a more concrete understanding of the technologies discussed here, hopefully with real missions to contextualize that analysis.

Similarly, the roadmap given for choosing a technology and an asteroid are preliminary. Any number of unforeseen technological developments could entirely change the conversation and modify which technologies are better suited for which missions. The decision points for this roadmap were not conclusive and were given as common-sense mission considerations and inhibitions. It is likely that any mission considering asteroid capture would have decision points not included here. Once asteroid capture has been accomplished and has gained mission legacy and the associated design experience, this roadmap should be redone with a more concrete understanding of the major roadblocks and complications that mission designers should consider.

6.2 Conclusions

This work succeeded in accomplishing its major goals. The asteroid capture optimization problems were generalized to any system of dynamics, and any technology, and tested against a large range of asteroids, different levels of thrust, and in the presence of different perturbations. The optimization effort was successful with the developed optimizer able to find solutions close to the theoretical energy minimum transfers, Hohmann transfers, and having trends matching JPLs optimization tool MATLO. Two major conclusions were found with this optimizer: 1) The time of flight itself does not impact the cost of the transfer. Above some minimum time, which varies based on the asteroid, the thrust, the initial orbit, and the final orbit, every flight time yields a nearly optimal transfer solution of equivalent cost. This is also true for any epoch - for any epoch, there exists some minimum time-of-flight above which equivalently costly solutions could be found. This leads to the second conclusion, 2) The epoch does not affect the transfer cost. For any epoch, there exists nearly optimal transfer solutions so long as the time-of-flight is high enough. Together, these two solutions are significant from a mission design perspective. These results show that time-of-flight and epoch, two things generally considered to be important and coupled factors in spacecraft transfers are unimportant in and of themselves. For a given flight time, there may only be certain epochs that allow nearly optimal solutions at that time, and for a given epoch, only a certain range of flight times will yields quality transfers, but either of these can be chosen arbitrarily (above some minimum flight time) and the other can be chosen to allow for nearly optimal transfer solutions. These conclusions were found to be true regardless of the asteroid, thrust, or dynamics tested.

In the context of the tested perturbations, solar radiation pressure, and n-body gravitational effects from the Earth, the Moon, Jupiter, and Venus, it was found that these effects have no notable impact on the quality of the optimized transfer solutions. The runs tested with multiple perturbations surprisingly showed an increase in robustness and a more consistent trending, but the best-found solutions, and the trends did not change regardless of the dynamics set. This is also a valuable advantage from a mission design perspective. Without having to run complex dynamical models inside an optimization, mission designers can be confident that the inclusion of perturbations will not significantly affect the quality of the results. Once a mission transfer cost is understood, the found trajectories can be corrected into higher fidelity models without worry that the new dynamics will significantly impact the mission.

Not only did the trends show notable consistency, but the quality of the results did as well. Tested over several different analytic models, it was found that the cost of these nearly optimal solutions could be predicted. By combining the Hohmann transfer cost with the theoretical single-burn minimum inclination-matching cost, the transfer ΔV could be predicted analytically. This analytic value was found to match the optimized transfer cost with a standard deviation of 10% from the predicted value and a 95% lower confidence interval of approximately 1.10 of the predicted cost. This confidence interval tells mission designers, without ever running an optimizer, that it is reasonable to expect optimized transfer costs according to this model plus an addition 10% as an upper bound to the minimum transfer costs. While a full optimization would still be required for any mission, from a preliminary perspective, this is a valuable and easy-to-calculate first order idea of the transfer cost.

A similar effort was made to predict the theoretical minimum transfer time required for nearly-optimal transfers, but, despite a length effort with numerous different models tested, the best analytic model could only compare to the tabulated transfer results with a standard deviation of approximately 35%. While this might give some idea of how much time transfers should take, it is not conclusive enough to trust as a bound and an optimization should be run in order to determine these qualities.

Using these models, the known population of NEAs was examined to estimate the cost of transferring any of these objects while also estimating the minimum required transfer time. This population was reduced to a feasible set of asteroids by adding reasonable restrictions to the transfer time and cost, and this new population of NEAs was examined against the technological capabilities of several different technologies. From this analysis, the statistics of potentially capturable asteroids were found to given an overview of the use-cases for each technology It was found that destructive technologies such as nuclear blasts, kinetic impactors, and mass drivers have some of the highest momentum exchange capabilities, though, naturally, they damage the target. Gravity tractors were found to be ineffectual unless given a significant amount of transfer time or a very high launch mass. Once smaller asteroids are located and launch vehicles improve, gravity tractors will be one of the bets choices for asteroid capture. Otherwise, propulsive systems were found to be one of the best options. They have relatively high momentum exchange capabilities, the high have high control authorities, and they have long mission lifetimes. The only major drawback for these technologies is that they require the development of an attachment system, an attachment system that could easily cause surface damage or even breakup of the asteroid body.

REFERENCES

[1] Nocedal, J., & Wright, S. J. (1999). *Numerical Optimization* (P. Glynn & S. M. Robinson (eds.)). Springer-Verlag New York, Inc. https://doi.org/10.1117/3.1002609.ch49

[2] Vallado, D. A. (2013). *Fundamentals of Astrodynamics and Applications, 4th Ed.* (W. J. Larson (ed.); 4th ed.).

[3] Der, G. J. (2011). *The Superior Lambert Algorithm. DerAstrodynamics.*

[4] Potter, R., Woolley, R., Nicholas, A., & Longuski, J. (2018). *Features and characteristics of earth-mars bacon plots.* Advances in the Astronautical Sciences, 162, 3799–3817.

[5] Fu, L., Xu, M., An, X., & Yan, X. (2012). *Design and optimization of low-thrust orbit transfers using hybrid method.* Advanced Materials Research, 588–589, 335–339. https://doi.org/10.4028/www.scientific.net/AMR.588-589.335

[6] Wagner, S. A. (2014). *Automated trajectory design for impulsive and low thrust interplanetary mission analysis* [Iowa State University]. https://doi.org/10.31274/etd-180810-3789

[7] Wagner, S., & Wie, B. (2014). *Low-thrust trajectory optimization for asteroid exploration, redirect, and deflection missions.* Advances in the Astronautical Sciences, 152, 1219–1232.

[8] Knitter, W. (1988). *Convex Optimization.* Journal of Curriculum Studies (Vol. 20, Issue 6). https://doi.org/10.1080/0022027880200601

[9] Sims, J. A., & Flanagan, S. N., (1999) *Preliminary Design of Low-Thrust Interplanetary Missions*, AAS/AIAA Astrodynamics Specialist Conference, AAS Paper 99-338, Girdwood, Alaska, Aug. 1999. Also in Advances in the Astronautical Sciences, Univelt Inc., San Diego, CA, Vol. 103, Part I, 1999, pp. 583-592

[10] Yang, G., & Weiqi, L. (2009). *Systematic Direct Approach for Optimizing Continuous-thrust Earth-orbit Transfers.* Chinese Journal of Aeronautics, 22(1), 56–69. https://doi.org/10.1016/S1000-9361(08)60069-2

[11] NASA. (2006). *2006 Near-Earth Object Survey and Deflection Study Final Report*, (December), 275.

[12] National Research Council (2010), *Defending planet Earth: Near-Earth object surveys and hazard mitigation strategies*, Washington, D. C. , National Academies Press. https://doi.org/10.17226/12842

[13] Stahl, B. a, & Braun, R. D. (2008). *Low-Thrust Trajectory Optimization Tool to Assess Options for Near-Earth Asteroid Deflection.* Horizons, (August). https://doi.org/10.2514/6.2008-6255

[14] Izzo, D., Olympio, J., & Yam, C. (2009). *Asteroid Deflection Theory: fundamentals of orbital mechanics and optimal control. 1st IAA Planetary Defense Conference*, (1). Retrieved from http://www.esa.int/gsp/ACT/doc/MAD/pub/ACT-RPR-MAD-2009-AstDeflection.pdf

[15] Wie, B. (2008). *Dynamics and control of gravity tractor spacecraft for asteroid deflection. Journal of Guidance, Control, and Dynamics*, 31(5), 1413–1423. https://doi.org/10.2514/1.32735

[16] Ketema, Y. (2017). Asteroid deflection using a spacecraft in restricted keplerian motion. Acta Astronautica, 136, 64–79. https://doi.org/10.1016/j.actaastro.2017.03.004

[17] Mazanek, D. D., Reeves, D. M., Hopkins, J. B., Wade, D. W., Tantardini, M., & Shen, H. (2015). *Enhanced Gravity Tractor Technique for Planetary Defense.* 4th IAA Planetary Defense Conference - PDC 2015, (June), 29. Retrieved from https://ci.nii.ac.jp/naid/40022109555/

[18] Vasile, M., & Colombo, C. (2008). *Optimal impact strategies for asteroid deflection. Journal of Guidance, Control, and Dynamics*, 31(4), 858–872. https://doi.org/10.2514/1.33432

[19] Vasile, M., & Thiry, N. (2016). *Methods and Techniques for Asteroid Deflection. Asteroid and Space Debris Manipulation: Advances from the Stardust Research Network*, 429–494. https://doi.org/10.2514/5.9781624103247.0429.0494

[20] Olds, J., Charania, A., and Schaffer, M. G. (2007). "Multiple mass drivers as an option for asteroid deflection missions," Proceedings of the 2007 Planetary Defense Conference, Washington, DC, pp. S3-7.

[21] Paek, S. W., & Weck, O. de W. (2016). *Asteroid Deflection Campaign Design Integrating Epistemic Uncertainty*, (June). Massachusetts Institute of Technology.

[22] Eggl, S., Hestroffer, D., Cano, J. L., Avila, J. M., Drube, L., Harris, A. W., ... Michel, P. (2016). *Dealing with Uncertainties in Asteroid Deflection Demonstration Missions: NEOTwIST.* https://doi.org/10.1017/S1743921315008698

[23] Sánchez, J.-P., Neves, R., & Urrutxua, H. (2018). *Trajectory Design for Asteroid Retrieval Missions: A Short Review.* Frontiers in Applied Mathematics and Statistics, 4(October), 1–6. https://doi.org/10.3389/fams.2018.00044

[24] Yarnoz, D. G., Sanchez, J. P., & McInnes, C. R. (2010). *Easily Retrievable Objects Among the NEO Population.* Sea Technology, 51(5), 10–13. https://doi.org/10.1007/s10569-013-9495-6.Pre-print

[25] Baoyin, H. X., Chen, Y., & Li, J. F. (2010). *Capturing near earth objects.* Research in Astronomy and Astrophysics, 10(6), 587–598. https://doi.org/10.1088/1674-4527/10/6/008

[26] Brophy, J., Gershman, R., Landau, D., & Polk, J. (2011).*Feasibility of Capturing and Returning Small Near-Earth Asteroids.* 32nd International Electric Propulsion Conference, Wiesbaden, Germany, 1–15.

[27] Brophy, J. R., Culick, F., & Friedman, L. (2012). *Asteroid Retrieval Feasibility Study*, (April), 1–51.

[28] Liado, N., Ren, Y., Masdemont, J. J., & Gomez, G. (2012). *Capturing small asteroids into sun-earth lagrangian points for mining purposes*. Proceedings of the International Astronautical Congress, IAC, 7, 1–10.

[29] Strange, N. J., Landau, D., Longuski, J., & Chodas, P. (2014). Identification of Retrievable Asteroids with the Tisserand Criterion, (August). https://doi.org/10.2514/6.2014-4458

[30] Bao, C., Yang, H., Barsbold, B., & Baoyin, H. (2015). *Capturing near-Earth asteroids into bounded Earth orbits using gravity assist*. Astrophysics and Space Science, 360(2), 1–11. https://doi.org/10.1007/s10509-015-2581-3

[31] Urrutxua, H., Scheeres, D. J., Bombardelli, C., Gonzalo, J. L., & Peláez, J. (2015). *Temporarily captured asteroids as a pathway to affordable asteroid retrieval missions*. Journal of Guidance, Control, and Dynamics, 38(11), 2132–2145. https://doi.org/10.2514/1.G000885

[32] Tan, M., McInnes, C. R., & Ceriotti, M. (2018). *Low-energy near-earth asteroid capture using momentum exchange strategies*. Journal of Guidance, Control, and Dynamics, 41(3), 632–643. https://doi.org/10.2514/1.G002957

[33] Neves, R., & Sánchez, J. P. (2019). Multifidelity design of low-thrust resonant captures for near-earth asteroids. Journal of Guidance, Control, and Dynamics, 42(2), 335–346. https://doi.org/10.2514/1.G003599

[34] D.K. Yeomans, S. Bhaskaran, S.R. Broschart, S.R. Chesley, P.W. Chodas, M.A. Jones, T.H. Sweetser, E.T. Lu, R. L. S. (2008). *Using a Gravity Tractor to Help Mitigate Asteroid Collisions with Earth*. Asteroids, Comets, and Meteors, 5–26.

[35] Ketema, Y. (2017). *Asteroid deflection using a spacecraft in restricted keplerian motion*. Acta Astronautica, 136, 64–79. https://doi.org/10.1016/j.actaastro.2017.03.004

[36] Landau, D., & Strange, N. (2012). *Near-Earth asteroids accessible to human exploration with high-power electric propulsion*. Advances in the Astronautical Sciences, 142 (December), 635–654.

[37] Spencer, D.A., Johnson, L., and Long, A.C., "Solar Sailing Technology Challenges," Journal of Aerospace Science and Technology, Vol. 93, Oct. 2019, 10.1016/j.ast.2019.07.009.

[38] Jerome Wright (1992), *Space Sailing*, Gordon and Breach Science Publishers

[39] Bombardelli, C., Urrutxua, H., & Peláez, J. (2012). *Earth delivery of a small NEO with an ion beam shepherd*. Advances in the Astronautical Sciences, 143, 371–378.

[40] Bombardelli, C., Urrutxua, H., Merino, M., Peláez, J., & Ahedo, E. (2013). *The ion beam shepherd: A new concept for asteroid deflection*. Acta Astronautica, 90(1), 98–102. https://doi.org/10.1016/j.actaastro.2012.10.019

[41] Rubincam, D. P. (1998). *Yarkovsky thermal drag on small asteroids and Mars-Earth delivery*. Journal of Geophysical Research E: Planets, 103(E1), 1725–1732. https://doi.org/10.1029/97JE03034

[42] Thiry, N., & Vasile, M. (2014). *Recent advances in laser ablation modelling for asteroid deflection methods*. Nanophotonics and Macrophotonics for Space Environments VIII, 9226, 922608. https://doi.org/10.1117/12.2060810

[43] Lubin, P., Hughes, G. B., Eskenazi, M., Kosmo, K., Johansson, I. E., Griswold, J., Pryor, M., O'Neill, H., Meinhold, P., Suen, J., Riley, J., Zhang, Q., Walsh, K., Melis, C., Kangas, M., Motta, C., & Brashears, T. (2016). *Directed energy missions for planetary defense*. Advances in Space Research, 58(6), 1093–1116. https://doi.org/10.1016/j.asr.2016.05.021

[44] Stickle, A. M., Atchison, J. A., Barnouin, O. S., Cheng, A. F., Crawford, D. A., Ernst, C. M., ... Rivkin, A. S. (2015). *Modeling momentum transfer from kinetic impacts: Implications for redirecting asteroids*. Procedia Engineering, 103(February 2016), 577–584. https://doi.org/10.1016/j.proeng.2015.04.075

[45] Siddiqi, Asif A. (2018).*Beyond Earth: A Chronicle of Deep Space Exploration, 1958–2016* (PDF). The NASA history series (second ed.). Washington, DC: NASA History Program Office. p. 2. ISBN 9781626830424. LCCN 2017059404. SP2018-4041.

[46] Agle, D. C.; Webster, Guy; Brown, Dwayne; Bauer, Markus (12 November 2014). *Rosetta's 'Philae' Makes Historic First Landing on a Comet*. NASA.

[47] Brophy, J. R., & Friedman, L. (2012). *Returning an Entire Near-Earth Asteroid in Support of Human Exploration Beyond Low-Earth Orbit*. Global Space Exploration Conference.

[48] Brophy, J. R., & Muirhead, B. (2013). *Near-Earth Asteroid Retrieval Mission (ARM) Study*. The 33rd International Electric Propulsion Conference, (IEPC Paper 2013-082), 1–16.

[49] NASA. (2015). *Asteroid Redirect Mission (ARM) Formulation Assessment and Support Team (FAST) Final Report Draft for Public Comment*, (February). Retrieved from https://www.nasa.gov/sites/default/files/atoms/files/fast-final-report-draft-for-public-comment.pdf

[50] Barbee, B., Esposito, T., Piñon, E., Hur-Diaz, S., Mink, R., & Adamo, D. (2012). *A Comprehensive Ongoing Survey of the Near-Earth Asteroid Population for Human Mission Accessibility*, (August). https://doi.org/10.2514/6.2010-8368

[51] Gleaves, A., Allen, R., Tupis, A., Quigley, J., Moon, A., Roe, E., ... Lyne, J. E. (2012). *A survey of mission opportunities to trans-neptunian objects-Part II, orbital capture*. AIAA/AAS Astrodynamics Specialist Conference 2012, (August 2012). https://doi.org/10.2514/6.2012-5066

[52] Morbidelli, Alessandro; Bottke Jr., William F.; Froeschlé, Christiane; Michel, Patrick (January 2002). W. F. Bottke Jr.; A. Cellino; P. Paolicchi; R. P. Binzel (eds.). *Origin and Evolution of Near-Earth Objects* (PDF). Asteroids III: 409–422. Bibcode:2002aste.book..409M

[53] Bowell, Edward & Hapke, Bruce & Domingue, Deborah & Lumme, Kari & Peltoniemi, Jouni & Harris, Alan. (1989). *Application of photometric models to asteroids* in *Asteroids II*, pp. 524-556

[54] Britt, D.T., Yeomans, D., Housen, K., and Consolmagno, G. (2002). *Asteroid Densities*. EAR-A-5-DDR-ASTEROID-DENSITIES-V1.1. NASA Planetary Data System.

[55] Liu, Xiaodong & Baoyin, Hexi & Ma, Xingrui. (2012). *Long-term perturbations due to a disturbing body in elliptic inclined orbit*. Astrophysics and Space Science. 339. 10.1007/s10509-012-1015-8.

[56] Boudad, K. (2018). *Disposal Dynamics from the Vicinity of Near Rectilinear Halo Orbits in the Earth-Moon-Sun System*. 10.13140/RG.2.2.15568.94729.

[57] Aziz, Jonathan & Parker, Jeffrey & Scheeres, D. & Englander, Jacob. (2018). *Low-Thrust Many-Revolution Trajectory Optimization via Differential Dynamic Programming and a Sundman Transformation*. The Journal of the Astronautical Sciences. 65. 10.1007/s40295-017-0122-8.

[58] Zhu, K., Jiang, F., Li, J., & Baoyin, H. (2009). *Trajectory Optimization of Multi-Asteroids Exploration with Low Thrust*. Transactions of the Japan Society for Aeronautical and Space Sciences, 52(175), 47–54. https://doi.org/10.2322/tjsass.52.47

[59] Yam, C. H., Biscani, F., & Izzo, D. (2009). *Global optimization of low-thrust trajectories via impulsive delta-V transcription*. Paper ISTS, 2–7. Retrieved from http://www.esa.int/gsp/ACT/doc/MAD/pub/ACT-RPR-MAD-2009-GlobalOptLowThrust.pdf

[60] Wolpert, D. H., & Macready, W. G. (1997). No free lunch theorems for optimization. IEEE Transactions on Evolutionary Computation, 1(1), 67–82. https://doi.org/10.1109/4235.585893

[61] Lantoine, G., & Russell, R. P. (2012). *A Hybrid Differential Dynamic Programming Algorithm for Constrained Optimal Control Problems. Part 1: Theory*. Journal of Optimization Theory and Applications, 154(2), 382–417. https://doi.org/10.1007/s10957-012-0039-0

[62] Bezrouk, C., & Parker, J. (2014). *Long duration stability of distant retrograde orbits*. AIAA/AAS Astrodynamics Specialist Conference 2014, (August), 1–9. https://doi.org/10.2514/6.2014-4424

[63] Campagnola, Stefano & Skerritt, Paul & Russell, Ryan. (2012). *Flybys in the planar, circular, restricted, three-body problem*. Celestial Mechanics and Dynamical Astronomy. 113. 343-368. 10.1007/s10569-012-9427-x.

[64] Cox D.R., Hinkley D.V. (1974) *Theoretical Statistics*, Chapman& Hall, p49, p209. https://doi.org/10.2307/3616677.

[65] Petropoulos, A. E. (2003).*Simple Control Laws for Low-Thrust Orbit Transfers*. AAS/AIAA Astrodynamics Spe-cialist Conference, AAS Paper 03-630

[66] Petropoulos, A. E. (2005). *Refinements to the Q-law for low-thrust orbit transfers*, AAS Paper 05-162, AAS Space Flight Mechanics Meeting, https://doi.org/120. 963-982.

[67] Collins, G. S., Melosh, H. J., & Marcus, R. A. (2005). *Earth Impact Effects Program: A Web-based computer program for calculating the regional environmental consequences of a meteoroid impact on Earth*. Meteoritics and Planetary Science, 40(6), 817–840. https://doi.org/10.1111/j.1945-5100.2005.tb00157.x

[68] Ariane Group. (2017) *400 N Monopropellant Hydrazine Thruster*. Retrieved October 20, 2020, from https://www.space-propulsion.com/spacecraft-propulsion/hydrazine-thrusters/400n-hydrazine-thruster.html

[69] Boone, S., & Mcmahon, J. (n.d.). *AAS RAPID LOCAL TRAJECTORY OPTIMIZATION USING HIGHER-ORDER STATE TRANSITION TENSORS AND DIFFERENTIAL DYNAMIC PROGRAMMING*, 1–20.

[70] Brasser, R., & Wiegert, P. (2008). *Asteroids on Earth-like orbits and their origin. Monthly Notices of the Royal Astronomical Society*, 386(4), 2031–2038. https://doi.org/10.1111/j.1365-2966.2008.13146.x

[71] Capdevila, L., Guzzetti, D., & Howell, K. C. (2014). *Various transfer options from Earth into Distant Retrograde Orbits in the vicinity of the Moon*. Advances in the Astronautical Sciences, 152(1), 3659–3678.

[72] Carry, B. (2012). *Density of asteroids*. Planetary and Space Science, 73(1), 98–118. https://doi.org/10.1016/j.pss.2012.03.009

[73] Castelli, R. (2011). *Application of the Circular Restricted Three-Body problem to mission design*. Basque Center for Applied Mathematics, (March).

[74] Cellino, a, Bus, S. J., Doressoundiram, A., & Lazzaro, D. (2002). *Spectroscopic properties of asteroid families*. Asteroids III, 1, 633–643.

[75] Curtis, H. D. (2014). *Introduction to Orbital Perturbations*. Orbital Mechanics for Engineering Students. https://doi.org/10.1016/B978-0-08-097747-8.00012-8

[76] Ehresmann, M. (2020).*Asteroid control through surface restructuring*. Acta Astronautica, (October). https://doi.org/10.1016/j.actaastro.2020.09.024

[77] Fiedler, B., Gröger, K., Sprekels, J., Koon, W. S., Lo, M. W., Marsden, J. E., & Ross, S. D. (2013). *Dynamical Systems, the Three-Body Problem and Space Mission Design*. Equadiff 99, 1167–1181. https://doi.org/10.1142/9789812792617_0222

[78] Gong, S., & Li, J. (2015). *Asteroid capture using lunar flyby*. Advances in Space Research, 56(5), 848–858. https://doi.org/10.1016/j.asr.2015.05.020

[79] Helin, E. F., & Shoemaker, E. M. (1979). *The Palomar planet-crossing asteroid survey, 1973-1978*. Icarus, 40(3), 321–328. https://doi.org/10.1016/0019-1035(79)90021-6

[80] Holsapple, K. A., & Housen, K. R. (2012). *Momentum transfer in asteroid impacts. I. Theory and scaling*. Icarus, 221(2), 875–887. https://doi.org/10.1016/j.icarus.2012.09.022

[81] Hoyt, Robert & James, Karsten. (2015). *WRANGLER: Nanosatellite Architecture for Tethered De-Spin of Massive Asteroids*. 10.2514/6.2015-4533.

[82] Johnson, L. (2010). *Near Earth Object Observations Program - Presentation to Astronomy & Astrophysics Advisory Committee.*

[83] Kupershmidt, B. A. (1998). *The Variational Principles of Dynamics.* World Scientific. https://doi.org/10.1142/1135

[84] Laipert, F. E. (2015). *Design of Low-Thrust Missions to Asteroids with Analysis of the Missed-Thrust Problem.* Open Access Dissertations. 495. https://docs.lib.purdue.edu/open_access_dissertations/495. https://doi.org/UMI 3402307

[85] Landau, D. (2017). *Fast and Reliable Approximations for Interplanetary Low-Thrust Transfers*, AAS/AIAA Astrodynamics Specialist Conference, Stevenson, Washington, August 20-24.

[86] Laurin, D., Hildebrand, A., Cardinal, R., Harvey, W., & Tafazoli, S. (2008). *NEOSSat: a Canadian small space telescope for Near Earth asteroid detection*. Proceedings of SPIE, 7010, 701013-701013–12. https://doi.org/10.1117/12.789736

[87] Licandro, J., Alí-Lagoa, V., Tancredi, G., & Fernández, Y. (2016). *Size and albedo distributions of asteroids in cometary orbits using WISE data*. Astronomy and Astrophysics, 585, 1–12. https://doi.org/10.1051/0004-6361/201526866

[88] Lladó, Neus & Ren, Yuan & Masdemont, Josep & Gomez, Gerard. (2014). *Capturing small asteroids into a Sun–Earth Lagrangian point*. Acta Astronautica. 95. 176–188. 10.1016/j.actaastro.2013.11.007.

[89] Lubin, P., Hughes, G. B., Eskenazi, M., Kosmo, K., Johansson, I. E., Griswold, J., . . . Brashears, T. (2016). *Directed energy missions for planetary defense.* Advances in Space Research, 58(6), 1093–1116. https://doi.org/10.1016/j.asr.2016.05.021

[90] Lupishko, D. F., & Di Martino, M. (1998). *Physical properties of near-earth asteroids. Planetary and Space Science*, 46(1), 47–74. https://doi.org/10.1016/S0032-0633(97)00132-3

[91] Machado, J. A. T., Baleanu, D., Luo, A. C. J., & Castelli, R. (2011). *On the Relation Between the Bicircular Model and the Coupled Circular Restricted Three-Body Problem Approximation*. Nonlinear and Complex Dynamics, 53–68. https://doi.org/10.1007/978-1-4614-0231-2_4

[92] Machuy, A. L., Fernando, A., Almeida, B. D. E., & Stuchi, T. D. E. J. (2009). *Gravitational Capture Using a Four-Body Model*, WSEAS Transactions on Mathematics. 8. 2002.

[93] Mainzer, A., Grav, T., Bauer, J., Conrow, T., Cutri, R. M., Dailey, J., . . . Wright, E. L. (2015). *Survey simulations of a new near-earth asteroid detection system.* Astronomical Journal, 149(5), 1–51. https://doi.org/10.1088/0004-6256/149/5/172

[94] Mingotti, G., Topputo, F., & Bernelli-Zazzera, F. (2012). *Transfers to distant periodic orbits around the Moon via their invariant manifolds.* Acta Astronautica, 79, 20–32. https://doi.org/10.1016/j.actaastro.2012.04.022

[95] Moon, H. K., Byun, Y. I., Raymond, S. N., & Spahr, T. (2008). *Realistic survey simulations for kilometer class near Earth objects*. Icarus, 193(1), 53–73. https://doi.org/10.1016/j.icarus.2007.07.022

[96] Moon, H., Chun, M., Byun, Y., & Han, W. (2019). *Small-Telescope Astronomy on Global Scales ASP Conference Series*, Vol. 2J,6, 2001 W.P. Chen, C. Lemme, B. Paczyriski, 2, 240–244.

[97] Morais, M. H. M., & Morbidelli, A. (2002). *The population of near-Earth asteroids in coorbital motion with the Earth*. Icarus, 160(1), 1–9. https://doi.org/10.1006/icar.2002.6937

[98] NASA. (2009). *Near-Earth Object Surveys and Hazard Mitigation Strategies : Interim Report Committee to Review Near-Earth Object Surveys and Hazard Mitigation*. Review Literature And Arts Of The Americas.

[99] Ldro, R. O., Robinson-tillenburg, E. A., Viciano, I. E., Zhang, Z. J., & Meszaros, V. A. (n.d.). *NASA BIG Idea Challenge Technical Paper A Reusable Modular Solar Electric Propulsion (SEP) Space Tug to Transfer Payloads from Low Earth Orbit (LEO) to Lunar Distant* University of Maryland.

[100] Okutsu, M., Yam, C. H., & Longuski, J. (2012). *Low-Thrust Trajectories to Jupiter via Gravity Assists from Venus, Earth, and Mars*, 37(6). https://doi.org/10.2514/6.2006-6745

[101] Pascale, P. De, & Vasile, M. (2006). *Preliminary Design of Low-Thrust Multiple Gravity-Assist Trajectories. Journal of Spacecraft and Rockets*, 43(5), 1065–1076. https://doi.org/10.2514/1.19646

[102] Petropoulos, A. E. (2004).*Low-Thrust Orbit Transfers Using Candidate Lyapunov Funcitons with a Mechanism for Coasting*. 2. 10.2514/6.2004-5089.

[103] Petropoulos, A. E., & Longuski, J. M. (2004). *Shape-Based Algorithm for Automated Design*. Journal of Guidance, Control, and Dynamics, 41(5), 787–796.

[104] Petropoulos, A. E. (2004). *Low-thrust orbit transfers using candidate Lyapunov functions with a mechanism for coasting*. Collection of Technical Papers - AIAA/AAS Astrodynamics Specialist Conference, 2(August), 748–762. https://doi.org/10.2514/6.2004-5089

[105] Rabe, E. (1961). *Determination and Survey of Periodic Trojan Orbits in the Restricted Problem of Three Bodies*. The Astronomical Journal, 66(9), 500–513.

[106] Rashid, T., Crispin, Y., & Seo, D. (2016). *Lagrangian Points and Jacobi Constants for a Class of Asteroids*, (September). https://doi.org/10.2514/6.2016-5435

[107] Ren, Y., Pergola, P., Fantino, E., & Thiere, B. (2012). *Optimal low-thrust transfers between libration point orbits. Celestial Mechanics and Dynamical Astronomy*, 112(1), 1–21. https://doi.org/10.1007/s10569-011-9382-y

[108] Ryan, E. L., Mizuno, D. R., Shenoy, S. S., Woodward, C. E., Carey, S. J., Noriega-Crespo, A., . . . Price, S. D. (2015). *The Kilometer-Sized Main Belt Asteroid Population as Revealed by Spitzer*. 578. 10.1051/0004-6361/201321375.

[109] Sales, J. (2013). *Trajectory Optimization for Spacecraft Collision Avoidance.* Retrieved from http://www.dtic.mil/dtic/tr/fulltext/u2/a583484.pdf

[110] Sengupta, R. (2013). *Deflection Of An Asteroid By Laser Ablation And Laser Pressure Technique*. International Journal of Engineering Research and Applications, 3(2), 1049–1056.

[111] Shannon, J. L., Ozimek, M. T., Atchison, J. A., & Hartzell, C. M. (2019). *Q-law aided direct trajectory optimization for the high-fidelity, many-revolution low-thrust orbit transfer problem.* Advances in the Astronautical Sciences, 168(January), 781–800.

[112] Shen, H., Zhou, J., Peng, Q., Luo, Y., & Li, H. (2011).*Low-thrust trajectory optimization for multiple target bodies tour mission.* Theoretical and Applied Mechanics Letters, 1(5), 053001. https://doi.org/10.1063/2.1105301

[113] Stasko, S. E. (2007). *A Dynamic Study of an Earth Orbiting Tether Propulsion System.* PhD diss., University of Tennessee, 2007. https://trace.tennessee.edu/utk_graddiss/304

[114] Sweetser, T. H.(1993) *Jacobi's Intergal and DV-Earth- Gravity Assist (DV-EGA) Trajectories*, Advances in the Astronautical Sciences, Vol. 85, Univelt, San Diego, pp. 417–430.

[115] Taheri, E., & Mall, K. (2020). *MINIMUM-FUEL LOW-THRUST TRAJECTORY OPTIMIZATION USING TRIGONOMETRIC-BASED REGULARIZATION*, 1–19.

[116] Tricarico, P. (2017). *The near-Earth asteroid population from two decades of observations.* Icarus, 284, 416–423. https://doi.org/10.1016/j.icarus.2016.12.008'

[117] Weaver, H., A'Hearn, M., Fountain, G., Leary, J., & Niebur, C. (2007). *Comet Surface Sample Return.* Retrieved from http://www.lpi.usra.edu/opag/nov_2007_meeting/presentations/cssr.pdf

[118] Vetrisano, M. & Branco, J. & Sánchez, J.P. & García Yárnoz, D. & Vasile, M. (2013). *Deflecting Small Asteroids using Laser Ablation: Deep Space Navigation and Asteroid Orbit Control for LightTouch 2 Mission.* AIAA Guidance, Navigation, and Control (GNC) Conference. 10.2514/6.2013-5250.

[119] Whiting, J.K. (2005). *Orbital Transfer Trajectory Optimization.* Master's thesis, MASSACHUSETTS INSTITUTE OF TECHNOLOGY.

[120] Xu, M., & Xu, S. (2009). *Exploration of distant retrograde orbits around Moon.* Acta Astronautica, 65(5–6), 853–860. https://doi.org/10.1016/j.actaastro.2009.03.026

[121] Yam, C. H., Mcconaghy, T. T., Chen, K. J., Longuski, J. M., & Candidate, D. (2004). *Design of Low-Thrust Gravity-Assist Trajectories to the Outer Planets.* International Astronautical Federation - 55th International Astronautical Congress 2004. 1. 476-491.

[122] Zhang, Q., Walsh, K. J., Melis, C., Hughes, G. B., & Lubin, P. M. (2015). *Orbital simulations on the deflection of Near Earth Objects by directed energy.* Nanophotonics and Macrophotonics for Space Environments IX, 9616, 961604. https://doi.org/10.1117/12.2186368

VITA

Jay Iuliano earned his Bachelor of Science in Aerospace Engineering degree from California Polytechnic State University (Cal Poly - SLO) in 2015, and his Master of Science in Aerospace Engineering degree one year later from the same place. During his time at Cal Poly, he spent several years working as a Teacher's Assistant for both aerospace and philosophy courses. Jay also worked for a year at Polysat, a student program that designs, builds, and flies cubesats, as an engineer and a mission manager for the Ionospheric Scintillation Explorer (ISX). In 2016, he began his Ph.D. at Purdue University under the advisement of Professor David Spencer. During his time at Purdue, Jay worked for more than 3 years as a Teaching Assistant for the Department of Mathematics, lecturing on various topics in introductory calculus. From 2018-2020, Jay worked as a Research Assistant for Professor Spencer, alongside NASA's Jet Propulsion Laboratory (JPL) where he researched the thermal effects on dust particles during Earth atmospheric entry.